4 Simulation, computer tools, and metrology

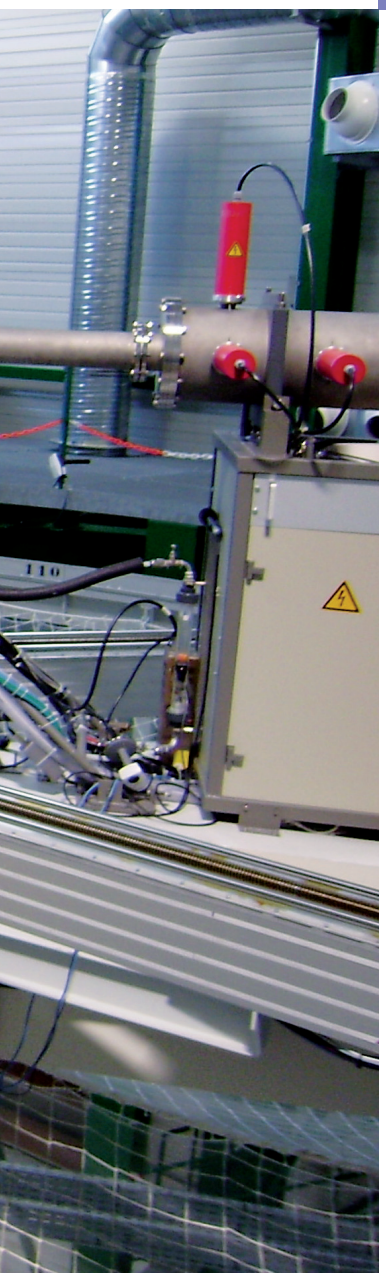

SIMULATION, computer tools, and metrology

Martial JOREL
Reactor Safety Division

The nuclear power plants currently operating in France can be considered highly satisfactory in terms of performance and safety levels. But performance and safety can only be preserved and, *a fortiori*, improved, through constant surveillance and a sustained research effort to reduce persistent uncertainties and obtain a better grasp of the phenomena at the root of accidents.

Research programs in this area are usually costly – sometimes very costly – but that is a price we have to pay if we are to rise to the many challenges associated with nuclear energy, such as aging facilities, new fuel management methods and, in the medium term, the arrival of new generations of reactors.

It is the research investment required if we are to reduce, or "practically eliminate", the occurrence of severe accidents or at least limit their impact on the environment and on human health and property.
This is no doubt ambitious, but it is crucial. Within this context, the solution is not to plan or recommend a line of additional protective systems, but rather to develop a probabilistic approach to incidents or accidents from the very beginning of the reactor design phase.
Any credible response to these technological, social, and regulatory challenges must take into consideration:

- new operating requirements (reactor units with a longer service life) and ecological challenges (optimizing resource management, reducing waste and recycling spent fuel);
- external factors (extreme weather conditions, acts of malice), which currently receive too little attention;
- public opinion and acceptance;
- maintaining skill levels in the nuclear field, primarily for operators, but also for authorities and experts;
- training and the need to attract fresh talent to hand down knowledge and know-how from one generation to another.

Then, there is the need to prepare for the future to pave the way for the gradual introduction of novel, innovative technology, such as fourth-generation – or GEN IV – reactors.

Safety research thus remains a vital and integral part of the use of nuclear energy for peaceful purposes, with which it shares the same essential characteristics, particularly in its forward-looking aspect. This perspective entails developing and initiating new, more robust, and more accessible computing programs that offer enhanced performance and more power, and that take into account an increasing range of physical parameters. Such programs will call for substantial experimental databases that are properly adapted to the development of software models and qualification. This makes it vital to preserve the necessary simulation tools by sharing costs and pooling knowledge within broader, well-organized international collaborative structures.

The feature articles contained in Chapter 4 are all very different and cover a wide variety of topics. They all seek, however, to main-

tain and, if possible, enhance the safety levels of reactors currently in service, while preparing a seamless transition to future systems. This will be achieved by drawing on the synergy between expert assessment requirements and controlled, well-directed, targeted research activities.

First of all, Article 3 by E. Raimond and N. Rahni, entitled "Level 2 PSA for 900 MWe PWRs: from Development to Lessons Learned", provides a very clear overview of severe accident phenomenology, and goes on to describe probabilistic safety assessment (PSA) objectives and methods, dividing them into Levels 1, 2, and 3 depending on the stage of the accident. The article then focuses on the sequences, starting with reactor core meltdown, that lead to the dispersion of contaminated products (Level 2 PSA). Lastly, it shows how Level 2 PSA assessments apply to studies of French 900 MWe reactors. It is important to observe that IRSN's expertise in these techniques is known and recognized around the world, which is why E. Raimond was asked to coordinate the ASAMPSA-II project as part of the Seventh European Framework Program (FP7). The project is aimed at standardizing Level 2 PSA practices in industry and among safety organizations.

Vincent Koundy's article, "PWR Reactor Vessel Lower Head Failure in a Severe Accident Situation and Research Program on Material Tearing in French Reactor Vessels", complements and follows on from the above article. It adds a precise phenomenological description and considers research requirements concerning some of the sequences studied during Level 2 PSA work. It does this by relating the molten material (corium) produced during a severe accident to the risk of high-temperature failure in the lower vessel head and the spread of this material towards the reactor containment.

Hazards – both internal and external, including earthquakes – are among the key issues addressed by safety assessment activities. This is why it is so important to determine reference values for use in design work. Luis Fabián Bonilla's article "Effects of Local Geology on Seismic Motions: Site-specific Estimation of the Seismic Hazard" provides a very thorough look at this question. The article shows how the geotechnical properties of the ground can affect the amplification of seismic motion and considers the consequences from the safety analysis point of view.

Reinforced and prestressed concrete is commonly used to build various parts of nuclear facilities. Its use in reactor building containments is not purely structural, for it also contributes to the containment function for environmental protection. In order to prevent any leaks in the event of a nuclear accident, the inner concrete wall of containments is biaxially prestressed. Nanthilde Reviron's article, "Creep Study on Concrete in Tension: Application to Containment Structures in Pressurized Water Reactor Nuclear Power Plants", investigates the behavior of this material in tension to provide some useful insight for assessment work.

Vincent Gressier's exhaustive article on "Neutron Metrology" analyzes the process used to guarantee accurate measurements in neutron dosimetry. The quality requirement for such measurements can be specified in international standards, for use as a reference in assessing the conformity of a product, process, system, person, or organization. Significant scientific progress has been made over the last few decades, bringing with it a great deal of new technology and novel products. This makes it all the more important for metrology to measure the quality of new products and services with increasing precision, and with reference to the International System of Units.

The article by Jean-Christophe Sabroux on the search for radon on Mars, conducted by IRSN and the CNES, the French space agency, also provides an illustration of some innovative products in the field of metrology. In a thesis written in collaboration with the CNES, the author develops a method for revealing the presence of radioactive gases on Mars. The Institute is working on an instrument specifically designed to measure radon on the Red Planet. The instrument is a likely candidate for a place on board the Mars probe, proof, if needed, that the skills acquired by the Institute in its traditional fields of activity can be put to use successfully in more "exotic" ventures.

The article "Using the CALIES computer code" by Caroline Ringeard, describes a code developed by IRSN to measure the environmental impact of chemical effluent. Three short articles complete this rich and varied chapter. All three deal with the safety problems inherent in the disposal of irradiated materials. The first, "Recent Developments in MELODIE Software" by Marc Bourgeois, describes the capabilities of the code acquired by IRSN to perform simulations in the field of surface facilities, for the export market in particular. The second, "IRSN's Contribution to the European NF-PRO Project on the Disposal of Radioactive Waste in Geological Repositories" by Gregory Mathieu, offers an overview of the studies carried out to control the behavior of a geological repository after closure. The third, "Safety of Deep Geological Radioactive Waste Repositories: IRSN Expands its Experimental Station in Tournemire and Sets up a New Research Program" by Justo Cabrera, provides the experimental backup required for these studies.

Although the studies and research activities related in these articles address a wide range of topics and themes, they share the same objective: to provide safety organizations with all the support they need to conduct exhaustive and independent assessments.

CREEP STUDY ON CONCRETE IN TENSION: application to containment structures in pressurized water reactor nuclear power plants

Nanthilde REVIRON, Georges NAHAS
Civil Engineering and Structural Analysis Unit

Reinforced pre-stressed concrete is commonly used for construction work in nuclear facilities. In reactor containments pre-stressed reinforced concrete is used not only for structural but also for containment purposes, in order to protect the environment. The research work carried out for the investigation reported here aimed to assess the effect of tensile creep in concrete, first, when cracks appear during ten-yearly inspections, and second, when microcracks occur in concrete, reducing its containment properties and life span.

Containment design on French nuclear power plants

In French PWR nuclear power plants with double-walled containment, the pre-stressed concrete wall is designed to withstand an increase in internal pressure under accident conditions of about 0.5 MPa absolute pressure during a loss-of-coolant accident (***Figure 1***).

EDF, the operator of the PWR nuclear power plants currently in service in France, must demonstrate that their containment structures are capable of ensuring a leakage rate of less than 1.5%/24 hours of the total mass of gas (air/steam mixture) inside the containment. To confirm that the structure is able to perform its containment function in the event of an accident, each containment is subjected to periodic testing (before the plant is commissioned, and then every ten years). The test is conducted at full scale, in dry air at ambient temperature and at design pressure: this is the "containment test".

During these tests, which last for several days – including a step-by-step rise in pressure and a return to "normal" pressure – the containment is subjected to stresses during which tensile forces may appear in singular zones (equipment hatch, personnel airlock, etc.).

In addition, over the very long term (beyond the structure's expected life span), these tensile stresses may also appear in straight sections of the containment if the delayed deformations (shrinkage and creep) were underestimated during structure design [Benboudjema, 2002]. Creep deformations caused by tension may appear under these conditions, accompanied by cracking and/or contributing to the growth of pre-existing cracks.

Concrete creep is one of the main features of the mechanical behavior of concrete. The corresponding tests are lengthy and the results obtained are strongly influenced by the age of the concrete at the time of loading, the level of stress applied, and the environmental conditions of testing (temperature, humidity, etc.).

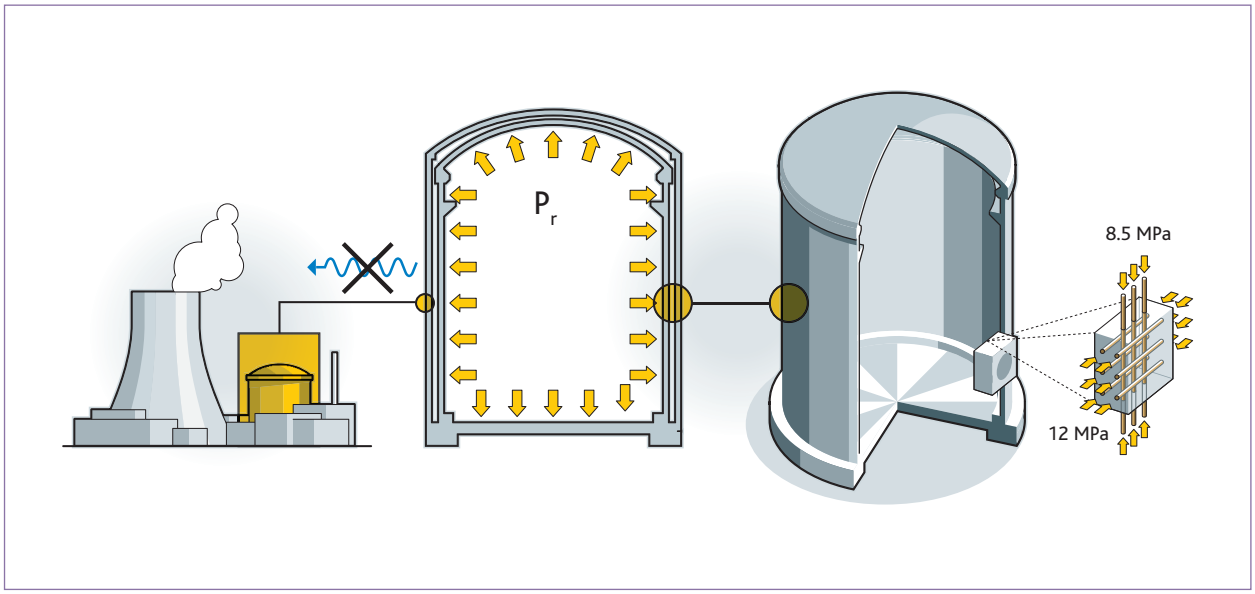

Figure 1 *Containment: prediction of delayed behavior [Granger, 1996].*

While concrete creep under compression, bending, and indirect tension at an early age (shrinkage-prevention system) has been studied extensively [Omar, 2004; Granger, 1996; Kovler, 1994], this is not the case for creep in hardened concrete in direct tension, which is poorly understood [Berthollet, 2003; Brooks and Neville, 1977; Morin and Maso, 1982]. In particular, the region where creep compliance in direct tension is independent of applied stress has not been investigated thoroughly, as is also the case for the risk of concrete failure upon loading.

Creep of concrete in tension at an early age has been investigated more frequently [Kovler et *al.*, 1999]. When concrete deformation (endogenous shrinkage and thermal deformation) is restricted or prevented, the development of tensile stresses may lead to cracking. A number of complex phenomena are involved, however, (in particular changes in the hydration reaction and temperature), which complicates the interpretation of the creep and relaxation curves.

As regards hydrated concrete, when designing structures, the behavior of the concrete in tension is not usually considered. In reinforced concrete structures the tensile stresses are taken up by the rebars. In addition, constructing an experimental setup is a tricky matter. As a result, very few data are available at present.
In spite of the large number of studies carried out on the phenomenon of creep, the mechanisms involved are not yet completely understood.

Sustained scientific initiative

In order to meet the needs of safety assessments, the behavior of concrete subjected to the mechanical stresses caused by uniaxial tension must be understood. Accordingly, it is important to determine the various physical and mechanical couplings that may affect this material.
For this reason a major experimental study of creep in hydrated concrete – at least 90 days old and representative of a containment wall subjected to tensile forces – was conducted, using various levels of stress.
Four types of test were carried out in parallel: measurements of deformations of thermal origin, deformations due to drying shrinkage, deformations due to basic creep, and delayed total deformations. An experimental study on concrete drying in the absence of mechanical stress was also performed.

The results obtained will be compared with those reported by EDF as part of the thesis work conducted by Laurent Granger [Granger, 1996] on compression creep in a material of almost identical composition.

Experimental investigation of creep in uniaxial tension

Test description

For the purposes of this study, two frame structures were constructed so that several tests could be conducted in parallel (***Figure 2***).

Figure 2 *Tensile creep test facility.*

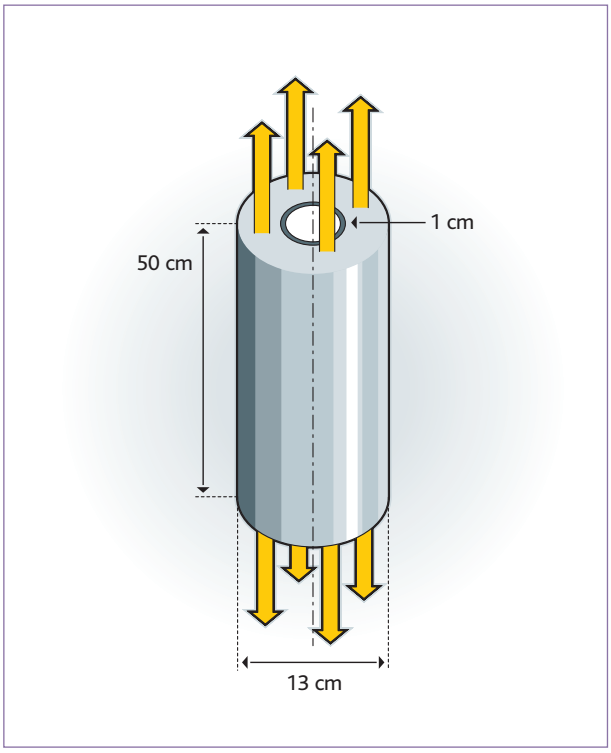

Figure 3 *Diagram of test specimen.*

They were used to apply a tensile force directly to a test specimen using a stack of 13-kg weights. The weights ensured constant loading during the test, whatever the deformation of the concrete and the environmental conditions, and also eliminated the constraints associated with the use of a hydraulic servo-mechanism, in particular the system's instability (applied load less constant over time, emission of heat). The test specimen was attached to the frame using aluminum caps that were screwed to the frame and bonded on the specimen side.

The test specimens were cylindrical, with a diameter of 13 cm and a height of 50 cm (***Figure 3***). As part of another study (not included in this report) concerning measurement of the permeability of the test specimens to air, they were given a central, i.e., cylindrical hole 1 cm in diameter, running their full length. By measuring permeability, it was possible to quantify the development of cracking during the test. The choice of cylindrical test specimens made it easier to interpret the results.

For all these tests the concrete was allowed to harden for at least 90 days and was preserved in endogenous conditions (cling wrap + self-adhesive aluminum foil) upon removal from the mold, in an atmosphere at 20°C (± 1°C) and 50% (± 5%) relative humidity.

The experimental work conducted on the hardened material addressed only the pre-peak phase of the concrete's uniaxial behavior. Various levels of loading (50%, 70%, and 90% of the tensile strength) were checked before reaching the peak stress. The specimens were subjected to these various loadings for three days. Several series of tests were carried out for each level of loading to quantify dispersion. The test specimens were then completely "unloaded" over 24 hours to characterize their recovery, and were then loaded until failure under direct tension (on the same frame), to assess the effects of creep on their residual mechanical properties.

Formulation selected

To ensure that the results would be representative, a concrete formulation provided by EDF was used. However, the rheological properties of concrete poured in the laboratory (to test slump, strength, and Young's modulus) were different from those of construction-site concrete; for this reason the formulation had to be adjusted. This step was very important because no model can reliably predict a concrete's characteristics based on its formulation. It was therefore necessary to vary the parameters one by one to arrive at a formulation whose characteristics were as close as possible to the rheological and mechanical data provided by EDF. This phase of experimentation was relatively lengthy. The formulation

Cement (Airvault) CEMI 42.5R	Sand	Aggregates 5-12.5 mm	Aggregates 12.5-20 mm	Water	Plastiment HP	Slump	Occluded air
kg/m³	kg/m³	kg/m³	kg/m³	l/m³	0.35 %	cm	%
350	772	316	784	201	1.225	11	2.33

Rc	Rc	Rc	Splitting	Splitting	Modulus	Modulus
7 days	28 days	90 days	28 days	90 days	28 days	90 days
MPa	MPa	MPa	MPa	MPa	GPa	GPa
39.34	46.5	49.35	3.29	3.42	31.34	33.81

Table 1 *Concrete formulation and characterization results (compression strength, splitting, Young's modulus).*

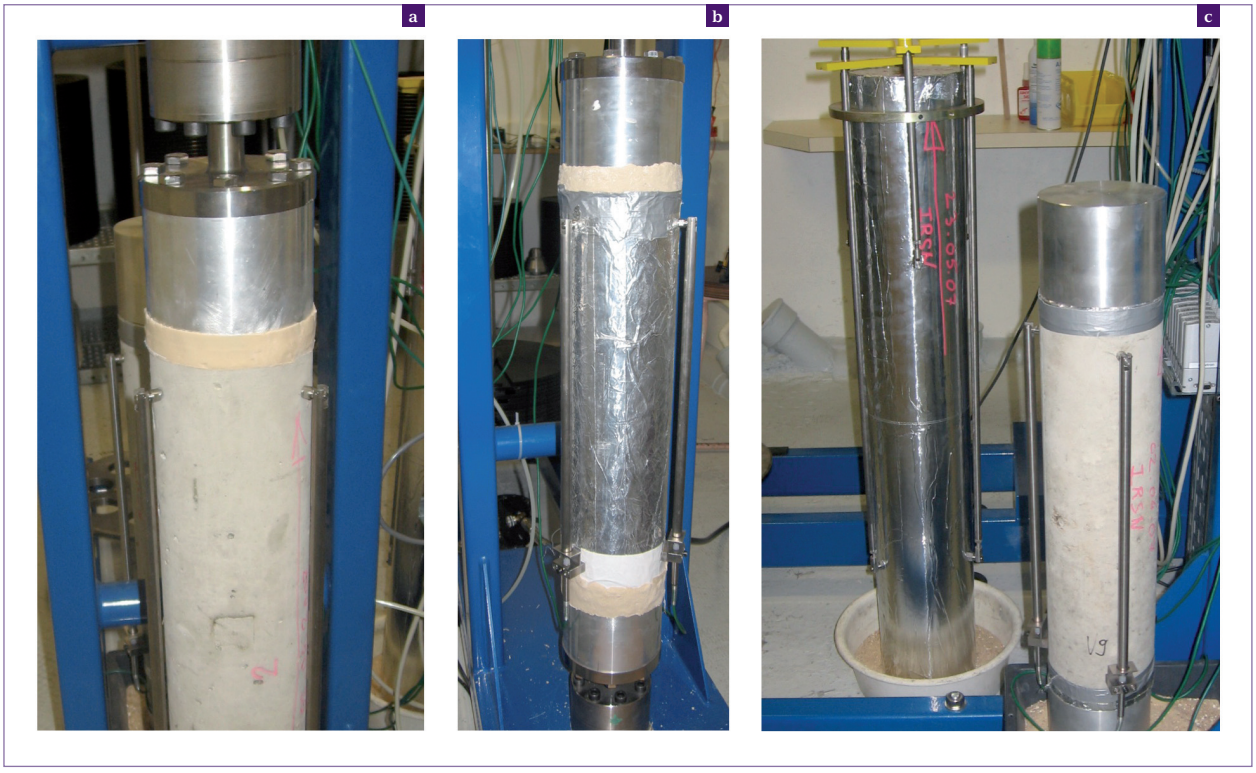

Figure 4 *Measurement of deformation* ***a)*** *total delayed deformation;* ***b)*** *basic creep;* ***c)*** *due to heating and drying shrinkage.*

(based on dry aggregates) and the properties of the concrete utilized are shown in ***Table 1***. [Granger, 1996] worked with the same concrete. The cement used in the study described here, however, is slightly different in composition (the cement used in 1996 is no longer manufactured); in addition, the water content was increased by six liters to meet the Abrams cone (slump) test and to allow for variation in absorption of the current aggregates. Although the aggregates still come from the same quarry, absorption rose from 1.3% to 1.6%.

Test description

In order to obtain the data needed to characterize the delayed behavior of concrete and then model it, a variety of tests were carried out to assess the influence of the various parameters on:

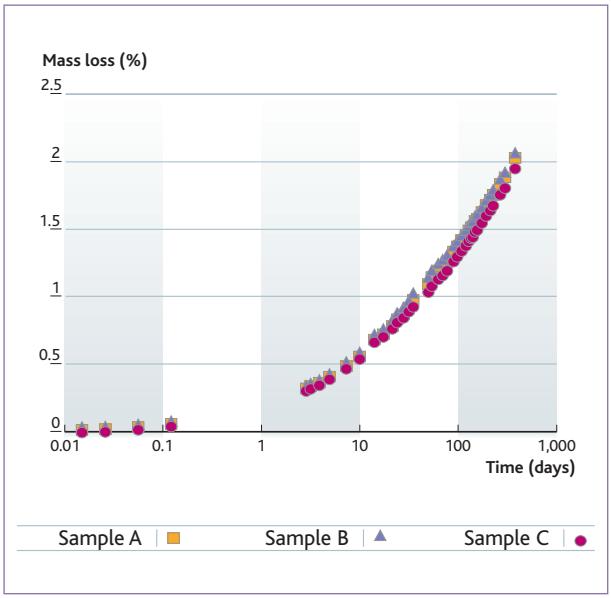

Figure 5 *Variation of mass loss with time (90-day-old concrete).*

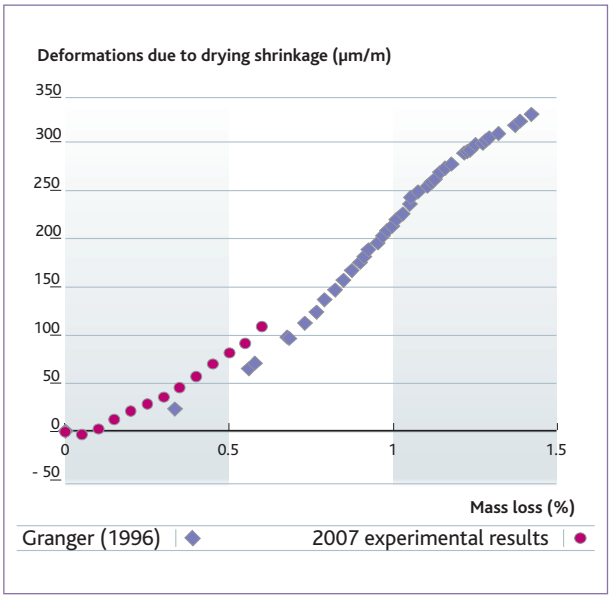

Figure 6 *Variation of deformations due to drying shrinkage with mass loss.*

- characterization tests (test specimens 16 cm in diameter and 32 cm high). These specimens were used to describe the creep loading level in direct tension. Splitting tensile tests (or "Brazilian" tests), which consist in crushing a sample of concrete between the plates of a press, were carried out before each tensile-creep campaign;
- measurement of mass loss (test specimens 13 cm in diameter and 10 cm high). The test determined the kinetics of concrete drying (three specimens). For this test the upper and lower surfaces were protected to prevent desiccation;
- measurement of the total delayed deformation (test specimens 13 cm in diameter and 50 cm high) (***Figure 4a***). The specimens unpacked at the beginning of the test were loaded in direct tension, maintained for three days. Recovery was monitored for 24 hours;
- measurement of basic creep deformation (test specimens 13 cm in diameter and 50 cm high) (***Figure 4b***). The specimens were loaded in direct tension, maintained for three days, while being protected against hydric exchanges. Recovery was also monitored for 24 hours;
- measurement of deformations of thermal origin (test specimens 16 cm in diameter and 100 cm high) (***Figure 4c left***). The test identified the proportion of thermal deformation caused by fluctuations in ambient temperature. The test specimen was maintained in endogenous conditions during the test. A single test specimen was used for the entire series of experiments;
- measurement of deformation due to drying shrinkage (test specimens 13 cm in diameter and 50 cm high) (***Figure 4c right***).

The specimens were dried under the same conditions as the specimens used to determine mass loss and those used to measure total delayed deformation. Three tests were carried out during the experimental campaign.

Test instrumentation

Displacements were measured against a 40-cm scale in the central portion of the test specimen (eliminating edge effects), using three LVDT (Linear Variable Differential Transformer) sensors set at 120°C, which eliminated movements of the rigid components on the concrete. The inserts supporting the extensometer bars and the aluminum caps were bonded using a methacrylate adhesive.

Result analysis

Mass loss and drying shrinkage

Figure 5 shows the gradual loss of mass against time under the test conditions: 20°C (±1°C) and 50% (±5%) RH. Mass loss was about 0.39% after four days (corresponding to the total duration of the shrinkage and creep tests).

The variation of shrinkage with mass loss is represented in ***Figure 6***, which also shows a "dormant" region at the beginning of the tests. Microcracking on the surface of the test specimens masks the deformation due to contraction caused by water loss. This is followed by a region where drying shrinkage is proportional to the observed

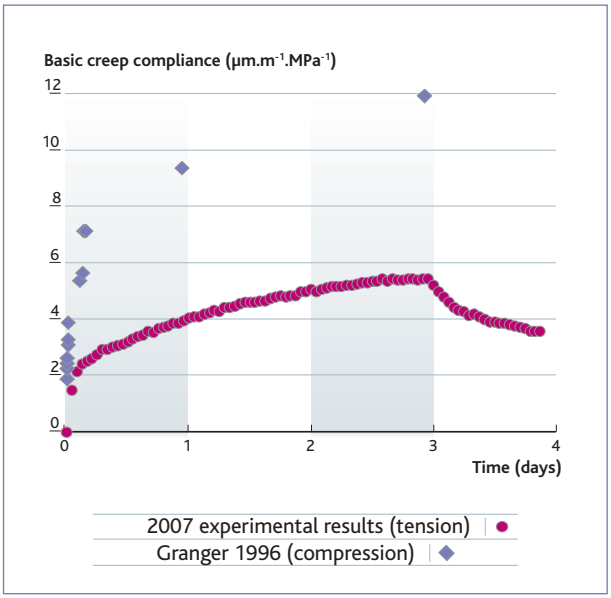

Figure 7 *Changes in basic creep compliance over time and comparison with [Granger, 1996].*

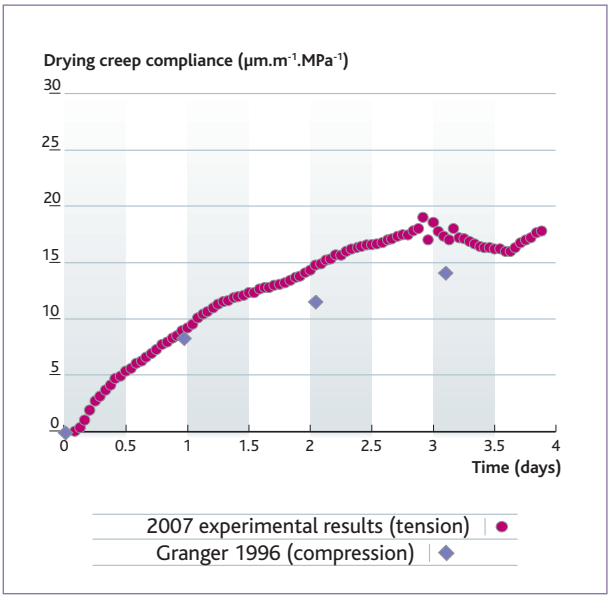

Figure 8 *Changes in drying creep compliance over time and comparison with values from [Granger, 1996].*

mass loss. These observations are consistent with those obtained by other authors [Granger, 1996] for various concrete compositions.

Basic creep

Basic creep compliance of concrete in tension corresponded to the raw test data, which served to deduce elastic deformations and deformations of thermal origin. The progress of basic creep compliance was compared to that obtained in compression by [Granger, 1996] for the same concrete (***Figure 7***). The graph of basic creep compliance of concrete in tension shown here represents the average of six tests. Observations did not discern any influence from the loading level on basic creep compliance, which confirms that the deformations are indeed proportional to the applied stress.

The deformation figures were about one fifth of those measured by Granger during compression tests (after three days). This notable contrast with the tests by [Granger, 1996] may be explained by differences in the materials utilized or by different creep mechanisms in compression and tension. It should be noted that, using the same concrete, [Brooks and Neville, 1977] measured a deformation by basic creep in tension that was greater than that in compression.

Experimental investigation of basic creep in tension is seen to be far from easy. On the one hand the two test specimens experienced failure, one of them in the useful zone after only a few hours, the other at the interface with the adhesive, due to poor adhesion; the deformation figures obtained during these tests were ignored in calculating creep compliance. On the other hand, the figures for deformation by basic creep were very small (similar in magnitude to the deformations of thermal origin).

The experimental results do not allow any conclusion to be drawn as to whether basic creep deformation is reversible or not, because the "unloading" period was too short. Nevertheless, after one day of "unloading", about 34% of creep deformation in tension was found to be reversible. This result is similar to what was observed during compression tests (see in particular [Illston, 1965], who found that about 30% of basic creep deformation was reversible). On the other hand, this result contradicts those of [Morin and Maso, 1982], who observed a completely irreversible behavior during tests in tension.

Drying creep

In parallel with the tests on basic creep, tests to measure total delayed deformation were conducted. Drying creep compliance was obtained by processing all the preceding tests. Deformations due to drying creep were determined by subtracting from the total delayed deformations the elastic deformations, the deformations of thermal origin, and the deformations from drying shrinkage and from all the basic creep tests (average figure for all the corresponding tests). The changes in drying creep compliance of concrete in tension are presented in ***Figure 8*** (average of five tests). As with

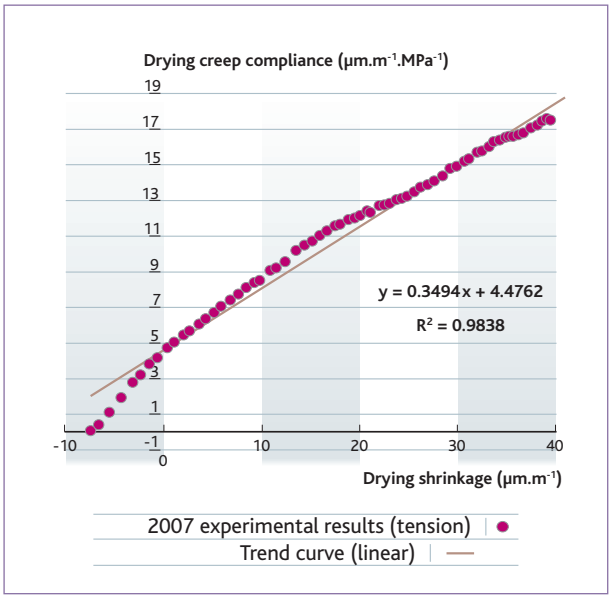

Figure 9 *Drying creep compliance versus drying shrinkage.*

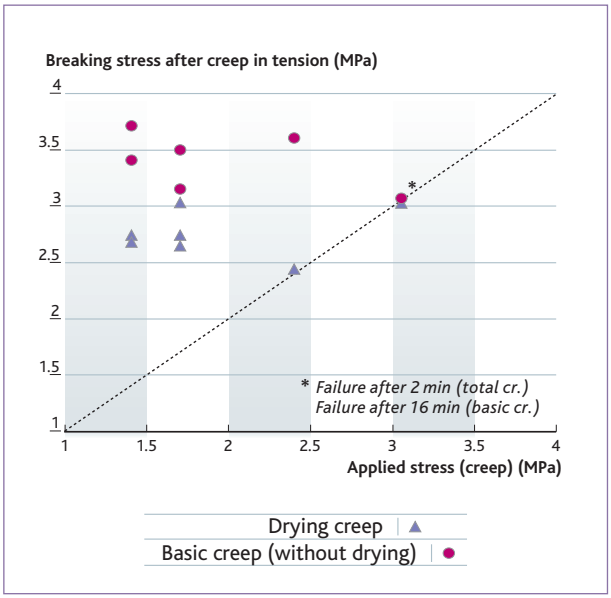

Figure 10 *Breaking stress (after creep) versus applied stress.*

basic creep, the level of loading does not appear to influence drying creep compliance.

The results obtained from our experimental campaign are in agreement with those produced in tension [Brooks and Neville, 1977]; these authors also observed a recovery of about 20% during unloading. As with basic creep, the result for tension is similar to what has been observed in compression [Illston, 1965].
When recovery was complete, an increase in deformations due to drying creep was noted, which cannot be explained physically.

Figure 9 shows that drying creep compliance of concrete in tension is proportional to drying shrinkage (a phenomenon also observed in compression [Gamble and Parrott, 1978]. The negative region at the start of the curve is explained by the "dormant" zone observed in ***Figure 6***. The specimens were unloaded after three days. Results show that creep was partially reversible (about 24%).

Moreover, a comparison of the results from this campaign with those obtained by [Granger, 1996] in compression shows that they are similar.

Effect of drying and creep on (residual) tensile strength

The variation of breaking stress (after basic creep or drying creep in tension) with applied stress is shown in ***Figure 10***.

Overall, concrete test specimens tested under drying conditions have a breaking stress (after deformation) that is lower than that of test specimens loaded under endogenous conditions. Breaking stress after basic creep tests was 3.47 MPa on average, whereas it was about 2.72 MPa for the total creep tests. In view of these results it seems that the microcracking on the skin of the test specimens was caused by differential drying. The breaking stress does not seem to depend on the stress applied during creep. However, this result remains to be confirmed, in particular by carrying out direct tension tests on specimens kept under drying conditions for four days (duration of testing), but without mechanical loading.
Comparison with results in the "technical literature" is difficult, because there are few results concerning changes in the mechanical properties of concrete subjected to tension after drying (as compared to concrete subjected to compression).

For example, during a splitting tensile test, [Hanson, 1968] observed a slight (3%) increase in strength. During a bending test [Pihlajavaara, 1974; Kanna et *al.*, 1998], a decrease in strength was observed down to a relative humidity of 70%, and then a gradual increase until a relative humidity of 0% was reached. For direct tension tests on specimens maintained at 21°C with 55% relative humidity, it appears that during sealed curing, the tensile strength first rose owing to the hydration effects, then fell [Fouré, 1985; de Larrard and Bostvirronois, 1991], and then rose again [Fouré, 1985].

It should be noted that [Morin and Maso, 1982] found no change in concrete strength after creep in tension (loading to produce creep at 25% and 50% of the tensile strength).

These tests produced new results that will be useful for modeling the behavior of containment structures in areas where tensile stresses may develop.

Conclusion and outlook

The tests performed led to a better understanding of the behavior of concrete subjected to tensile stresses causing creep, and improved our knowledge of the behavior of containment structures that may be subjected to this type of loading. The study is particularly important because the phenomenon is poorly understood and has received little attention. The "scientific literature" mainly offers works concerning compressional creep in concrete. The comparison made above between creep compliance in tension and in compression naturally leads to a numerical simulation of creep. The goal is to model both compressional and tensile creep by applying the same rheological principle, building on existing creep models [Benboudjema, 2002; Granger, 1996] and thereby develop a reliable tool for numerical simulation of the delayed behavior of prestressed reinforced concrete structures considered to be "sensitive" as regards nuclear safety, such as reactor containment structures.

Several avenues of research could provide further information in this area, e.g., a study of creep in tension over a long period (several months), since time has an effect on concrete deterioration in terms of its strength and resistance to water. In this regard it should be emphasized that the test facilities utilized were designed to conduct tests of this type.

Other important subjects remain to be investigated, such as the multiaxial aspects of creep (tension/tension, and tension/compression). An experimental program was initiated using the triaxial Astrée press at the Laboratory of Mechanics and Technology (LMT-Cachan), with test specimens sized and optimized by finite-element numerical simulations (CAST3M). This R&D work is particularly important because the type of stress being studied corresponds to the *in situ* stresses to which containment structures are subjected.

References

- F. Benboudjema (2002). Modélisation des déformations différées du béton sous sollicitations biaxiales. Application aux enceintes de confinement de bâtiments réacteurs des centrales nucléaires, thèse de doctorat de l'université de Marne-la-Vallée.
- A. Berthollet (2003). Contribution à la modélisation du béton vis-à-vis du vieillissement et de la durabilité : interaction des déformations de fluage et du comportement non linéaire du matériau, thèse de doctorat de l'Insa Lyon.
- J.J. Brooks, A.M. Neville (1977). *A comparison of creep, elasticity and strength of concrete in tension and in compression, Magazine of Concrete Research,* vol. 29, n° 100, p. 131-141, septembre 1977.
- B. Fouré (1985). Note sur la chute de résistance à la traction du béton léger consécutive à l'arrêt de la cure humide, Annales de l'Institut technique du bâtiment et des travaux publics, 432, p. 3-14.
- B.R. Gamble, L.J. Parrott (1978). *Creep of concrete in compression during drying and wetting, Magazine of Concrete Research, 104 (30), p. 129-138.*
- L. Granger (1996). Comportement différé du béton dans les enceintes de centrales nucléaires. Analyse et modélisation, thèse de doctorat de l'ENPC, avril 1996.
- J.A. Hanson (1968). *Effects of curing and drying environments on splitting tensile strength of concrete, Journal of the American Concrete Institute, 65 (7), p. 535-543.*
- J.M. Illston (1965). *The components of strains in concrete under sustained compressive stress, Magazine of Concrete Research, vol. 17 n° 50, p. 21-28.*
- V. Kanna, R.A. Olson, H.M. Jennings (1998). *Effect of shrinkage and moisture content on the physical characteristics of blended cement mortars, Cement and Concrete Research, 18 (10), p. 1,467-1,477.*
- K. Kovler (1994). *Testing system for determining the mechanical behaviour of early age concrete under restrained and free uniaxial shrinkage, Materials and Structures, vol 27, p. 324-330.*
- K. Kovler, S. Igarashi, A. Bentur (1999). *Tensile Creep behaviour of high strength concretes at early ages, Materials and structures,* vol. 32, p. 383-387, juin 1999.
- F. de Larrard, J.L. Bostvirronois (1991). *On the long term losses of silica fume high strength concretes, Magazine of Concrete Research, 43 (155).*
- D. Morin, J.C. Maso (1982). Fluage en traction des bétons ordinaires et des bétons légers, *Materials and Structures,* vol. 15, n° 89, p. 469-473, septembre 1982.
- M. Omar (2004). Déformations différées du béton : étude expérimentale et modélisation numérique de l'interaction fluage-chargement, thèse de doctorat de l'École centrale de Nantes.
- S.E. Pihlajavaara (1974). *A review of some of the main results of a research on the aging phenomena of concrete: effect of moisture conditions on strength, Shrinkage and creep of mature concrete, Cement and Concrete Research, 4 (5), p. 761-771.*

4.2

PWR REACTOR VESSEL LOWER HEAD FAILURE IN A SEVERE ACCIDENT SITUATION
and research program on material tearing in French reactor vessels

Vincent KOUNDY
Physics of Severe Accidents Unit

In the postulated case of a PWR(1) core meltdown accident, a significant quantity of corium (mixture of molten metals and oxides) is likely to accumulate in the lower head of the reactor vessel (Figure 1). This results in a risk of vessel lower head failure at high temperatures and spreading of corium in the confinement. Knowing the exact time of lower head failure and the failure mode is important in preparing for this type of accident. By knowing the size of the breach, it is possible to define the conditions of corium ejection, making breach size one of the primary parameters for predicting the consequences of reactor vessel failure and subsequent ex-vessel phenomena (steam explosion, direct heating of containment, interaction between corium and the basemat).

IRSN has developed two-dimensional (2-D) and three-dimensional (3-D) computer models to study the thermal-mechanical behavior of the PWR reactor vessel lower head in the event of a severe accident, which will be used in studies to support the Level 2 PSA(2) developed by IRSN. In this modeling work, lower head penetration was not taken into consideration(3), since the main purpose was to obtain models that were simple, but advanced enough to predict the overall behavior of the reactor vessel lower head, then integrate these models in the standard European severe accident code, ASTEC(4). The computer models developed were first used to interpret and simulate experiments (American and Swedish) on lower head mock-ups to estimate the time of failure and breach size. Validation of the computer models is essential before they can be applied to a reactor-scale study.

(1) Pressurized Water Reactor.

(2) Level 2 Probabilistic Safety Assessments, which cover the progression of severe accidents from core uncovery up to radioactive release to the environment (see article on Level 2 PSA for 900 MWe PWRs: from Development to Lessons Learned).

(3) Cases involving a lower head with local variations in thickness and a lower head with penetrations are currently being studied by CEA and VTT, respectively.

(4) Accident Source Term Evaluation Code.

A look at questions concerning lower head failure

Since the accident at the Three Mile Island nuclear power plant (1979), many research studies have been conducted, including both experimental programs and theoretical work, concerning the behavior of the PWR reactor vessel in a severe accident situation.

The most significant experimental programs have been the LHF(5) [Chu et *al.*, 1998], OLHF(6) [Humphries et *al.*, 2002] and FOREVER(7) [Sehgal et *al.*, 2003] programs. The first two were undertaken by Sandia Laboratories in the US under the direction of the American Nuclear Regulatory Commission (NRC); the second was conducted in the context of an international program under the auspices of the OECD (8), in which IRSN was an active participant; the FOREVER program for its part was undertaken by the Royal Institute of Technology, KTH, in Stockholm.

These programs have furthered knowledge on the physical phenomena leading to failure of the PWR vessel lower head, while contributing to the advancement and validation of the computer codes developed by IRSN and its partners.

Comparisons between the model results and experimental results show that the time of failure and the breach location are correctly estimated by the models. They are also capable of correctly describing overall rupture behavior with core meltdown in the lower head in an accident situation.

The breach size remains difficult to evaluate, however, because it depends to a great extent on the failure mode of the steel. For nearly identical experimental conditions, the size of the breach can be very different from one experiment to another. Studies and analyses performed in the context of the LHF and OLHF programs have shown that embrittlement of vessel materials fully compliant with the same general manufacturing specifications can occur due to certain trace elements inherent in the materials, even at low concentrations. The applied metallurgy research department at CEA has shown that high-temperature embrittlement, which leads to a larger breach size, is mainly due to the sulfur content in the material.

Characterization tests conducted on the vessel materials used during the LHF and OLHF programs based on cylindrical specimens showed a significant difference in behavior between the LHF program vessel material, in which the sulfur concentration was significant, and the OLHF vessel material, where the sulfur concentration was 10 times less, especially for temperatures near 1,000°C (***Figure 2***).
Creep failure, when the temperature was near 1,000°C, was visibly "brittle" for the LHF program vessel material and "ductile" for the OLHF program vessel material. Considerable necking was observed in the second case with a very pointed failure zone.

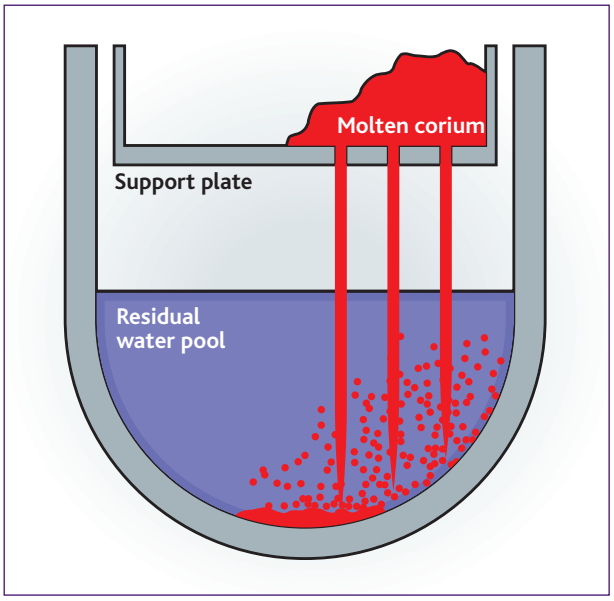

Figure 1 *Accumulation of molten corium in the vessel lower head (schematic representation).*

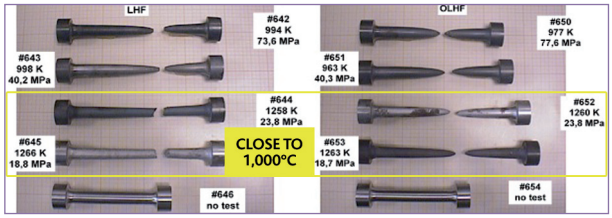

Figure 2 *Characterization tests of the LHF/OLHF reactor vessel materials.*

Although these observations involve American reactor vessel materials, it is appropriate to note that the same embrittlement phenomenon was observed for French reactor vessel materials during the RUPTHER program test campaign [Devos et *al.*, 1999] conducted by the CEA.

This variability in the behavior of the reactor vessel steel must therefore be taken into consideration when preparing the failure criteria used in numerical models, in order to correctly estimate breach size on the lower head. In 2003 IRSN therefore undertook an experimental and numerical modeling research program aiming primarily to gain a better understanding of the high-temperature steel tearing mechanism in French reactor vessels and establish an appropriate failure criterion for modeling.

(5) Lower Head Failure Program (1994-1999).
(6) OECD Lower Head Failure Program (1999-2002).
(7) Failure of Reactor Vessel Retention Program (1999-2002).
(8) Organization for Economic Cooperation and Development.

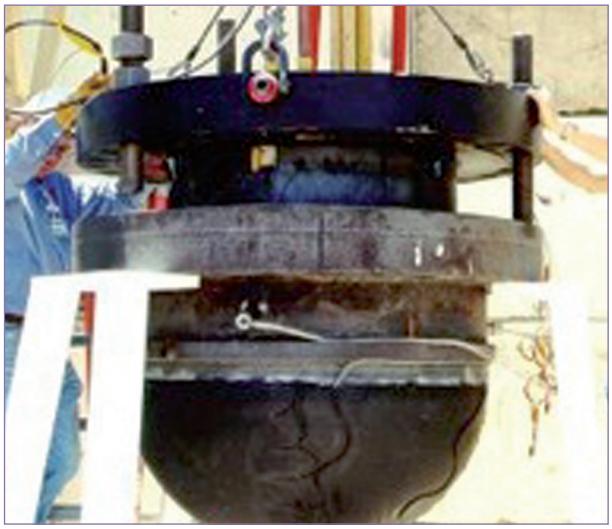

Figure 3 *Mock-up of the lower head from the OLHF program and installation of the induction and radiation heating system.*

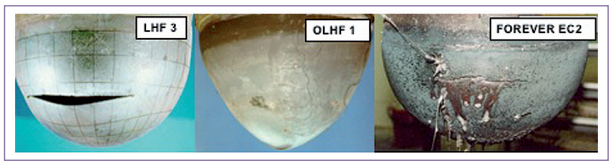

Figure 4 *Photograph of the mock-ups after failure: LHF program Test 3, OLHF program Test 1, and FOREVER program Test 4.*

Experimental programs on reactor vessel lower head failure

The LHF and OLHF programs consisted in performing "failure" tests (eight LHF and four OLHF tests), using PWR lower head mock-ups built to a scale of 1:5. The internal diameter was about 91.4 cm. The lower head thickness of the LHF program mock-ups was about 2.9 cm, while that of the OLHF program was greater, at 7.6 cm, in order to assess the influence of the temperature gradient in the thickness of the lower head material. In the LHF tests (***Figure 3***), the temperature difference observed through the total thickness was less than 80°C, whereas in the case of a reactor core meltdown accident, this difference could reach about 400°C. Most tests were performed at constant pressure (between 2 and 10 MPa) with an internal temperature that rose (up to 1,250°C) until mock-up failure. Taking into account the scaling factor, the internal pressure values applied during the tests were identical to the reactor vessel design pressure. In this way the local state of stress and deformation was the same on the reduced scale and the reactor scale. The internal temperature was obtained using induction heating and radiation heating.

The FOREVER program included nine tests performed on PWR lower head mock-ups built to a scale of 1:10. The mock-up dimensions were about 39 cm for the average diameter and 1.5 cm for thickness. The experimental protocol consisted in pouring a binary oxide melt simulating corium at approx. 1,200°C into the mock-up. An electrical resistance in direct contact with the simulated corium held the temperature at the desired value. The internal pressure in the reactor vessel was assumed constant and kept at 2.5 MPa until failure of the lower head. Two PWR vessel steels, French and American, were used for the FOREVER program tests.

Figure 4 shows a mock-up sample after failure for the LHF, OLHF and FOREVER experimental programs.

Development and validation of the numerical models

The experimental programs mentioned previously provided data that were important to understanding vessel lower head failure phenomena and were necessary to model this event. Several computer models were developed and validated by the various program partners. In this context, IRSN developed a simplified 2-D computer model and, jointly with CEA, developed a 2-D and a 3-D finite element model using CEA's standard code CAST3M. EDF and FZD[9] each developed a 2-D finite element model using their respective standard codes CODE_ASTER and ANSYS. The French partners used the same creep laws (developed by Sandia for the US vessel steel and by CEA for the French vessel steel), whereas FZD used its own creep law.

The simplified 2-D model based on equations expressing the behavior of shells of revolution subject to an axisymmetric load, describes elongation of the lower head along an egg-shell shape [Koundy and Cormeau, 2005], representing the overall deformation observed on the LHF and OLHF mock-ups (***Figure 3***).

Compared to the finite element models, the simplified 2-D model can be used to quickly test model assumptions: with analytical equations, it is easier to determine the relationship between assumptions and results, and to determine the most important parameters in the problem. The simplified 2-D model is also convenient because it is easy to adjust the grid and data, and calculation time is short. This model is therefore particularly appropriate for performing repetitive parametric calculations, which are fundamental for the development of probabilistic studies. The model was of course

(9) *Forschungszentrum Rossendorf Dresden.*

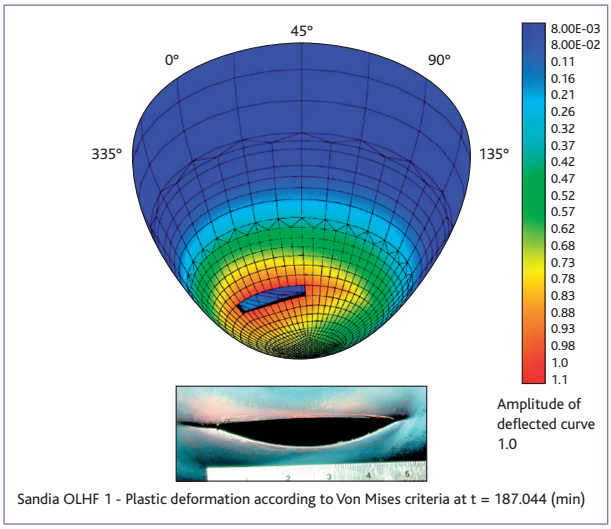

Figure 5 *Overall view of the experimental breach during OLHF Test 1 (14 cm²) and the calculated breach (17.6 cm²).*

limited to calculating the time of lower head failure and the location of the failure zone, and describing the overall behavior of the structure (just before cracking occurred and was propagated geometrically in three dimensions).

The 2-D and 3-D finite element models and the summary on comparison of the experimental results and modeling results from the OLHF 1 lower head test are described in detail in [Koundy et *al.*, 2008a]. Conclusions found that the overall mechanical behavior of the OLHF 1 test was well represented by the 2-D models (simplified model and finite element model), that the experimental and computed deflected curves were consistent, and that the estimated time of failure and the failure zone were in good agreement with the experimental results. Interpretation of the FOREVER EC2 test using the simplified 2-D model and the FZD 2-D finite element model also showed good agreement [Koundy and Hoang, 2008].

For interpretation of the OLHF 1 test, the 3-D finite element model (obtained by CAST3M) produced more detailed calculation results than the other models. It provided local details that were entirely consistent with the experimental results, in particular the zones where lower head thickness was reduced. This 3-D model also made it possible to study initiation of the crack and its propagation. ***Figure 5*** shows the experimental breach and the calculated breach. The areas of both breaches have the same order of magnitude: 14 cm² and 17.6 cm². In this three-dimensional calculation, the selected failure criterion corresponded to a total deformation set to 100% (which means that a small geometric element of the grid was assumed to be failing if its total calculated deformation exceeded this value). The failure elements were then eliminated from the grid and led to a three-dimensional development of the breach.

It should be emphasized that while the failure criterion considered in the 3-D model was appropriate for interpreting the OLHF 1 test, it was not valid for interpreting the LHF program tests. Consequently, during the LHF 5 test, where a very long circumferential tear was observed, the initial failure time and the crack propagation rate calculated by the 3-D model varied noticeably from the experimental results. This was explained by the fact that the failure criterion depends to a great extent on the failure mode of the material ("ductile" for OLHF and "brittle" for LHF). It is therefore necessary to choose a more appropriate failure criterion that takes into account the variability of material failure behavior, which is one of the objectives of the joint research program currently being conducted by IRSN, CEA and Insa Lyon [Koundy et *al.*, 2008b].

Research program to study material tearing on French reactor vessels

This IRSN research program, conducted in close cooperation with CEA and Insa Lyon, began in 2003, just after completion of the OLHF experimental program. Research work has set out to study French PWR vessel materials, with the twofold objective of building up the existing database that characterizes these materials, and applying the results to studying severe accidents on French reactors.

The program consisted in first taking inventory of the physical properties as well as the chemical and metallurgical composition of French PWR vessel materials, in cooperation with Framatome. At the end of this work, five materials (more specifically five families of materials) with sufficiently varied mechanical and metallurgical properties, all compliant with the general manufacturing specification for steel used in French PWR reactor vessels, were selected for testing.

Three types of additional tests were defined and conducted in three centers:

- the CEA Grenoble Center conducted materials characterization tests at high temperature (900°C-1,100°C) using small cylindrical test specimens. These tests were followed by image analysis. The tests aimed to further understanding of what causes the variability in the material failure modes, i.e. to identify the microstructures responsible for this variability.

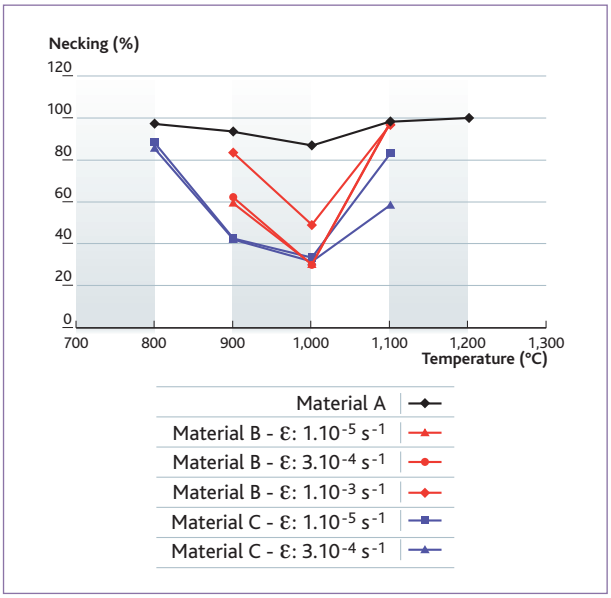

Figure 6 *Necking values observed during the tensile tests, as a function of temperature and strain rate, for three reactor vessel materials A, B, and C (with increasing sulfur concentrations).*

Figure 6 shows that decreases in ductility occurred during tensile tests, defined by the drop in the specimen necking values as a function of temperature and strain rate. The corresponding tests were conducted on three vessel materials, A, B and C, with increasing concentrations of sulfur. The ductility of each material was measured based on these necking values. Material A, for which necking was less than 90%, was the most ductile material. Material C, with the highest sulfur concentration, was the most brittle, showing a necking value of less than 30%. For materials B and C, embrittlement was greatest at around 1,000°C.

Hot embrittlement of the steel is therefore a function of temperature: materials B and C, brittle at 1,000°C, may be ductile at 800°C or 1,100°C. Microscopic observations of the fracture face on material C specimens that failed at 1,000°C show small amounts of aluminum nitride precipitates and large quantities of manganese sulfide precipitates (which are absent or present in very small amounts in the case of material A).

A curve showing necking versus sulfur content is being developed for the five families of selected materials, which will be used to describe the behavior of these materials as a function of their sulfur content. It will then be possible to predict the failure mode (brittle or ductile) based on knowledge of the vessel material and its sulfur content, and to obtain an initial quantification of the probability of having a small or large breach.

■ CEA Saclay conducted high-temperature materials characterization tests with Compact Tension (CT) specimens to assess tear resistance and the crack propagation rate for these materials. These tests are important for failure modeling and serve to study the influence of the material's chemical and metallurgical composition on tearing kinetics. ***Figure 7*** shows the shape of a CT specimen (where F represents the tensile force, δ the opening, and "da" the average progress of the crack across the entire thickness of the sample) and gives the force applied as a function of the opening for materials A and B (two tests for each curve).

A clear difference in behavior between the two materials is observed (material A is more ductile than material B). Based on these curves and using analytical equations, it is possible to obtain curves establishing a relationship between the integral "J[(10)]" and the progress of the crack "da".

Each slope of the curve (J, da) is an "energy parameter Gfr" that serves to evaluate material embrittlement. This method, referred to as the "Gfr method", conveniently transposes data directly from specimens to structures.

This stage of tear characterization is an essential step in developing the new failure criterion. The Gfr parameters resulting from the CT tests will be entered in the 3-D finite element model (obtained with CAST3M). This model will then be validated, first on the same CT tests, and then again on the LHF and OLHF program tests, by determining crack length and breach size, respectively. More analytical tests on tubes (see below) will be interpreted using this 3-D model as soon as the experimental results are available.

■ Insa Lyon is conducting pressurized tear tests on plates and tubes at high temperature in order to determine crack initiation thresholds and propagation rates. The test bench was designed and built jointly by IRSN and Insa Lyon.

The plate tests, considered as preliminary tests, provided the opportunity to finalize the high-temperature electrical and optical measurement systems and to study tearing on plane structures.
Tube tests are currently in progress, and will serve not only to study material tearing, but also to establish the depressurization law required for modeling (internal pressure drop following the first through-wall crack). The pressure values selected for the tube tests are equivalent to the imposed primary pressure (defined to the nearest factor, as in the case of the LHF and OLHF mock-ups), in order to obtain the same local state of stress and deformation in

(10) The integral J represents the potential energy growth rate of the structure.

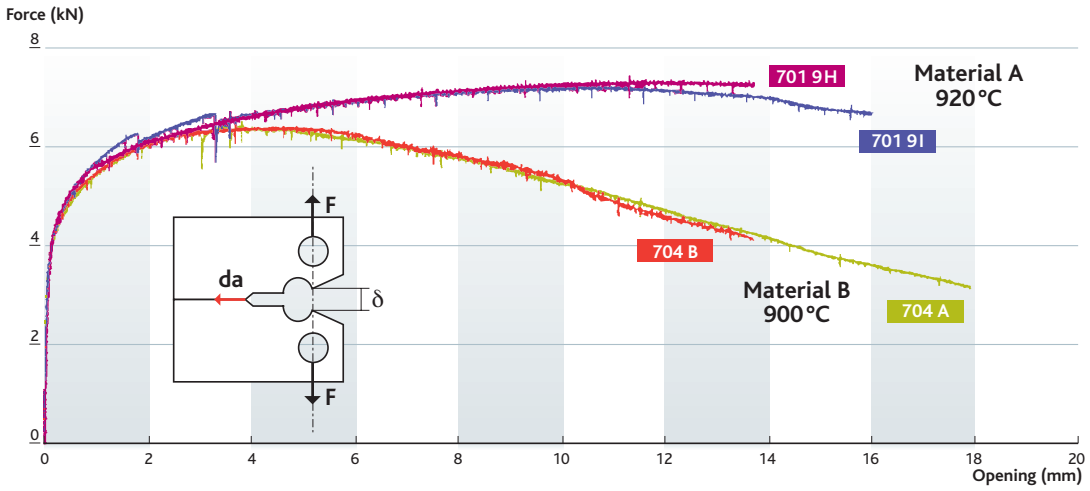

Figure 7 *Curves presenting tensile force F as a function of the opening δ for materials A and B (tests around 900°C, with two tests per curve).*

the tube and in application to reactors. This will avoid the problem of scaling in studying applications for the reactor. These tests will subsequently be used for "structure type" validation of the numerical models.
Four tube tests were performed in 2008, and four others should take place in 2009.

In conjunction with the plate and tube tests, a second 3-D finite element model was jointly developed by IRSN and Insa Lyon using ABAQUS/Standard code (the first model used the CAST3M code). These two models take into account variability of the material failure mode at high temperature and use two different methods to evaluate the final size of the breach.

The first model uses the Gfr method, whereas the second model is based on "cohesive" finite elements. The cohesive finite elements are connection elements placed in advance on the path of the crack and whose nodes are arranged on each side of the lips of the crack. Crack propagation is then verified by a behavior law establishing a relationship between "stress within the element" and "relative displacements of element nodes".

This law can describe both brittle failure behavior and ductile failure behavior, by taking into account the energy deduced from the experimental behavior curve. The model was first used to interpret the CT tests (mentioned above). It is capable of determining cracking under high necking.

Figure 8a shows the final state of the tear and visualizes the different levels of stress intensity. The state was estimated using a second computer model for a CT test.

Figure 8b shows good agreement between the experimental and calculated tensile force curves. The calculation also achieved a good estimate of experimental crack propagation as a function of the crack opening. Model validation continues with simulations of the LHF and OLHF tests and the tube tests.

Conclusion and outlook

To achieve a more accurate assessment of the thermal-mechanical behavior of the lower head on a PWR reactor vessel during a postulated accident with core meltdown and the possible consequences of lower head failure, parameters such as failure time, failure mode, breach location and breach size are essential.

Numerical models (simplified model or finite element model) developed by the various LHF and OLHF program partners (AVN, CEA, GRS, IRSN, SNL, UJV and VTT), can predict the time of failure on the lower head and the breach location. Because it is easy to use, fast, and provides good numerical results, the simplified 2-D model was developed by IRSN as part of the European ASTEC severe accident code.
It should be noted, however, that only a 3-D finite element

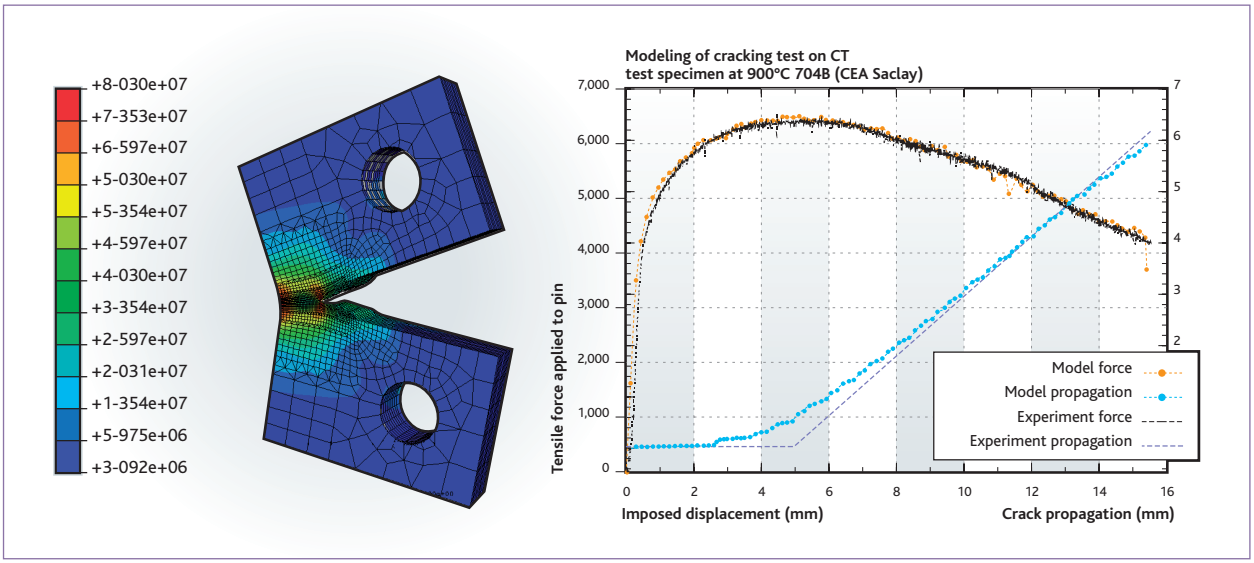

Figure 8 ***a)*** *Simulation of a CT test.* ***b)*** *Comparison of the force/opening and propagation/opening curves.*

model can be used to study a three-dimensional tear in a material. To date, no 3-D finite element model is capable of correctly evaluating the final size of the breach, since size depends to a great extent on the high-temperature failure mode of the vessel materials. The failure criterion used in the models must take into account the variability of material failure behavior (either ductile or hot embrittlement failure).

To improve the failure criterion and more accurately evaluate breach size in various severe accident scenarios, in 2003 IRSN undertook a research program conducted in partnership with CEA and Insa Lyon, concerning tearing on various French reactor vessel materials. Today this program is well advanced, and ultimately aims to:

- characterize material tearing properties at high temperature;
- gain a better understanding of the influence that material chemical composition has on tearing kinetics;
- define a new failure criterion that takes into account the variability of material failure behavior, for both 3-D finite element models developed, in order to assess breach size. These models must first be validated by interpreting the tube failure tests before they are applied to PWR power reactor studies.

References

- T.Y. Chu *et al.* (1998). *Lower Head Failure Experiments and Analyses, NUREG/CR-5582, SAND98-2047, Sandia National Laboratories, Albuquerque, NM, USA.*
- J. Devos *et al.* (1999). *CEA programme to model the failure of the lower head in severe accidents, Nuclear Engineering and Design, Volume 191, p. 3-15.*
- B.R. Sehgal *et al.* (2003). *Assessment of Reactor Vessel Integrity (ARVI), Nuclear Engineering and Design, volume 221, p. 23-53.*
- V. Koundy, I. Cormeau (2005). *Semi-analytical modelling of a PWR lower head failure under severe accident conditions using an axisymetrical shell theory, Nuclear Engineering and Design, volume 235, p. 845-853.*
- V. Koundy *et al.* (2008a). *Progress on PWR lower head failure predictive models, Nuclear Engineering and Design, Volume 238, p. 2,420-2,429.*
- V. Koundy, N.H. Hoang (2008). *Modelling of PWR lower head failure under severe accident loading using improved shells of revolution theory, Nuclear Engineering and Design, Volume 238, p. 2,400-2,410.*
- V. Koundy *et al.* (2008b). *Study of tearing behaviour of a PWR reactor pressure vessel lower head under severe accident loadings, Nuclear Engineering and Design, Volume 238, p. 2,411-2,419.*
- L.L. Humphries *et al.* (2002). *OECD Lower Head Failure Project Final Report, Sandia National Laboratories, Albuquerque, NM 87185-1139, USA.*

4.3

LEVEL 2 PSA FOR 900 MWE PWRs: from development to lessons learned

Emmanuel RAIMOND, Nadia RAHNI, Karine CHEVALIER-JABET, Thomas DURIN
Severe Accident Probabilistic Assessment Unit

Since the accident that occurred on March 28, 1979 on Reactor No. 2 of the Three Mile Island nuclear power plant (TMI-2), resulting in partial core meltdown and limited release of fission products, nuclear safety authorities have implemented research programs to achieve a better understanding of the potential consequences of a severe core meltdown accident and thereby improve applicable prevention or mitigation measures. Such measures may involve the installation of new reactor equipment, or the reinforcement of existing equipment. They may also consist in optimizing operating procedures under accident conditions, or improving severe accident guidelines. Within the framework of its activities, IRSN assesses measures adopted by operators, taking into account the results of severe accident research programs, numerical simulations, and Level 2 probabilistic safety assessments.

This article describes the development by IRSN of a Level 2 Probabilistic Safety Assessment for CPY-series 900 MWe Pressurized Water Reactors (referred to hereafter as the PWR 900 Level 2 PSA study), its articulation with related research programs, the results obtained, and the conclusions to be drawn.

Foreword: progression of a severe accident scenario and the three levels of PSA

In a pressurized water reactor (PWR), a severe accident is defined as an accident causing significant fuel degradation, with a risk of radioactive release outside the facility. Given the design and operating conditions of PWR facilities (***Figure 1***), this type of accident can only result from a highly improbable sequence of equipment failures and human errors.

As an example, various physical phenomena potentially occurring during a severe accident are shown in ***Figure 2***. The different phases of a severe accident and the various possible containment failure modes are briefly presented below. A more complete description of severe accidents is provided in a reference document [IRSN and CEA report, 2006].

If a reactor core remains uncovered for an extended period of time, the fuel temperature rises gradually due to the loss of residual heat removal. The water vapor causes an exothermic oxidation reaction of the Zircaloy fuel cladding, leading to significant hydrogen production and heat release. In addition, metallurgical reactions between the fuel and the cladding produce low-melting-point eutectics, causing relocation of materials within the reactor core. The temperature rise causes the most volatile fission products to be released from the fuel, followed by semi-volatile fission products.

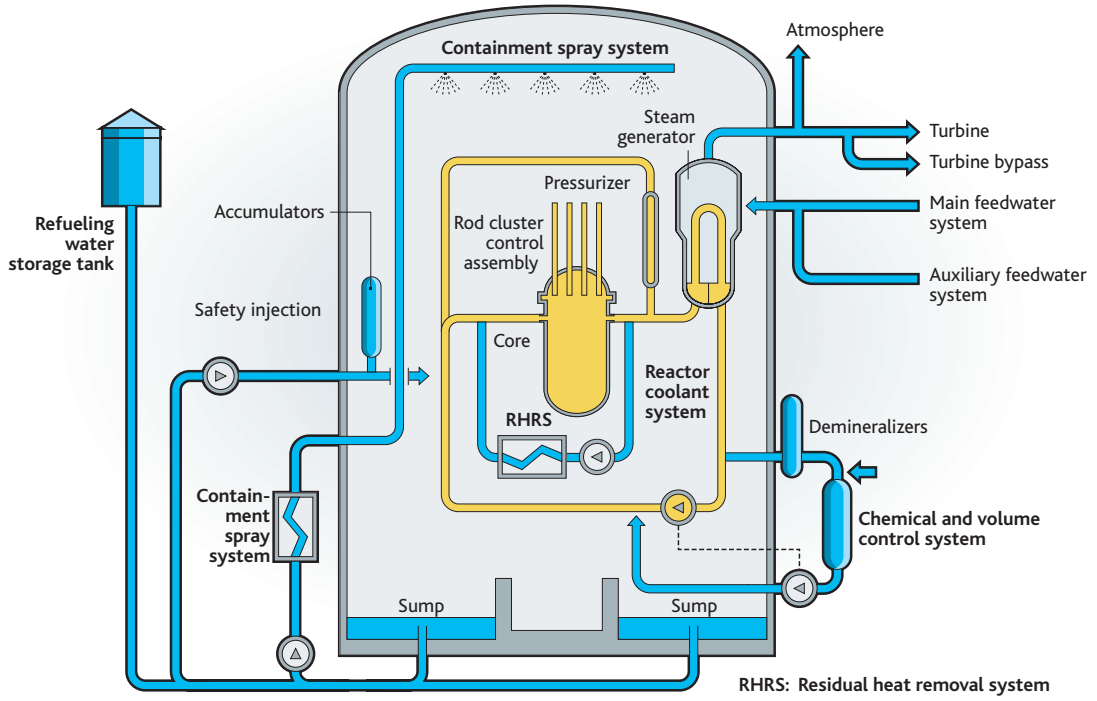

Figure 1 *PWR safeguard systems (schematic diagram).*

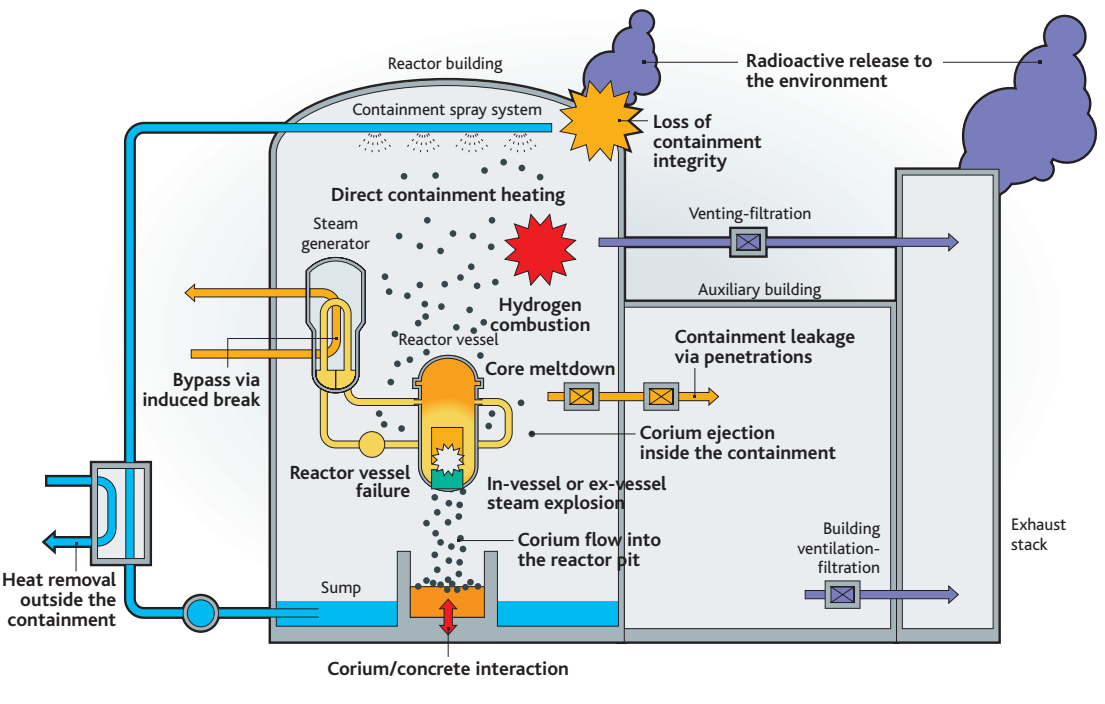

Figure 2 *Physical phenomena potentially occurring during a severe accident.*

A pool of molten materials, referred to as corium, is gradually formed within the reactor core. When the corium comes into contact with the core baffle, it flows through the reinforcements between the core baffle and the core barrel. Upon contact with the water remaining in the vessel lower head, the corium is grossly fragmented, possibly leading to a more violent phenomenon referred to as in-vessel "steam explosion". This type of explosion can cause a lower head failure, and can also eject a fraction of the corium onto the vessel closure head, with a risk of ejected debris reaching the containment.

During core degradation, some makeup systems can be used to inject water into the primary or secondary cooling system. Reflooding a degraded core produces complex phenomena, but can in certain cases stop the accident progression. However, reflooding can also cause an increase in hydrogen production, thereby increasing the associated risk of hydrogen combustion in the containment, and can lead to additional release of fission products.

The temperature of the reactor coolant system walls and steam generator tubes may increase significantly. If this temperature rise is coupled with high pressure in the reactor coolant system, an "induced break" may occur in this system. This break leads to depressurization of the reactor coolant system, contributing positively to the accident progression. Nevertheless, if this break occurs on the steam generator tubes, the reactor core would be connected to the outside *via* the primary and secondary reactor systems, and it would constitute a containment "bypass"; the presence of water in the steam generator secondary system would significantly reduce release outside containment.

The hydrogen produced during core degradation is released in the containment, and its combustion can lead to a pressure and temperature peak potentially compromising containment integrity. This combustion can be slow (slow deflagration), rapid (fast deflagration) or even explosive (detonation).

The molten corium accumulates in the vessel bottom more or less rapidly, leading to a potential vessel lower head failure. In the event of such a failure, particularly under high pressure conditions, part of the corium is dispersed inside the containment, potentially creating a pressure peak due to "direct containment heating" (DCH).

Moreover, in the event of vessel lower head failure, the corium may come into contact with water present in the reactor pit, particularly due to the operation of the containment spray system. The contact of the corium (heated to over 2,500°K) with the water in the reactor pit can cause almost instantaneous vaporization of the water present. This vaporization could lead to a very sudden, localized pressure increase capable of damaging the reactor pit walls or even causing some movements of the internal containment structures, which is referred to as the "ex-vessel steam explosion" phenomenon.

After the lower head failure, the corium flows to the bottom of the reactor pit, where it causes gradual thermal ablation of the concrete basemat, thereby releasing significant quantities of noncondensable gases inside the containment. These gases induce a gradual pressure increase within the containment. In order to prevent a containment failure due to overpressure, a "venting and filtration" system has been installed in PWR units currently in service. These systems are designed to prevent pressure from significantly exceeding the containment design pressure.

During a severe accident, containment leakage may occur through containment penetrations. These leaks may be pre-existing or due to containment isolation failures, and they may also occur in the lines that recirculate water recovered in the containment sump, namely from the containment spray system. They flow into auxiliary buildings, where they are recovered by ventilation systems equipped with various types of filtration devices, and are subsequently released to the environment.

Probabilistic safety assessments (PSAs) are developed to analyze and classify all potential severe accident scenarios as exhaustively as possible. Three levels of assessment are generally used, depending on the impact considered:

- Level 1 PSAs are used to identify accident scenarios involving a sequence of equipment failures and human errors leading to fuel degradation, and to determine the frequency of these scenarios;
- Level 2 PSAs are used to assess the nature, significance and frequency of environmental radioactive releases associated with the core meltdown accident scenarios identified in Level 1 PSAs;
- Level 3 PSAs are used to quantify the economic, human health and environmental consequences.

IRSN conducts Level 1 and Level 2 PSAs.

Structure of the PWR 900 Level 2 PSA study

Interface with Level 1 PSA

The first step of the Level 2 PSA is to establish an interface with the Level 1 PSA with a view to satisfying the following objectives:

- ensuring, for each level 1 PSA scenario, the transmittal of reactor status datas, which have a significant impact on the subsequent

progression of the accident, particularly in terms of potential containment failure modes and the amount of radioactive release;

- grouping the several thousand accident scenarios in the Level 1 PSA study in a limited number of plant damage states (PDS), on the basis of accident sequences deemed "equivalent" in terms of progression after fuel damage.

In practice, for the purpose of the PWR 900 Level 2 PSA study, a little over 300 PDS were defined from the Level 1 PSA accident scenarios leading to core damage (for in-power and shutdown reactor states).

"Severe accident" event tree

The approach adopted by IRSN for the PWR 900 Level 2 PSA study aims to construct an "event tree" accurately representing the various events that condition the progression of an accident until the radioactive release phase, including the potential physical phenomena and their dependencies, human actions, system failures, and system repairs.

The resulting event tree is then used to identify the various possible accident sequences for each PDS, including any containment failures, and to estimate the corresponding annual frequencies. Detailed models based on a large number of supporting studies are developed within the event tree to determine the sequence of significant events (lower head failure, basemat penetration, loss of containment integrity, etc.) and facility conditions (reactor coolant system pressure, composition of containment atmosphere, etc.) during accident progression.

The PWR 900 Level 2 PSA study conducted by IRSN comprises a sequence of approximately 100 events (physical phenomena, human actions, system failures or restarts), requiring the probabilistic quantification of several thousand accident scenarios. In addition, a Monte Carlo algorithm is used to quantify uncertainties.

The methods used are described in detail in various reference documents [Raimond et *al.*, 2004; Charpin et *al.*, 2005; Raimond et *al.*, 2005; Raimond et *al.*, 2006; Villermain et *al.*, 2008; Raimond et *al.*, 2008].

Radioactive release categories

The various accident sequences are then grouped into a number of "accident scenarios families". This classification is based on variables (referred to as "accident scenario family" variables) indicating the magnitude and kinetics of the radioactive releases associated with the accident scenarios, the variable values being determined using the event tree.

A calculation of radioactive releases is then performed for each accident scenario family.

These various steps (event tree construction, quantification and classification of accident scenarios, calculation of radioactive releases) are carried out using the KANT software tool developed by IRSN, in combination with a specific radioactive release calculation tool.

Physical studies to support the PWR 900 Level 2 PSA study and results from R&D programs

The development of the PWR 900 Level 2 PSA study involved significant work in terms of the analysis of accident scenarios, and the use of results from numerous test programs.

Accident progression

The Level 1 PSA study identified a large number of accident scenarios up to the core meltdown phase. The number of post-meltdown scenarios to be analyzed increases significantly when the following are taken into consideration: success or failure of operator actions, system failures or restarts. IRSN considers that the findings from a Level 2 PSA study are more robust when the event tree is based on a sufficient number of calculated accident scenarios. In the case of the PWR 900 Level 2 PSA study, the ASTEC code (1) was used to calculate approximately 100 accident scenarios for at-power conditions, and approximately 40 scenarios for shutdown conditions.

IRSN also considers that by including models of actual physical phenomena in the event tree, it is possible to obtain a description of the facility's physical state as the accident progresses. Dependency between phenomena and the associated uncertainty are also more easily determined.

The development of these models is largely based on the use of computer codes. A specific method based on experimental design and response surface techniques is used for certain event tree models. The results of international R&D programs devoted to severe accidents are also used extensively to validate and supplement the results obtained. IRSN has implemented specific methods for certain analyses (e.g. mechanical strength of reactor coolant system under high-pressure and high-temperature conditions). A few examples are shown in ***Table 1***.

(1) ASTEC (Accident Source Term Evaluation Code): computer code for severe nuclear reactor accident analysis, developed by IRSN and its German counterpart GRS.

Containment strength

Containment structures on 900 MWe reactors consist of a pre-stressed concrete wall with an internal metal liner ensuring leak integrity. These structures are designed for a pressure of about 5 bar absolute. Their design pressure resistance is periodically verified by the operator during "periodic tests". The leak rate measured during these tests must not exceed a value derived from a regulatory requirement specified in the construction license for the corresponding facility.

During a severe accident, the containment structure may be subjected to pressures exceeding the design pressure due to the occurrence of an energy phenomenon (hydrogen or carbon monoxide combustion, direct containment heating). To limit the risks associated with combustion reactions, passive autocatalytic hydrogen recombiners are installed inside the containment. In addition, a manually operated venting system (the "U5" system) may be used in the case of slow containment pressurization, so as to limit containment pressure to a value between the design pressure and the ultimate pressure capacity of the containment, while keeping radioactive release to a minimum by means of the filtration feature included in this system.

In order to conduct a Level 2 PSA study, it is necessary to assess the containment pressure capacity beyond the design pressure. This is only possible using numerical simulation tools. For example, IRSN used the CAST3M code, combined with specific models, to describe the behavior of the containment concrete, metal liner, equipment hatch, reinforcements and prestressing tendons. The models used were improved to perform 3D calculation of an entire containment structure [Nahas and Cirée, 2007]. This "multiscale" approach is illustrated in ***Figure 3***.

These studies identified two possible containment failure modes:

- shear failure of the equipment hatch fastening bolts;
- liner tearing in the straight portion of the containment.

The "realistic" pressure values obtained for these two failure modes (7 and 10 bar absolute, respectively) led IRSN to consider the equipment hatch as the weakest point of the containment (under pressure conditions exceeding the design pressure). EDF agrees with this conclusion and has undertaken to reinforce the equipment hatch closure system during the third ten-yearly inspection of 900 MWe reactor units.

In the PWR 900 Level 2 PSA study, it was assumed that a liner tear or equipment hatch closure failure would lead to a containment failure with a very high containment leak rate. Fragility curves taking into account containment capacity uncertainty were developed to estimate the conditional failure probability for each stress level (***Figure 4***), depending on whether or not the equipment hatch was reinforced (both cases will coexist for approximately 10 years, given the ten-yearly inspection schedule)(2).

Phenomenon	Analysis method
Thermohydraulic phenomena (before fuel degradation)	CATHARE 2 code and SIPA2 simulator
In-vessel core degradation	ASTEC code (CESAR-DIVA)
Modification of the composition of the atmosphere inside the containment	ASTEC code (CPA)
Core meltdown under pressure and induced steam generator tube rupture	ICARE-CATHARE code and the results of an R&D program focused on the mechanical strength of the reactor coolant system
Reactor vessel failure	Development and use of a specific model
Corium ejection inside the containment during direct containment heating (DCH)	Development and use of a specific model suited for the 900 MWe PWR geometry and implemented in the ASTEC code; use of specific R&D programs
Steam explosion in the reactor vessel and reactor pit	MC3D code (steam explosion code) coupled with the EUROPLEXUS code (mechanical code)
Thermal erosion of the basemat	ASTEC code (MEDICIS)
Hydrogen or carbon monoxide combustion during interaction between corium and basemat concrete	Development of a specific model in the event tree based on results obtained using the ASTEC code
Slow containment pressurization (with or without reflood) during the corium/concrete interaction phase	Use of ASTEC code

Table 1 *Methods adopted for the analysis of certain physical phenomena.*

The PWR 900 Level 2 PSA study was also quantified (in a sensitivity analysis), assuming that failure of at least one penetration (other than the equipment hatch penetration) is inevitable if the containment pressure temporarily exceeds 6 bar. This value of 6 bar corresponds to a mechanical strength requirement for containment equipment and structures formulated in EDF's draft "guidelines for severe accidents".

Radioactive releases and radiological impact

As mentioned earlier, a Level 2 PSA study involves calculating the release of radioactive substances to the environment for each "accident scenario family".

(2) CPY-series reactors were commissioned in France between 1980 and 1987.

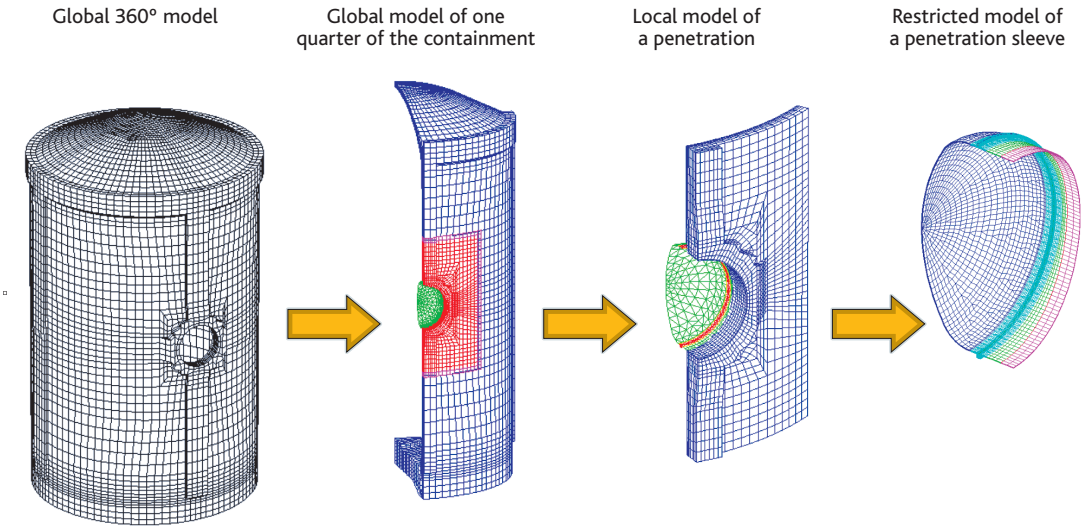

Figure 3 *"Multiscale" modeling of a CPY-series containment vessel.*

IRSN has developed a computer code for this purpose, used to calculate the release of radioactive substances from the reactor core into the containment vessel, the behavior of these substances within the containment, and potential releases to the environment. Four groups of radioactive substances are considered (noble gases, molecular iodine, organic iodine, aerosols). For each group, the released activity is estimated using models developed on the basis of results from research programs such as PHÉBUS and VERCORS. These models will be subsequently updated once the results of the International Source Term program (ISTP), coordinated by IRSN, become available.

The amplitude of the radiological impact associated with the "accident scenarios families" considered in the Level 2 PSA study was assessed, supposing some meteorological standard conditions. This assessment was performed using tools developed by IRSN for the emergency response center. The results obtained provide a better classification of the scenarios considered.

Results of the PWR 900 Level 2 PSA study

Containment failure mode

Given the number of degraded states of the facility considered and the fineness of the event tree constructed, the PWR 900 Level 2 PSA study involved several thousand "accident scenarios families". To facilitate the presentation and analysis of results, these families were classified into approximately 20 situations, referred to as "grouped accident scenarios families", where the distinguishing factor is the associated containment failure mode(s).

Figure 5 shows the average calculated frequency of containment failure (per year and per reactor, taking into account the first containment failure mode[3], for at-power and shutdown conditions (assuming the equipment hatch has been reinforced).

A few details regarding the failure modes considered are described below:

- "successful reflood and containment integrity maintained" scenarios correspond to situations where the accident sequence has been stopped in-vessel (or ex-vessel without basemat penetration or any other containment failure). These scenarios nevertheless result in (limited) release to the environment due to the "normal" containment leak rate;
- the initiating events consisting of "initial SGTR" and "V-LOCA" (containment bypass by a line connected to the reactor cooling system) are specific to at-power conditions;
- the frequency of the initiating events leading to a V-LOCA scenario significantly exceeds that of the other initiating events considered, due to a specific core melt sequence (with reactor coolant pump thermal barrier leakage). It should be noted that as part of the safety review associated with the third ten-year inspection of

(3) A large number of Level 2 PSA scenarios result in multiple containment failure modes. For example, in a core meltdown scenario involving a small leak in a containment penetration leading to release, as pressure rises, it may also be necessary to open the controlled and filtered containment venting system through the U5 procedure.

this reactor series, the standing group for reactor surveillance has recommended that EDF define and implement specific measures to reduce the frequency of this scenario;

- under shutdown conditions, "heterogeneous dilution" initiating events are characterized by a relatively high frequency, also due to a specific sequence;
- "line break" scenarios correspond to situations with ex-vessel leakage *via* penetrations connected to the reactor coolant system or via containment sump water recirculation. Unlike the case of V-LOCA scenarios, this type of leakage occurs during the accident and is not considered as an initiating event;
- "non-closure of equipment hatch" scenarios are specific to maintenance outage conditions and include cases of unsuccessful closure of penetrations opened for maintenance operations (equipment hatch, personnel air lock, etc.);
- "post-reflood hydrogen combustion" scenarios correspond to cases where borated water is injected into the reactor coolant system during in-vessel core degradation, with an increase in hydrogen generation due to Zircaloy oxidation (not compensated by the recombiners) and with containment failure subsequent to hydrogen combustion;
- "ex-vessel steam explosion" scenarios correspond to situations leading to loss of containment integrity after a steam explosion in the reactor pit;
- "isolation valve failure" scenarios correspond to a loss of integrity on a containment penetration isolation valve due to containment pressure, temperature, and radiation conditions during a severe accident.

Influence of ultimate pressure capacity values considered for the containment

Sensitivity analyses were conducted for the containment ultimate pressure capacity values considered (i.e. assuming a non-reinforced equipment hatch, or highly pessimistic assumptions on penetration failure under pressure conditions exceeding 6 bar absolute). The results obtained show that these assumptions have a significant impact on the frequency of the following containment failure modes (***Figure 6***):

- containment failure due to hydrogen combustion after degraded core reflood (quite logically, the lower the ultimate pressure capacity, the higher the probability of occurrence);
- slow containment pressurization during in-vessel core degradation, and no-successful opening of the U5 venting and filtration system less than 24 hours after the beginning of fuel degradation (formally, the severe accident guidelines recommend waiting more than 24 hours). It should be noted that emergency response teams would probably recommend opening the system earlier (this is not taken into consideration in the PWR 900 Level 2 PSA study).

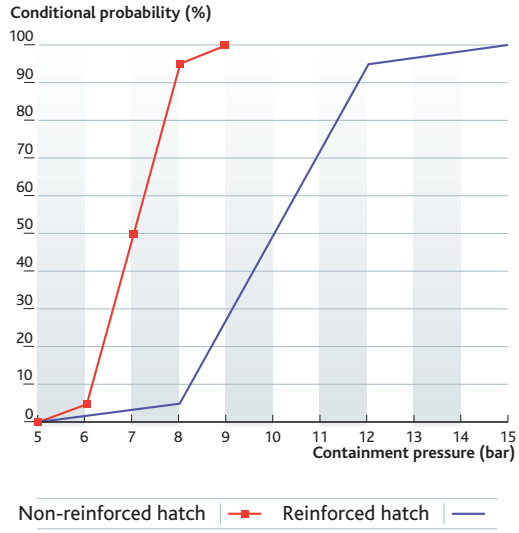

Figure 4 *Probability of containment failure as a function of pressure.*

Prioritization of accident situations

As explained earlier, the PWR 900 Level 2 PSA study includes an assessment of radioactive releases and the associated impact for each accident sequence family considered. Frequency/impact pairs are then used to classify the various scenarios. Particular focus is placed on the scenarios associated with the highest frequencies and the most severe impact.

Figure 7 shows the distribution of the "accident sequence families" identified in the Level 2 PSA study in a frequency/impact diagram. The IAEA's International Nuclear Event Scale (Ines) has been used to position the accident scenarios in a qualitative manner with respect to their impact.

Families 1 to 5 are characterized by the release of a significant quantity of fission products in aerosol form (particularly cesium-137, which causes long-term environmental contamination). For these accident families, the magnitude of the environmental impact mainly depends on the aerosol fraction deposited in the containment vessel or in the auxiliary buildings.

In the case of families 8 and 9, most of the aerosols would remain trapped in the containment and only fission products in gaseous form would be released to the environment, i.e. noble gases and iodine for family 8. Families 6 and 7 show intermediate characteristics, where the accident impact is of the same order of magnitude as the quantity of fission products released in aerosol or gaseous form.

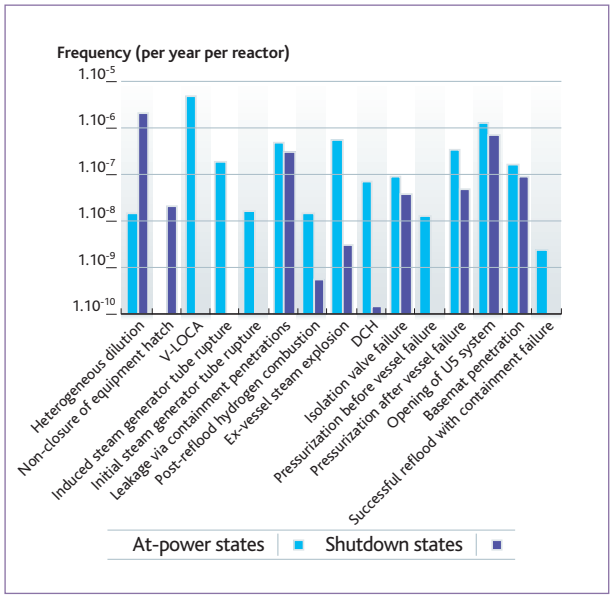

Figure 5 *Average frequency of containment failure scenarios.*

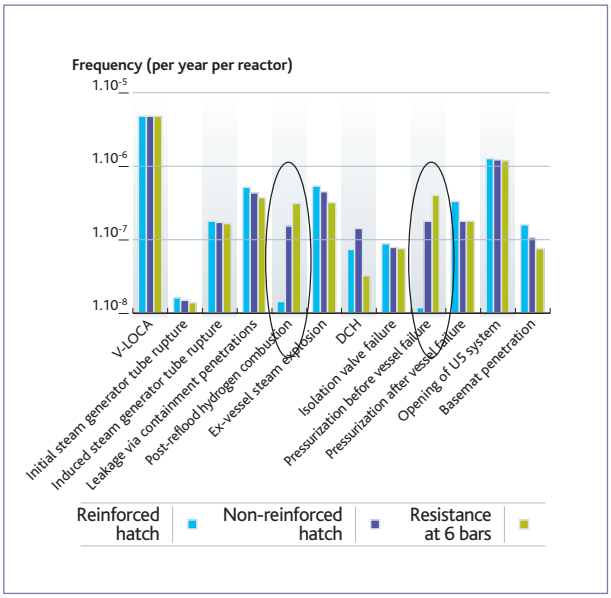

Figure 6 *Influence of ultimate pressure capability values.*

Findings from the PWR 900 Level 2 PSA study

The PWR 900 Level 2 PSA study is an important tool for IRSN. It should be recalled that, in France, reference PSAs are established by the operator (according to the Basic Safety Rule issued by the ASN, the French nuclear safety authority).
IRSN is developing its own studies to facilitate analysis of the results and conclusions of studies conducted by the operator. The PWR 900 Level 2 PSA study was conducted primarily for this purpose.

It is therefore intended to contribute to a continuous facility improvement approach. The results obtained are used to identify relatively weak points in facilities, or specific issues for which additional knowledge may be required. A few examples are described below:

- the calculated frequency of the heterogeneous dilution sequence seems high, considering the associated impact. Since this frequency is mainly due to a specific scenario identified by IRSN (heat exchanger leakage), analysis of this scenario should be actively pursued;
- the calculated frequency of the loss-of-containment-integrity sequence after a steam explosion in the reactor pit also seems relatively high. This issue is currently the subject of technical discussions with EDF. Additional studies regarding induced loads and containment strength under this type of loading seem to be necessary. In addition, the presence of water in the reactor pit and its favorable effect on cooling the corium after vessel failure and preventing basemat penetration should also be considered;
- the study indicates a risk of containment failure due to hydrogen combustion after in-vessel water injection. The calculated frequency of this type of scenario is low, due to the precautions already taken by the operator (prohibition of low-flow water injection at the beginning of core degradation). Nevertheless, IRSN considers that the actions recommended in the severe accident guidelines could and should be optimized [Raimond and Laurent, 2007];
- certain sequences correspond to core-meltdown-under-pressure scenarios, with risk of containment bypass in the case of steam generator tube rupture, despite the implementation of specific control measures to depressurize the reactor coolant system before (or during, at the latest) core degradation. These sequences will be reexamined in detail in more in-depth studies;
- sequences potentially leading to the opening of the U5 system less than 24 hours prior to the beginning of core degradation will be reexamined in detail;
- the study shows the importance of the ultimate pressure capacity of the containment (i.e. beyond the initial design pressure) and recalls the importance of maintaining containment structures in good condition. It also shows the relevance of making changes to reinforce containment structures beyond their initial design strength (reinforced equipment hatch).

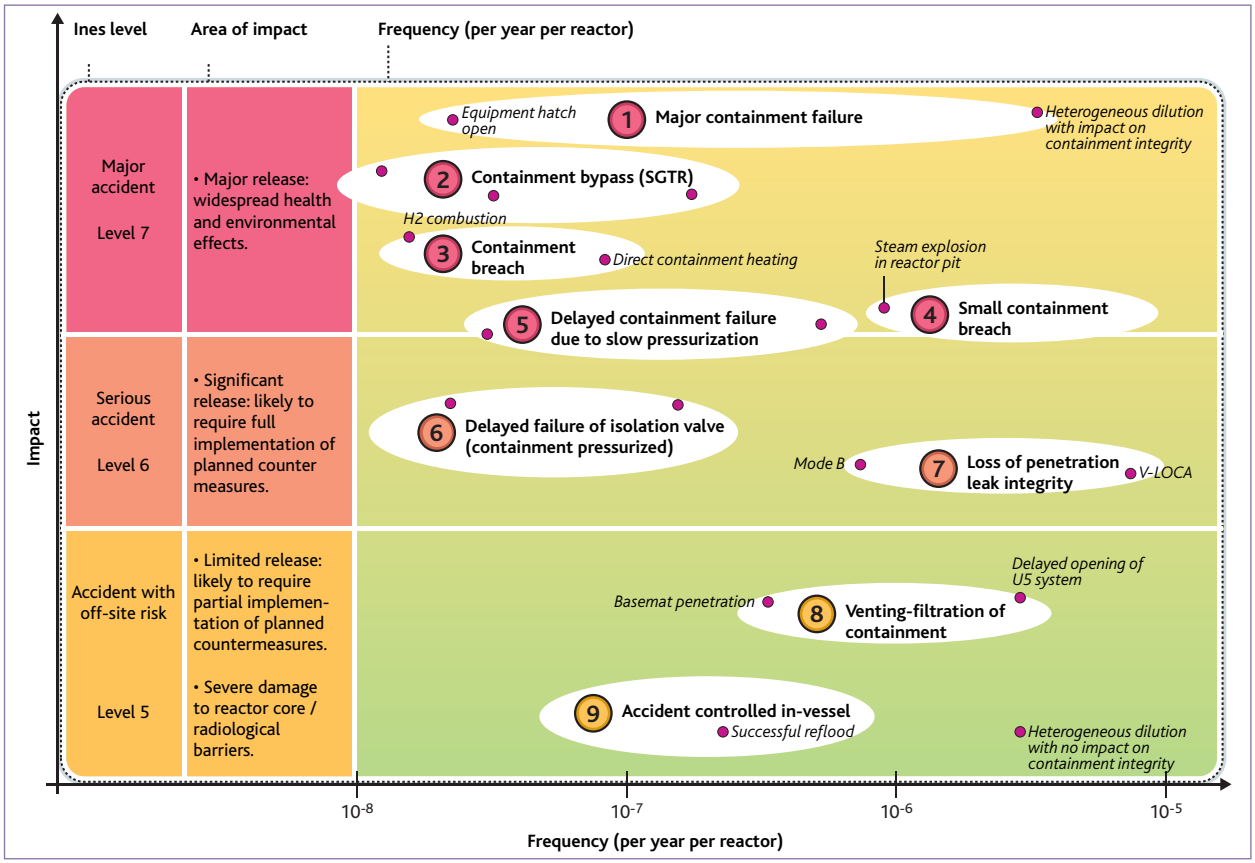

Figure 7 *Frequency-impact diagram*

Generally speaking, the PWR 900 Level 2 PSA study and the associated supporting studies provided a vast amount of knowledge on the potential consequences of a severe accident on a 900 MWe reactor. This knowledge was established using state-of-the-art R&D techniques and numerical simulation tools. It has improved communication with EDF on these very complex issues.

Nonetheless, although this type of study provides essential insight and information, the numerical simulation results must be considered with great caution. A thorough understanding of the models used and their limitations (particularly considering the available validation data) is indeed necessary in order to properly interpret these results.

Conclusion and outlook

The version of the PWR 900 Level 2 PSA study discussed in this article was developed during the period from 2004 to 2008. The results obtained reflect the approach adopted by IRSN engineers on the basis of the experimental results and simulation tools available during this period.

Certain aspects are still currently being addressed in research programs (identification of radioactive releases, steam explosion, impact of reflooding a degraded core, risk of hydrogen combustion in case of in-vessel water injection, etc.). The outcome of some of these research efforts could subsequently modify the results of the PWR 900 Level 2 PSA study. IRSN plans to develop an equally detailed study on 1,300 MWe reactors, before preparation of the third series of ten-yearly inspections for these reactors (scheduled to begin in 2010), followed by development of a specific study for the EPR plant.

References

- ASN – Règle fondamentale de sûreté n° 2002-01 – Développement et utilisation des études probabilistes de sûreté pour les réacteurs nucléaires à eau sous pression.
- F. Charpin, E. Raimond, B. Chaumont, Petten (2005). *Technical basis for off-site emergency planning in France, Seminar on Emergency & Risk Zoning around Nuclear Power Plants, The Netherlands.*
- G. Nahas, B. Cirée. IRSN – Rapport scientifique et technique 2007 – Analyse du comportement mécanique des enceintes de confinement des REP 900 MWe CPY en conditions d'accident grave.
- E. Raimond, C. Caroli, B. Chaumont (2004). *Status of IRSN level 2 PSA, CSNI/WG Risk, workshop level 2 PSA and severe accident management, Koln, Germany.*
- E. Raimond, R. Meignen, J. Dupas, D. Plassard, B. Laurent (2004). *Advanced modelling and response surface method for physical models of level 2 PSA event tree, CSNI/WG risk, workshop level 2 PSA and severe accident management, Koln, Germany.*
- E. Raimond, N. Rahni, M. Villermain (2005). *Method implemented by the IRSN for the evaluation of uncertainties in level 2 PSA. Some examples, Workshop on evaluation of uncertainties in relation to severe accidents and level 2 PSA, Cadarache, France.*
- E. Raimond, K. Chevalier, F. Pichereau (2006). *Link between Level 2 PSA and off-site emergency preparedness, PSAM8, New Orleans, USA.*
- E. Raimond, B. Laurent. IRSN – Rapport scientifique et technique 2007 – Application des EPS de niveau 2 et des techniques de fiabilité dynamique à la validation des guides d'intervention en cas d'accident grave.
- E. Raimond, T. Durin, B. Laurent, K. Chevalier-Jabet (2008). *L2 PSA: a dynamic event tree approach to validate PWR severe accident management guidelines, PSA2008, Knoxville, USA.*
- Rapport IRSN et CEA (2006). R&D relative aux accidents graves dans les réacteurs à eau pressurisée : bilan et perspectives (rapport IRSN 2006-73 rév. 1 – rapport CEA 2006/474). *Research and development with regard to severe accidents in pressurized water reactors: Summary and outlook* – Rapport IRSN-2007-83.
- M. Villermain, E. Raimond, K. Chevalier, N. Rahni, B. Laurent (Mai 2008). *Method for Examination of Accidental Sequences with Multiple Containment Failure Modes in the French 900 MWe PWR Level 2 PSA, PSAM9, Hong-Kong.*

4.4

EFFECTS OF LOCAL GEOLOGY ON SEISMIC MOTIONS: site-specific estimation of the seismic hazard

Luis Fabián BONILLA, Stéphane NECHTSCHEIN, Céline GELIS, Sylvette BONNEFOY-CLAUDET, David BAUMONT
Seismic Risk and Facility Safety Assessment Unit

The assessment of the seismic hazard at a given site consists of estimating the ground motion that could result from an earthquake affecting the site. Motion of this type observed on the surface results from a combination of the action of the seismic source, which generates seismic waves, the propagation of these waves between the source and the site, and the local geologic conditions at the site (*Figure 1*).

In the frequency domain (Fourier spectrum), the mathematical representation of a seismic ground motion i recorded at a station j, $O_{ij}(f)$, corresponds to the following product (***Equation 1***):

$$O_{ij}(f) = S_i(f)\, P_{ij}(f)\, F_j(f)\, I_j(f)$$

where $S_i(f)$, $P_{ij}(f)$, $F_j(f)$, and $I_j(f)$ are terms respectively representing the seismic source i, the propagation effects j, the site conditions beneath station j, and the instrumental response of the seismometer at station j. This mathematical operation is called a convolution. The motion can be assessed in terms of the displacement, velocity, or acceleration of the ground during the earthquake.

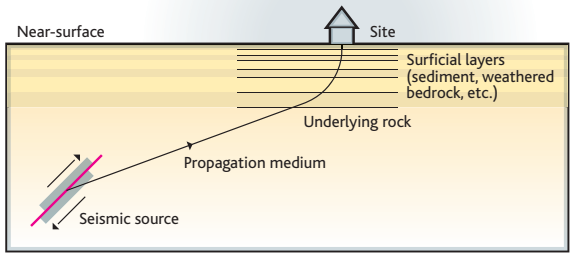

Figure 1 *Diagram of the propagation of seismic waves from the seismic source where they are generated to the study site where they are observed. The local site conditions are characterized by the presence of surficial layers whose geotechnical properties are different from those of the underlying rocks (modified after [Kramer, 1996]).*

This article illustrates the need to consider local geologic conditions when estimating the seismic motion at a given site (site or site-specific estimate). This term is also referred to as the site effect, the site's response, or the site's transfer function.

Definition of a site effect

A site effect is a modification of the seismic motion produced by the local geology. The study of site effects is now one of the most important aspects of earthquake engineering. Analysis of seismic recordings highlights the fact that local geology has a strong influence on the spatial variation of the seismic motion. The material damage and casualties caused by earthquakes are often the direct results of local site effects. Accordingly, any attempt at seismic zoning must include a detailed consideration of site effects.

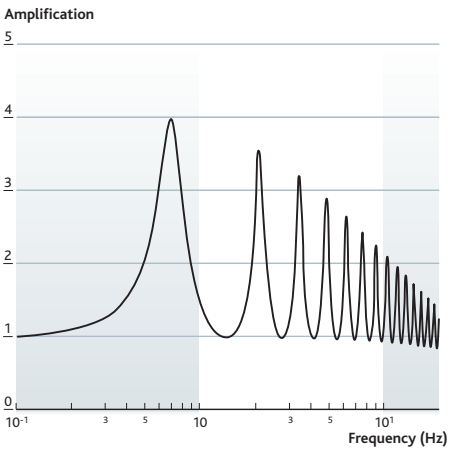

Figure 2 *Amplification as a function of frequency (|F(f)|) for a unidimensional model of a ground layer overlying a half-space.*

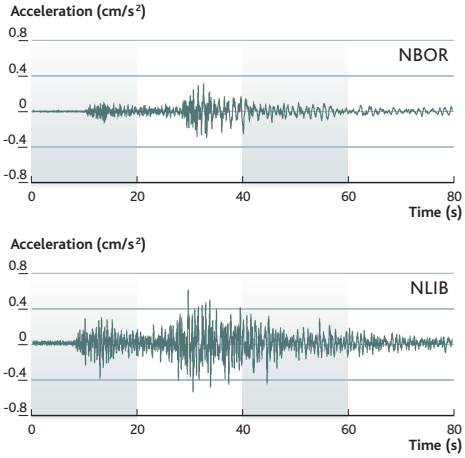

Figure 3 *Accelerograms (east-west components) recorded at the NBOR (bedrock) and NLIB (sediment) stations, located 2 km apart at Nice. These recordings correspond to a magnitude-5 seismic event on Aug. 21, 2000, located at an epicentral distance of 158 km (in northern Italy).*

For a one-dimensional model consisting of a layer of ground of thickness H overlying a half-space, the term F(*f*) has an analytic solution [Kramer, 1996]:

$$F(f) = \frac{1}{\cos(\kappa_s^* H) + \zeta^* i \sin(\kappa_s^* H)}$$

where κ_s^* is the number of waves and ζ^* is the impedance contrast. These two terms are defined as follows:

$$\kappa^* = 2\pi f \sqrt{\frac{\rho}{G}}$$

$$\zeta^* = \frac{\kappa_s^* G_s^*}{\kappa_r^* G_r^*}$$

$$G^* = G(1 + 2i\xi)$$

where ρ is density, ξ is damping, G is the shear modulus, and the indices s and r respectively identify the ground layer and the half-space. The shear modulus G is equal to the product $\rho\beta^2$, β being the velocity of the shear waves. Although the term F(*f*) is a complex number, the site effect is usually represented by its modulus |F(*f*)| which shows the amplification as a function of frequency (***Figure 2***).

Investigation of the term |F(*f*)| shows that an increase in the velocity contrast between the ground and the half-space is expressed by an increase in the amplification. This term reaches its maximum at the resonant frequency, defined by:

$$f = \frac{\beta}{4H}$$

However, estimating the resonant frequency is not enough to define the site effect. As shown in ***Figure 2***, the site's response is a broadband phenomenon.

Influence of site effect on seismic motion

The site effect is described by the transfer function in the frequency domain. In the time domain, it is expressed by an increase in the amplitude and duration of the seismic signals. ***Figure 3*** shows the effect of local geologic conditions on seismic motion by comparing the recording on bedrock (Station NBOR) and the recording on sediments (Station NLIB, located about 2 km from NBOR) of a magnitude-5 earthquake located at an epicentral distance of 158 km. Note that the signal recorded on sediments has a higher amplitude and a longer duration than the one recorded on bedrock. The site effects can be intensified by the presence of positive and negative relief (media that are heterogeneous in two dimensions, or even in three) affecting the propagation of the seismic waves.

What impact do site effects have on buildings? Each building has its own resonant frequency. It is therefore essential to determine whether the local geology might induce resonance effects at a frequency close to that of a structure's resonant frequency, as happened during the 1985 earthquake in Michoacán, Mexico. In that case, although the epicenter of the earthquake

was located some 400 km from Mexico City, a large number of eight- to twelve-story buildings in the city collapsed, because their resonant frequency was close to that of the Mexico City Basin. The sedimentary fill in this basin amplified the 0.5-Hz seismic ground motion up to forty times, compared with the motion recorded on the surrounding bedrock [Singh et *al.*, 1988]. This tragedy marked the beginning of the modern study of site effects.

Estimating the site effect

The analytical approach described in the preceding section is valid only for a unidimensional geometry consisting of a single layer overlying a half-space, a situation very rarely encountered in nature. In more complex real cases (one-dimensional geometry with several layers, and two- or even three-dimensional configurations), no analytical solutions exist. It therefore becomes necessary to employ numerical solutions to assess the site effects. For this type of solution it is essential to create a model of the geologic structure. The site effects can also be estimated empirically, for any type of geometric configuration, by using earthquake recordings.

Work by [Borcherdt, 1970] and [Hartzell, 1992] shows that with a pair of seismometer stations, one installed on sediments and the other on bedrock, the amplification produced by the sedimentary layers is obtained by calculating the ratio between the Fourier spectra of signals recorded simultaneously on the sediments and on the bedrock. This empirical technique for the estimation of site effects is based on the assumption that the seismic motion on the bedrock comes directly from the source, without being modified by the sediments.

For this reason the bedrock seismometer station is called the "reference station". ***Equation 1*** represents the Fourier spectrum of a seismic signal. For the same seismic source, the ratio of the signal at a given site to that at the reference station makes it possible to eliminate the term identifying the source, $S(f)$. Moreover, if the distance between the sediment station and the reference station is small in comparison to their distances from the hypocenter (focus), the propagation effects between the seismic source and each station, represented by the term $P(f)$, are also canceled. Since the bedrock station is the reference station, its site term $F_r(f)$ is equal to 1. Lastly, the spectral ratio is proportional to the site term $F_s(f)$ for the sediments.

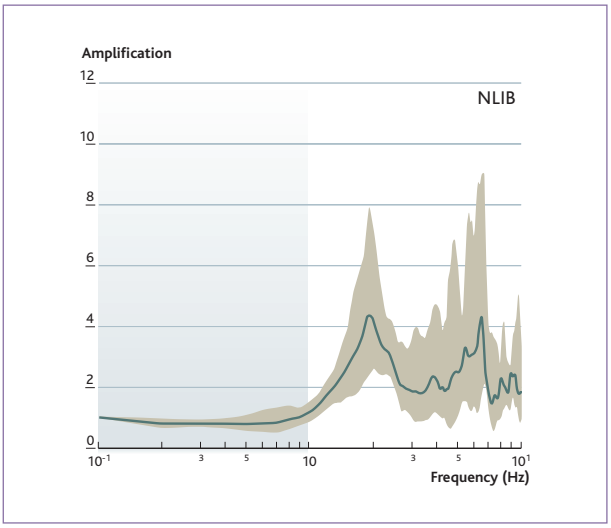

Figure 4 *Empirical transfer function for the NLIB station (a station in the permanent RAP accelerometer network, at Nice). The green line represents the mean function and the beige area indicates the 68% confidence limits. The reference station is NBOR.*

For a particular site, and for each earthquake, the recordings at the seismometer stations (sediments and reference) allow this ratio to be determined. Since the direction and distance of the foci of the seismic sources vary, the site effect for the sediment station is estimated by calculating the geometric mean of these ratios. ***Figure 4*** is an example showing the mean and 68% confidence limits (+/- one standard deviation) of an empirically-calculated transfer function. The advantage of this empirical calculation is that the result contains information from the various sources, and thus on the complexity of the propagating medium in two- or even three- dimensions.

The method described above is one of the simplest and most reliable for estimating the site effect [Hartzell, 1992; Bonilla et *al.*, 1997]. However, it is expensive because it requires the installation of a significant number of seismometer stations, over a long period of time, so as to be able to record a large number of earthquakes. For this reason another technique, based on the analysis of ambient noise, was developed in the early 1980s and has been in common use for the last ten years, especially in Europe and Japan [Bonnefoy-Claudet et *al.*, 2006]. This technique consists of presenting, by frequency, the ratio of the Fourier transform moduli of the horizontal and vertical components of the ambient noise (H/V spectral ratios).

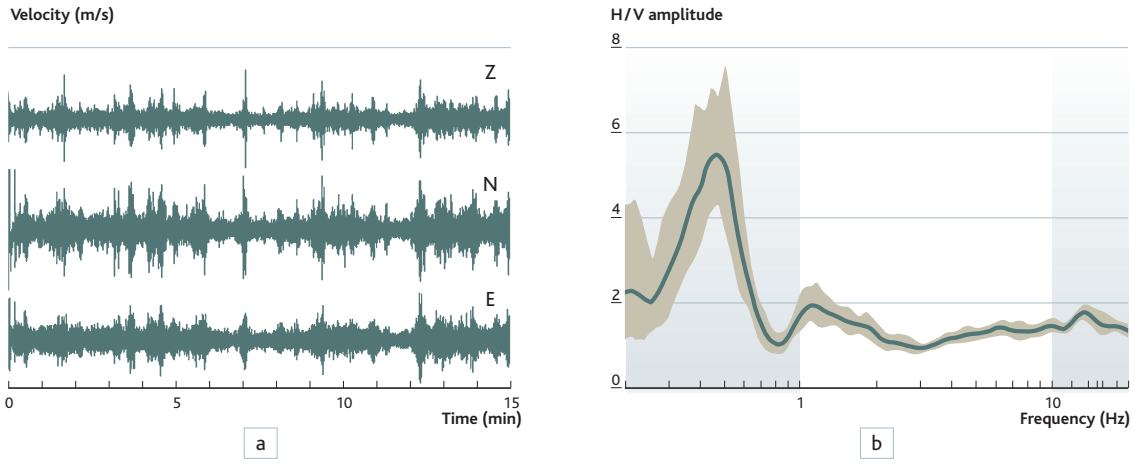

Figure 5 ***a)*** *Example of a recording of ambient vibrations – vertical (Z), north-south (N), and east-west (E) components.* ***b)*** *H/V ratio calculated from the recordings shown in (a). The green line represents the mean ratio and the beige area indicates the 68% confidence limits. After* [*Bonnefoy-Claudet et al., 2008a*].

Figure 5 shows an example of an ambient-noise recording and H/V spectral ratios obtained during a survey in Chile [Bonnefoy-Claudet et *al.*, 2008a]. The frequency of the main peak generally corresponds to the site's resonant frequency. Although the principle of the H/V method is simple, its theoretical foundation is not fully accepted by the scientific community. Based on explanations that are more qualitative than quantitative, [Nakamura, 1989] concluded that the peak observed on the H/V curve is due to the resonance of SH waves trapped in layers of unconsolidated sediments. These explanations were sharply disputed by a number of studies [Lachet and Bard, 1994; Kudo, 1995; Bard, 1998; Konno and Ohmachi, 1998], which show that the peak seen on the H/V curve is due to the horizontal polarization of Rayleigh waves, which takes place at a frequency close to the medium's resonant frequency. Recent work using a numerical approach has shown that the source of the H/V peak is not unique, and depends on the physical composition of the ambient vibrations' wave field [Bonnefoy-Claudet et *al.*, 2008b].

Although the technique identified has been very successful for the calculation of a site's resonant frequency and for seismic micro-zoning studies, the amount of amplification is never obtained. Knowledge of the resonant frequency is a useful but limited piece of information. Moreover the H/V technique does not generally bring out the other amplification peaks (higher modes) present in a transfer function (***Figure 2***). The site effect is therefore not fully characterized by this technique [Bonnefoy-Claudet et *al.*, 2008a].

Determination of uncertainty in the site effect

The site effect is thus characterized by its transfer function. During the empirical calculation it is important to show the average value of the amplification according to frequency, accompanied by the 68% confidence limits which represent a measure of uncertainty (***Figure 4***). In this way, if the confidence limits are large, the transfer function is not well characterized.

When a transfer function is calculated from a numerical model of a column of ground, the assessment of uncertainty is not so trivial. The complexity of the calculation depends on the geometric configuration of the seismic waves' medium of propagation. For example, in a unidimensional configuration the ground response is quickly calculated. It then becomes possible to explore a number of numerical models of the medium, in order to determine an average response and an estimate of the associated uncertainty. However, for a 2-D or especially a 3-D geometry, modeling the propagation of seismic waves requires the provision of a large quantity of data for describing the geologic environment, and is very costly as regards computing time. This tends to restrict the number of models investigated, and it therefore remains of limited use.

Figure 6 illustrates the calculation of a transfer function using a 1-D model of the ground in which the average shear-wave (S wave) velocity over the first 30 meters (Vs30) is 400 m/s. Several transfer functions (yellow curves) were calculated using

the Monte Carlo method, by randomly varying velocity, thickness, density, and damping of the ground column. The solid red line represents the mean response of all the transfer functions obtained, and the dotted red lines indicate the 68% confidence limits. Uncertainty increases with frequency, which corresponds to a lack of information regarding thin layers of ground. This kind of calculation for 2-D or 3-D geometric configurations is still at the research stage, for the reasons mentioned earlier [Bonilla et *al.*, 2006].

Including site effects in empirical equations for predicting seismic ground motion

In earthquake engineering, the measurement of a seismic ground motion is generally represented not by a Fourier spectrum (***Equation 1***), but by a response spectrum, which indicates the maximum response of a harmonic oscillator to the seismic motions for a given range of frequency and damping [Kramer, 1996]. The harmonic oscillator is an approximation of a building. On a response spectrum, the spectral acceleration at infinite frequency is likened to the maximum acceleration observed in the time domain (called the PGA, or Peak Ground Acceleration).

The equation for this type of spectrum (Sa), called the empirical ground-motion prediction equation, is (***Equation 2***):

$$\log Sa_{ij}(f) = a(f) \log M_i - \log R_{ij} + b(f) \log R_{ij} + c_k(f)$$

where the seismic source ($S_i(f)$ in ***Equation 1***) is represented here by its magnitude M_i. The effects of geometric and anelastic attenuation depend on the distance between the source i and the site j (R_{ij}) and on damping in the propagating medium. The R_{ij} terms in ***Equation 2*** thus correspond to the term $P_{ij}(f)$ in ***Equation 1***. Lastly, the coefficient $c_k(f)$ models the site effects for a ground type k (corresponding to $F_j(f)$ in ***Equation 1***).

The terms in this equation may be more or less complicated and numerous, but the goal is always to predict the response spectrum using data on the magnitude, the source/site distance, and the site conditions only [Bommer, 2006]. The coefficients $a(f)$, $b(f)$, and $c_k(f)$ are obtained by applying a statistical regression to a database. The assessment of seismic hazard at French nuclear facilities employs an equation of this kind, obtained from a European seismic database [Berge-Thierry et *al.*, 2003].

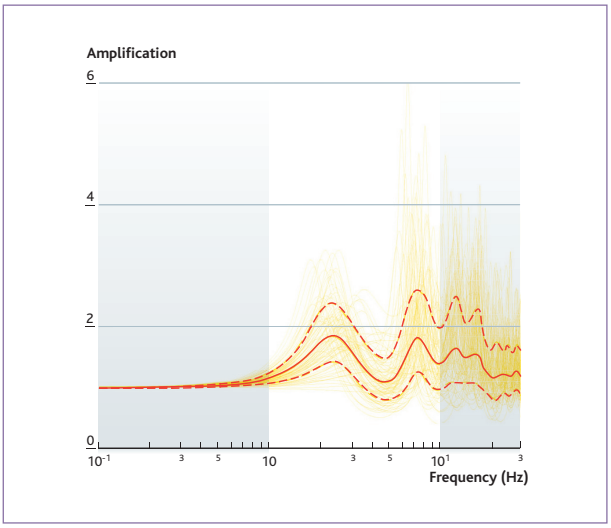

Figure 6 *Illustration of the application of the Monte Carlo method, in which the properties of the ground column are varied to obtain a mean transfer function and an estimate of the associated uncertainty. The yellow curves represent the transfer functions of various ground models. The red lines indicate the mean amplification (solid line) and the 68% confidence limits (dotted).*

	EC8	NEHRP
A	Vs30 > 800 m/s	Vs30 > 1,500 m/s
B	360 < Vs30 < 800 m/s	760 < Vs30 < 1,500 m/s
C	180 < Vs30 < 360 m/s	360 < Vs30 < 760 m/s
D	Vs30 < 180 m/s	180 < Vs30 < 360 m/s
E	Type D or C ground with a thickness of 20 m underlying a type A ground	Vs30 < 180 m/s

Table 1 *Classification of site conditions used in Europe (EC8) and in the United States (NEHRP).*

Calculation of the coefficient $c_k(f)$ in ***Equation 2*** requires that the geotechnical classification of the ground be known. For most of the world's seismometer stations, this type of information about site conditions is far from complete. For example, the stations in the Japanese Knet network are characterized to a maximum depth of only 20 m.

As for the Kiknet network, also Japanese, it consists of stations installed both on surface and underground. For each of these there are geotechnical data for a ground column between 100 m and 200 m deep. Information on a geotechnical profile such as this is not usual for European seismic networks.

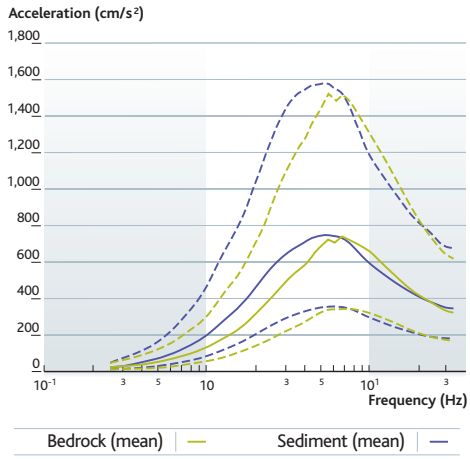

Figure 7 *Response spectrum for a magnitude-6 event whose hypocenter is 8 km from a "sediment" site (blue line) and a "bedrock" site (green line). The solid lines indicate themedian values and the dotted lines indicate the 68% confidence limits. The coefficients used are taken from the motion-prediction equation of [Berge-Thierry* et al.*, 2003].*

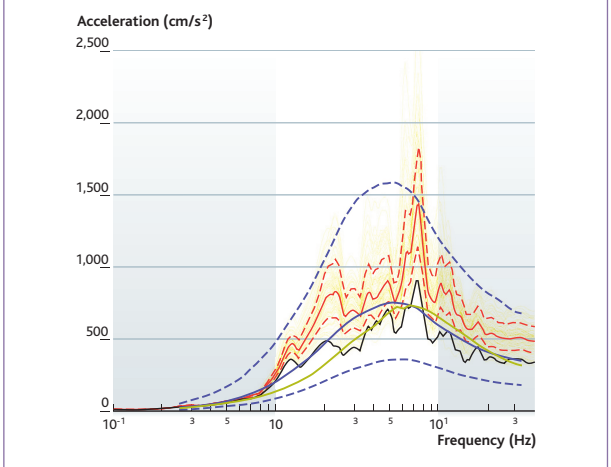

Figure 8 *Estimation of site-specific response spectra (yellow curves) obtained by propagating an incident signal (black line) in a 1-D stochastic medium. The red lines indicate the mean value (solid line) and the 68% confidence limits (dotted). The "bedrock" response spectrum(Vs30 > 800 m/s) predicted by the model of [Berge* et al.*, 2003] for a magnitude/distance pair (6/8 km) is also shown (green line), as well as the "sediment" response spectrum (300 m/s < Vs30 < 800 m/s) (blue line) and the median "sediment" response spectrum +/– one standard deviation (dotted blue lines).*

Ground types are classified by using information on the velocity of shear waves in the ground column. Knowing this velocity, it is possible to determine the material's shear modulus ($G = \rho\beta^2$). The higher the velocity, the stronger the material. In earthquake engineering, the average velocity of shear waves in the uppermost 30 meters of ground, Vs30, is used for site characterization. For example, in the United States the standard classification is defined in the NEHRP program [BSSC, 2000] and in Europe in Eurocode 8 [EUROCODE 8, 2002]. These two classifications are shown in ***Table 1***.

Of course, if information on Vs30 is not available, this means that the classifications in ***Table 1*** cannot be used in the empirical ground-motion prediction equations. In this case, geological and geotechnical criteria can be used to distinguish between so-called "sediment" and "bedrock" conditions [Berge-Thierry et *al.*, 2003]. Recently [Zhao et *al.*, 2006] and [Fukushima et *al.*, 2007] proposed predictive equations based on a classification employing the site's resonant frequency.

Figure 7 shows two response spectra calculated for "bedrock" (green line) and "sediment" (blue line) conditions, using the equation of [Berge-Thierry et *al.*, 2003], based on a magnitude-6 event at a distance of 8 km from the hypocenter. The median spectral acceleration is indicated by solid lines, and the 68% confidence limits are indicated by dotted lines. This figure illustrates three important aspects of the representation of seismic motions by a response spectrum. Firstly, at intermediate frequencies (from 3 to 8 Hz in this example), the spectral acceleration is distinctly higher than that predicted by the PGA. Secondly, for intermediate to low frequencies (frequencies below 5 Hz in ***Figure 7***), the predicted spectral acceleration for "sediment" type conditions (blue line) is stronger than that predicted for "bedrock" type conditions (green line), which corresponds to the site effect. Thirdly, for high frequencies (between 8 and 20 Hz in ***Figure 7***), the predicted "bedrock" spectral acceleration is higher than the predicted "sediment" one. This difference at high frequency results both from the enhancement of ground motions for the sites located on a weathered bedrock and/or the absorption of high-frequency energy in the sediments. It may also arise from a non-linear ground response. Non-linear behavior of a material implies a change in its strength depending on the deformation. A description of this type of rheology goes beyond the scope of this article, but it should be noted that non-linearity of the ground is generally expressed by attenuated seismic motion at high frequencies.

The coefficient c_k used in the empirical ground-motion prediction equations thus represents an average site effect for each type of ground, defined by a wide range of Vs30 values (***Table 1***). It cannot reflect the specific properties of a particular site. The use of this coefficient can then lead to response spectra that are somewhat different from those calculated using a so-called site-specific estimate, i.e., one based on the geotechnical and seismic data for that site.

Site-specific estimation: a 1-D multilayer model

To estimate the seismic motion at a specific site for a given magnitude/distance pair, it is necessary to represent the surface geologic medium and the seismic stresses incident on the base of this medium [Archuleta et *al.*, 2003; Heuze et *al.*, 2004]. The 1-D multilayer model in question is the one used to determine the transfer function described in ***Figure 6*** and the magnitude/distance pair selected is (6.8 km). To represent the incident seismic stresses, a number of synthetic accelerograms were calculated for this magnitude/distance pair, using the model of [Pousse et *al.*, 2006]. The synthetic accelerogram adopted is the one whose response spectrum is the closest to the "bedrock" response spectrum predicted by the equation of [Berge-Thierry et *al.*, 2003] (***Figure 8***).

This signal was altered to take into account the specific local properties of the surface geologic environment. In order to allow for the lack of knowledge concerning the geotechnical properties of this environment, numerous geologic models were generated using the Monte Carlo method (as shown in ***Figure 6***). The seismic motion for a particular site and the associated response spectrum were calculated for each geologic model. The results obtained are summarized in ***Figure 8*** in the form of a mean response spectrum and its 68% confidence limits (yellow and red lines) and are compared to the predicted "sediment" response spectrum (blue line) using the predictive equation of [Berge-Thierry et *al.*, 2003].

The specific consideration of the surface geologic environment is expressed by an increase in the acceleration spectrum over a wide range of frequencies (red lines) in comparison to the "sediment" prediction (blue line), particularly at the 2 and 7 Hz frequencies. To allow for uncertainty in knowledge of the environment, the response spectrum adopted could correspond to the median spectrum plus one standard deviation (dotted blue line).

Site-specific estimate: propagation of seismic waves in a 2-D medium

The examples discussed until now have described the site effects produced by a 1-D configuration. When the propagating medium can no longer be considered to be a stacking of flat beds (sedimentary basins and mountainous regions), other phenomena, in particular the generation of surface waves at the edges of basins, may also cause increases in the amplitude and duration of the seismic signals. Research efforts have therefore been devoted to the characterization of the propagating medium and the numerical simulation of seismic-wave propagation.

Currently, modeling of the propagation of seismic waves in 3-D media is limited to frequency domains of less than 1 to 4 Hz for major basins (several thousand km^2) such as those of Los Angeles in the United States, Sendai in Japan, and Wellington in New Zealand [Olsen and Archuleta, 1996; Satoh et *al.*, 2001; Benites and Olsen, 2005]. However, for earthquake engineering purposes, it is necessary to calculate a sedimentary basin's response up to frequencies of nearly 10 Hz, and sometimes even higher. This requirement leads to a practical difficulty, because it requires knowledge of the geologic environment for wavelengths close to the maximum frequency used in the calculations. For example, for frequencies close to 10 Hz the associated wavelength is several meters; the geologic environment must then be known at this scale if 3-D simulations are to be performed. This level of knowledge is impossible to obtain at present. Moreover, it would be difficult to store the corresponding volume of geologic information, and the computing time required would be prohibitive.

For a less extensive sedimentary basin (a few tens of km^2), which could be treated using a 2-D configuration (assuming that the incident wave can be likened to a plane wave), existing computing resources permit simulation of the basin's response at frequencies above 4 Hz. Even in the simplest case, however, the propagating medium must be characterized at the scale of the wavelength (about ten meters) that corresponds to the maximum frequency of calculation, which is not always the case.

Nevertheless, there are basins, like the one at Nice, where the underground geology is known in sufficient detail to allow the propagation of seismic waves to be simulated. A compilation of geotechnical and geophysical studies carried out for this basin enabled the construction of a 3-D velocity model [Gemgep, 2000]. Using an east-west section of this model, simulations in one and two dimensions were carried out along the profile that

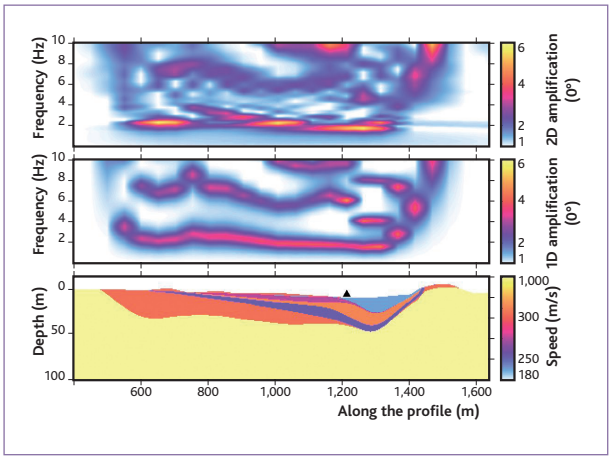

Figure 9 *Examples of transfer functions calculated for a 2-D model (upper panel) and from 1-D ground columns (center panel), for a vertically-incident plane wave. The black triangle shows the location of the NLIB station; after [Gélis et al., 2008].*

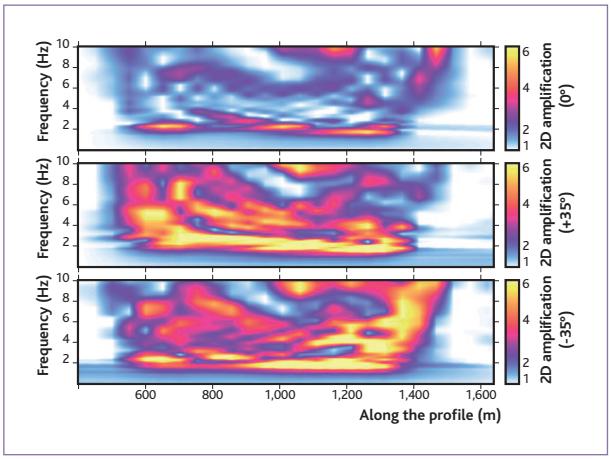

Figure 10 *Transfer functions calculated for a 2-D model of a plane wave with vertical incidence (upper panel), +35⁰ incidence from left to right (center panel), and – 35⁰ incidence from right to left (lower panel), after [Gélis et al., 2008].*

includes the NLIB station mentioned in ***Figures 3*** and ***4*** [Gélis et *al.*, 2008]. The depth of this section is 125 m and its width is 2.2 km. The minimum and maximum shear-wave velocities are 180 m/s and 1,000 m/s respectively. The finite differences method was used to calculate the propagation of the P and SV waves in this configuration [Saenger et *al.*, 2000].

Figure 9 shows the transfer function obtained from the propagation of a synthetic accelerogram, for a vertical incidence of the incident plane SV wave. The lower panel illustrates the geometry of the east-west section of the basin mentioned above. The center panel shows the transfer function calculated from the ground columns (1-D information) by sampling the 2-D model every 50 m. The upper panel shows the 2-D model's real transfer function. The 1-D calculation models the overall response of the basin's 2-D profile with a maximum amplification of about 4, while the 2-D calculation shows higher amplifications (about 6) for the fundamental frequency, and at the edges of the small basin (located between 1,200 and 1,400 m along the profile).

In this type of configuration, the effect on the basin's response of the angle of incidence of the waves arriving directly from the seismic source is also very significant. ***Figure 10*** illustrates the case of two plane waves propagating, one from right to left with an incident angle of –35⁰ (lower panel) and the other from left to right with an incident angle of +35⁰ (center panel).

The upper panel shows the results obtained for a vertical incidence. With regard to this incidence, examination of ***Figure 10*** shows that the amplification observed for incident waves of +/–35⁰ is greater, and extends over a wider range of frequencies. This broadband phenomenon cannot be modeled by a 1-D calculation, hence the need to perform a site-specific estimate for this kind of configuration, when possible.

Conclusions

This article describes the importance of the site effect in estimating seismic hazards. The site effect is represented by the site's transfer function, which defines the amplification of the seismic signal according to frequency. There are several methods for characterizing a site's transfer function. The ambient noise method is inexpensive, but is used only to obtain the site's resonant frequency. Although this information is very useful, the site effect is not completely characterized by this method. On the other hand, although it is more costly, the empirical sediment/reference method, based on calculating the spectral ratios of signals simultaneously at a sediment site and a bedrock site, is capable of completely determining the transfer function. This second method is, however, tainted by an intrinsic uncertainty arising from the combined effect of the seismic source, the propagation of the waves, and their sampling of the upper layers of the earth's crust.

For this reason any study of site effects (empirical or numerical) must define the mean value of the transfer function and the corresponding confidence limits. In the absence of empirical data the uncertainty of the site's response is determined by numerical approaches employing Monte Carlo methods. For 2-D and especially 3-D geometric configurations, however, determining uncertainty is still a very tricky matter.

Site effects are partially included in the empirical ground-motion prediction equations. The terms that represent them correspond to the mean amplification figures, allowing for the wide variability in the geotechnical conditions at the sites used for deriving the equations. Nevertheless, the predictive equations cannot reflect the specific features of a given site. In some cases, moreover, these equations predict response spectra that are somewhat different from those calculated by using geotechnical characteristics specific to the site (site-specific estimation). Consequently, when geotechnical information for the site is available, a site-specific estimation is preferable to the application of empirical equations.

References

- R.J. Archuleta, P. Liu, J.H. Steidl, L.F. Bonilla, D. Lavallée, F. Heuze (2003). *Finite-fault site-specific acceleration time histories that include non linear site response, Physics of the Earth and Planetary Interiors, 137, 153-181.*
- P.Y. Bard (1998). *Microtremor measurements: A tool for site effect estimation? in Proceedings of the second International Symposium on the Effects of Surface Geology Seismic Motion, December 1-3, Yokohama, Japan 3, 1251-1279.*
- R. Benites, K.B. Olsen (2005). *Modeling Strong Ground Motion in the Wellington Metropolitan Area, New Zealand, Bull. Seism. Soc. Am., 97, 2180-2196.*
- C. Berge-Thierry, F. Cotton, O. Scotti, D.A. Griot-Pommera, Y. Fukushima (2003). *New empirical response spectral attenuation laws for moderate European earthquakes, J. Earthquake Eng., 7, N° 2, 193-222.*
- J.J. Bommer (2006). *Empirical estimation of ground motion: Advances and issues, In: Proceedings of the Third International Symposium on the Effects of Surface Geology on Seismic Motion, 30 August-1 September, Grenoble, France, 155-135.*
- L.F. Bonilla, J.H. Steidl, G.T. Lindley, A.G. Tumarkin, R.J. Archuleta (1997). *Site Amplification in the San Fernando Valley, California: Variability of Site-Effect Estimation Using the S-wave, Coda, and H/V Methods, Bull. Seism. Soc. Am., 87, 710-730.*
- L.F. Bonilla, J.H. Steidl, J.C. Gariel, R.J. Archuleta (2002). *Borehole Response Studies at the Garner Valley Downhole Array, Southern California, Bull. Seism. Soc. Am., 92, 3165-3179.*
- L.F. Bonilla, P.C. Liu, S. Nielsen (2006). *1D and 2D linear and non linear site response in the Grenoble area, in Proceedings of the Third International Symposium on the Effects of Surface Geology on Seismic Motion, 30 August-1 September, Grenoble, France.*
- S. Bonnefoy-Claudet, F. Cotton, P.Y. Bard (2006). *The nature of noise wavefield and its application to site effects studies. A literature review, Earth-Science Reviews, 79, N° 3-4, 205-227.*
- S. Bonnefoy-Claudet, C. Pasten, S. Baize, L.B. Bonilla, C. Berge-Thierry, J. Campos, R. Verdugo, P. Volant (en révision) (2008a). *Site effect evaluation in the basin of Santiago de Chile using ambient noise measurements, Geophys. J. Int.*
- S. Bonnefoy-Claudet, A. Köhler, C. Cornou, M. Wathelet, P.Y. Bard (2008b). *Effects of Love waves on microtremor H/V ratio, Bull. Seism. Soc. Am., 98, 288-300.*
- R.D. Borcherdt (1970). *Effects of local geology on ground motion near San Francisco Bay, Bull Seism. Soc. Am., 60, 29-61.*
- Building Society Safety Council (2000). *The 2000 NEHRP Recommended Provisions for New Buildings and Other Structures: Part I (Provisions) and Part II (Commentary), FEMA 368/369, Federal Emergency Management Agency, Washington, D.C.*
- Eurocode 8 : *Design of structures for earthquake resistance (2002). Part 1: General rules, seismic actions and rules for buildings, Revised Final Project Team Draft (preStage 49). Doc CEN/TC250/SC8/N317.*
- Y. Fukushima, L.F. Bonilla, O. Scotti, J. Douglas (2007). *Site classification using horizontal-to-vertical response spectral ratios and its impact when deriving empirical ground-motion prediction equations, Journal of Earthquake Engineering, 11, 712-724.*
- C. Gélis, L.F. Bonilla, J. Regnier, E. Bertrand, A.M. Duval (2008). *On the Saenger's finite difference stencil to model 2D P-SV nonlinear basin response: application to Nice, France, Proceedings in Seismic Risk 2008 - Earthquakes in North-Western Europe, 11-12 September 2008, Liège, Belgium.*
- Gemgep phase 1 (2000). Risque sismique sur Nice : étude de scénarios de gestion de crise sismique. Définition de l'aléa, de la vulnérabilité et des enjeux. CETE Méditerranée, laboratoire de Nice.
- S.H. Hartzell (1992). *Site response estimation from earthquake data, Bull. Seism. Soc. Am., 82, 2308-2327.*
- F. Heuze, R.J. Archuleta, L.F. Bonilla, S. Day, M. Doroudian, A. Elgamal, S. Gonzales, M. Hoehler, T. Lai, D. Lavallée, B. Lawrence, P.C. Liu, A. Martin, L. Matesic, B. Minster, R. Mellors, D. Oglesby, S. Park, M. Riemer, J.H. Steidl, F. Vernon, M. Vucetic, J. Wagoner, Z. Yang (2004). *Estimating site-specific strong earthquake motions, Soil Dyn. and Earth. Eng., 24, 199-223.*
- K. Konno, T. Ohmachi (1998). *Ground-motion characteristics estimated from spectral ratio between horizontal and vertical components of microtremor, Bull. Seism. Soc. Am., 88, 228-241.*
- S. L. Kramer (1996). *Geotechnical Earthquake Engineering, Prentice Hall, New Jersey, 653 p.*
- K. Kudo (1995). *Practical estimates of site response. State-of-art report, in Proceedings of the fifth International Conference on Seismic Zonation, Nice, France.*
- C. Lachet, P.Y. Bard (1994). *Numerical and theoretical investigations on the possibilities and limitations of Nakamura's technique, J. Phys. Earth., 42, 377-397.*
- Y. Nakamura (1989). *A method for dynamic characteristics estimation of subsurface using microtremor on the ground surface, Quarterly Report Railway Tech. Res. Inst., 30, 25-30.*
- K.B. Olsen, R.J. Archuleta (1996). *3D Simulation of Earthquakes on the Los Angeles Fault System, Bull. Seism. Soc. Am., 86, 575-596.*
- G. Pousse, L.F. Bonilla, F. Cotton, L. Marguerin (2006). *Non Stationary Stochastic Simulation of Strong Ground Motion Time Histories Including Natural Variability: application to the K-net Japanese Database, Bull. Seism. Soc. Am., 96, 2103-2117.*
- E. Saenger, N. Gold, S. Shapiro (2000). *Modeling the propagation of elastic waves using a modified finite-difference grid. Wave Motion, 31, 77-82.*
- T. Satoh, H. Kawase, T. Sato, A. Pitarka (2001). *Three-Dimensional Finite-Difference Waveform Modeling of Strong Motions Observed in the Sendai Basin, Japan, Bull. Seism. Soc. Am., 91, 812-825.*
- S.K. Singh, E. Mena, R. Castro (1988). *Some aspects of source caracteristics of the 19 September 1985 Michoacàn earthquake and ground motion amplification in and near Mexico City from strong motion data, Seism. Soc. Am., 78, 451-477.*
- J.X. Zhao, K. Irikura, J. Zhang, Y. Fukushima, P. G. Somerville, A. Asano, Y. Ohno, T. Oouchi, T. Takahashi, H. Ogawa (2006). *An Empirical Site-Classification Method for Strong-Motion Stations in Japan Using H/V Response Spectral Ratio, Bull. Seism. Soc. Am., 96, 914-925.*

4.5 RECENT DEVELOPMENTS in MELODIE software

Marc BOURGEOIS
Safety Assessment and Research Section for Radioactive Waste Disposal Facilities Unit

The new release of MELODIE, Version 5.0, an application developed by IRSN to simulate the transport of solutes in porous media, used in assessing the long-term safety of a radioactive waste repository, was installed for "regular service" in 2008. It includes numerical enhancements such as the new "finite volumes/finite elements" mixed discretization method, which, in comparison with the "finite elements" method, guarantees better simulation results when the proportion of convection in transport is not negligible with respect to diffusion. The new version also provides a better understanding of transport mechanisms in the sub-surface zone between the near-surface and the water table (the "non-saturated zone"), which is important in assessing surface storage and "sub-surface"-storage facilities.

During the promotion of MELODIE, Version 5 was made available to outside partners (BEL-V in Belgium, BNRA in Bulgaria, SEC/NRS in Russia), *via* a dedicated area on the Institute's computer network. One aim of providing external access to MELODIE is to obtain feedback that will contribute to improving the software, maintaining its position as the benchmark tool in safety assessment of radioactive waste repositories.

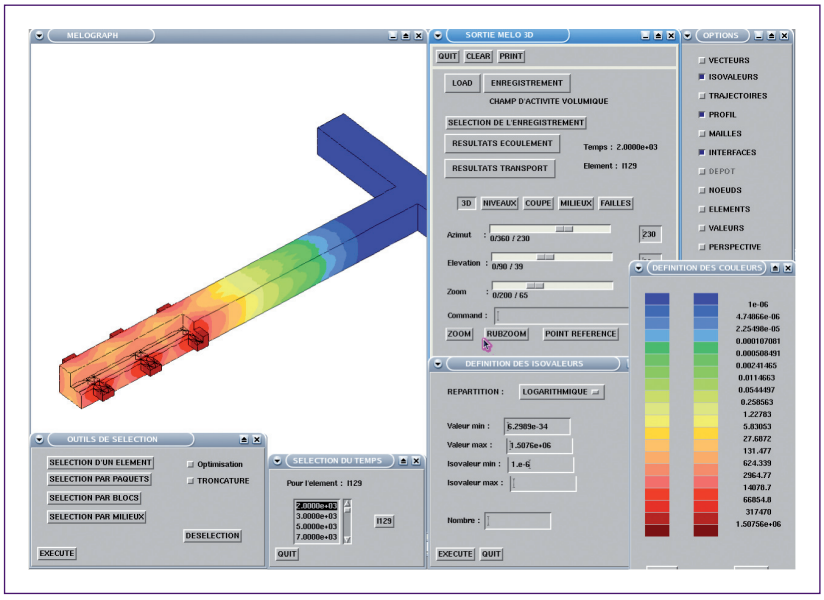

Figure 1 *The new release of MELODIE, Version 5.0.*

4.6 IRSN'S CONTRIBUTION TO THE EUROPEAN NF-PRO PROJECT on the disposal of radioactive waste in deep geological layer

Gregory MATHIEU
Safety Assessment and Research Section for Radioactive Waste Disposal Facilities Unit

NF-PRO(1) was a four-year project (2004-2007) of the 6th Framework Program (FP6) run by the European Commission (Euratom), bringing together more than 40 partners. Its main goal was to achieve progress in scientific and technical knowledge with a view to assessing the containment properties of near-field components(2) in a repository for high-level radioactive waste and spent fuel built in a geological formation (clay, granite or salt).

NF-PRO is structured in five Research and Technology Development Components (RTDCs), corresponding to experimentation and modeling work on changes in the main near-field components, (RTDC 1 to 4). It also analyzed the study results to determine whether they could be used in safety assessments (RTDC 5). RTDCs 1 to 4 dealt respectively with:

- the processes used to test waste dissolution and activity releases;
- the chemical processes that influence the performance of engineered components made of swelling clay;
- the thermal-hydromechanical development of the engineered barrier system;
- the characterization of and changes in the host rock zone damaged by excavation.

RTDC 5 addressed possible changes in the near-field components and the associated uncertainties. The results of RTDCs 1 to 4 were analyzed and integrated to establish a frame of reference based on their relative importance for safety assessments concerning waste disposal in geological formations.

IRSN's contributions to RTDC 4, especially Work Package 4.2, involved studying techniques for determining the extent of the excavation damage zones (EDZ), and understanding the mechanisms causing this phenomenon. In this context, IRSN interpreted an instrumented digging experiment (mine-by-test) at the Tournemire experimental station. The main findings from this experiment were as follows:

- evidence emerged of significant hydro-mechanical coupling, with a high rise in interstitial pressure occurring as gallery digging progressed;
- no EDZ was detected in the short term (after completion of digging), which is consistent with the predictive calculations carried out, but does not explain the damaged zone observed around the hundred-year-old railroad tunnel;
- the influence of desaturation was very clearly identified by the presence of cracking caused by the atmospheric water conditions in contact with the gallery walls;
- a hydromechanical behavior model taking into account the changes in massif saturation was integrated into the numerical simulations, improving the reproduction of measured displacements. A significant deviation was observed, however, in pore pressure values.

IRSN's contributions to RTDC 5 with regards to the concept of a high-level, long-lived waste repository in an argillaceous formation have led to the following conclusions:

- concerning the chemical changes in clay

(1) Acronym for Near-Field PROcesses.

(2) The near field of a repository includes the engineered components (waste packages, components made of swelling clay such as the plugs and drift seals), as well as the part of the host rock disturbed by the repository.

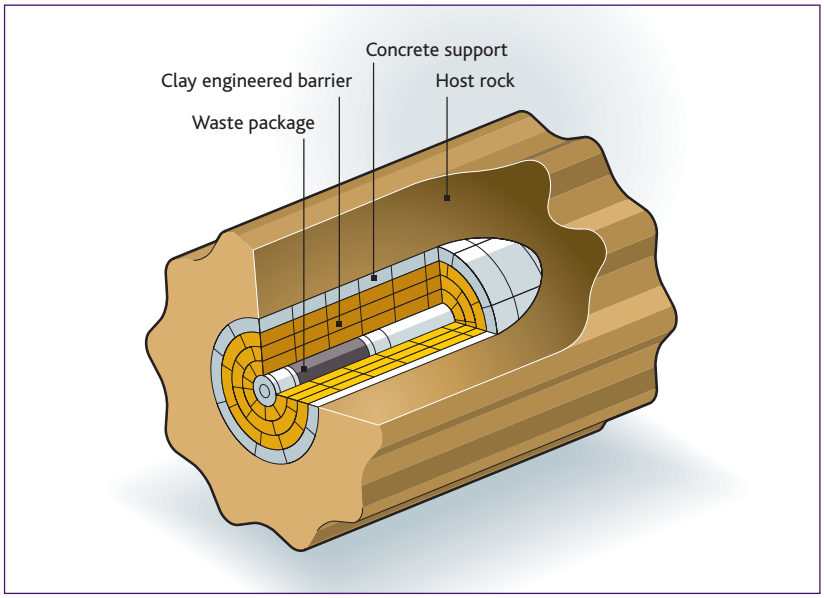

Figure 1 *Illustration of the near field and its components for spent fuel disposal (diagram: SCK-CEN, NF-PRO consortium).*

in the presence of cement-type materials, the study showed that the intensity and extension of clay alteration over a calculated period of 100,000 years, depends greatly on potential porosity clogging, the relevant reaction scheme, the diffusion rate, and the component dimensions. In general, the interaction between concrete and clay could lead to substantial but localized mineral disturbances in the clay, so that part of the engineered clay barriers of the disposal drifts could be preserved;

- with regard to changes in the free gas phase and its pressure in the near field, the simulations showed that gas migration does not have a significant effect on water saturation in the host rock. Nevertheless, the maximum pressure calculated in the reference case is close to the lithostatic pressure of the rock, which could lead to damage. Given data uncertainty and the simplifications made in modeling the processes, assessing damage to the rock caused by gas pressure will require a better representation of the phenomena involved and more accurate parameter values when running the model;
- as regards solute migration in the near field, and on the repository scale, it appears that most solutes migrate by diffusion through the host rock, due to the containment properties of clay and the repository architecture (sealed drifts, dead-end disposal cells), which help limit flows and therefore the transfer of solutes through the repository drifts by convection. Moreover, a study of the sensitivity of activity flux to parameters such as instantaneously released activity, the dissolution rate of the spent fuel matrix, and the chemical properties of the solutes, has advanced understanding of the overall behavior of the containment system.

4.7 SAFETY OF DEEP GEOLOGICAL RADIOACTIVE WASTE REPOSITORIES: IRSN expands its experimental station in Tournemire and sets up a new research program

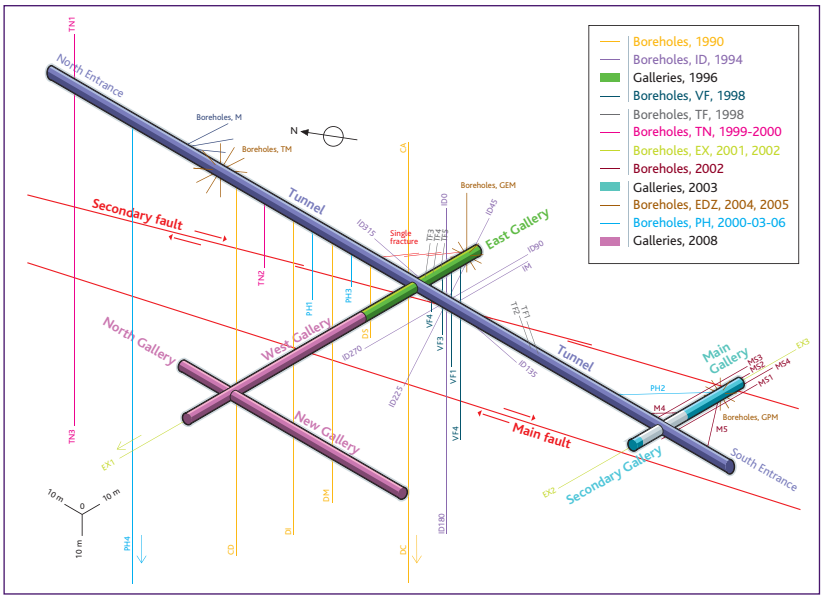

Figure 1 *Three-dimensional drilling plan for the experimental facility.*

Justo CABRERA
Research on Geological Waste Disposal and Near-Surface Transfers Laboratory

In June 2008, after several months of work, Eiffage completed digging the 170 m of new galleries at the IRSN experimental station in Tournemire. Built in a 1,885-meter long railway tunnel over 120 years old, the station has seen significant growth, with the total length of galleries now exceeding 270 m.

Thanks to these new structures, IRSN now has the space necessary to continue research and undertake a new experimental program started in 2009, designed to investigate the long-term behavior of the seals on disposal drifts. The program will study the effectiveness and resistance of different types of "plugs" over time, and will identify the parameters requiring special attention in assessing the projects to be presented by Andra before 2015, a date set in accordance with the Program Act of June 28, 2006. The experiments will be based on systems set up in the 60-cm diameter boreholes representative of the scale of certain drifts being considered for the disposal of long-lived, high-level radioactive waste.

In parallel with the installation of new experiments, as the station is expanded, studies are being conducted to monitor the damage induced by digging structures in indurated argillaceous formations, thereby contributing to a better understanding of this phenomenon. The new galleries are of particular interest in this respect, since they were designed to reach a zone located more than 100 m from the tunnel, thus providing access to argillaceous rock unaffected by the disturbances resulting from the 120-year existence of the earlier structure. Crossing these structures will make it easier to set up experimental and observation systems.

The galleries were completed according to stringent specifications, in order to limit immediate damage to the rock as much as possible while digging. Eiffage, engaged following a call for tenders by IRSN, used a tunnel-miner called a "roadheader", an innovative approach for this kind of rock, which met all the requirements stipulated by the Institute.

Figure 2 *Tournemire galleries*

Figure 3 *Digging a gallery at Tournemire.*

NEUTRON metrology

Vincent GRESSIER
Neutron Metrology and Dosimetry Laboratory

All countries rely on a viable infrastructure to achieve their societal objectives. Building this infrastructure in a sustainable development perspective depends on three keystones that are closely interdependent: metrology, standardization and conformity assessment [ISO, 2006].

■ In the field of Metrology, a distinction is made between fundamental and legal metrology. Fundamental metrology, coordinated by the BIPM (the International Bureau of Weights and Measures), deals with measurement standards and the International System of Units (SI)(1). The IRSN activities described in the article below come within this area of metrology. Legal metrology encompasses all the legislative, administrative and technical procedures used to specify and ensure the quality and credibility of measurements relative to official inspections, trade, health care, safety and the environment. Legal metrology, which is supported by fundamental metrology, is coordinated by the OIML (the International Organization of Legal Metrology). The OIML develops standard regulations and international recommendations used in drawing up national regulations for various categories of measuring instruments. These recommendations are prepared in liaison with international standards organizations.

(1) The International System (SI) includes seven basic units of measurement: meters, kilograms, seconds, amperes, kelvins, moles, and candelas, used to quantify independent physical magnitudes. Each unit of measure is represented by a symbol (for the basic units, in order: m, kg, s, A, K, mol, and cd). These basic units serve to define derived units, such as the SI unit for measuring speed, the meter per second, or dosimetric quantities.

■ International standards result primarily from the work of the International Organization for Standardization (ISO), the International Electrotechnical Commission (IEC) and the International Telecommunications Union (ITU). ISO deals with standards in all fields, except for the electrotechnical sector, which is covered by the IEC, and telecommunications, under the authority of the ITU. The three organizations work closely together in developing standards for information technologies.
These international standards are adopted at European level by the European Committee for Standardization (CEN) and, in France, by the *Association Française de Normalisation* (AFNOR).

Standards are divided into three main categories, according to whether they relate to products, processes or management systems. The first category involves the quality and safety of goods and services. The second deals with the conditions in which products and services are produced, packaged and developed. Standards related to management systems (such as ISO 9001) aim to assist companies in managing their business activities. They serve to define a framework enabling companies to systematically meet the requirements set out in the standards relative to products and processes.

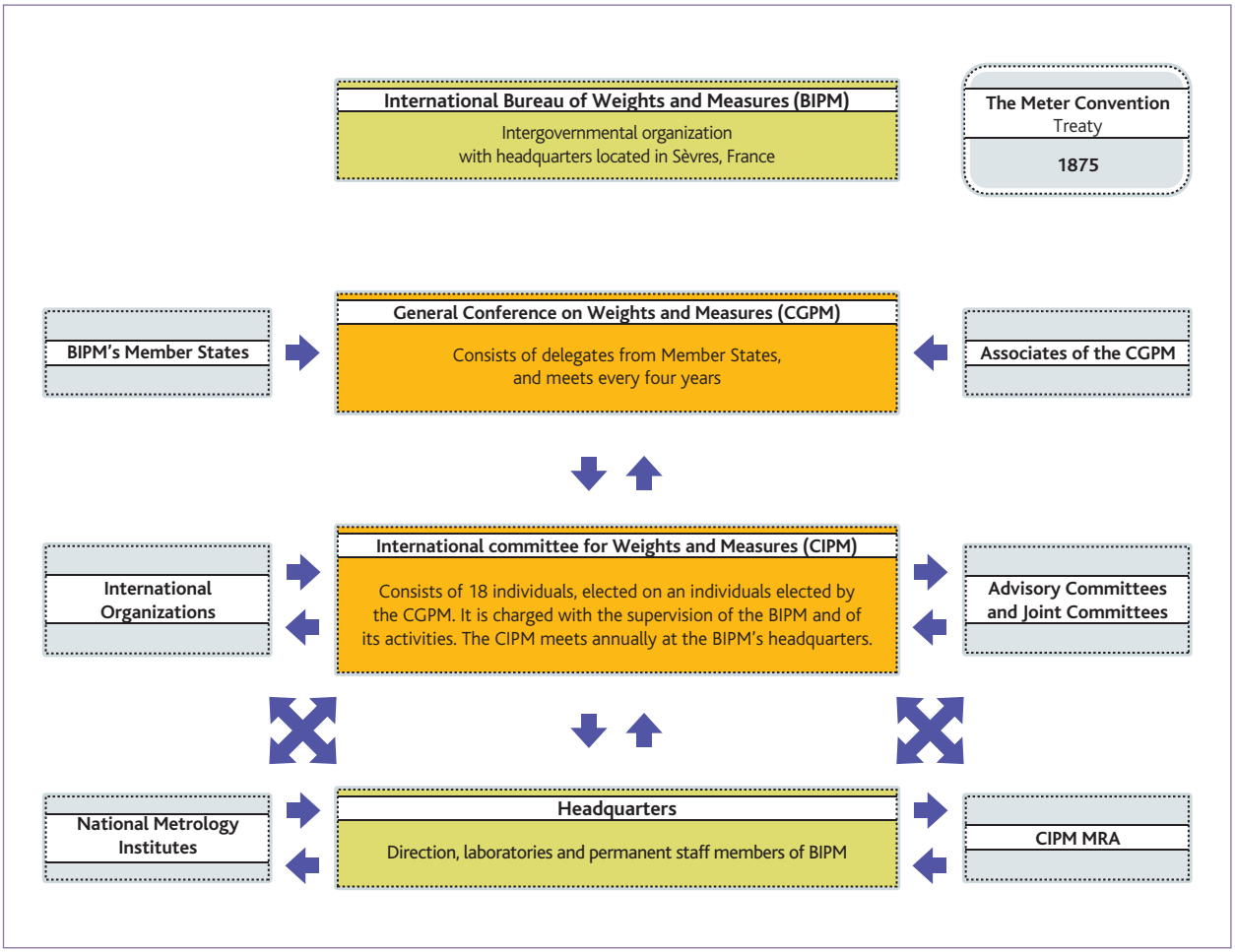

Figure 1 *Organization chart of the International Bureau of Weights and Measures (BIPM).*

Compliance is assessed by checking that the requirements specified for a product, process or system, a person or organization, are met. Conformity assessment procedures, such as tests, inspection and certification, provide assurance that the products meet the requirements specified in the regulations and standards. Accreditation is granted by an independent organization in either the public or private sector. ISO/IEC standards and guides regarding conformity assessment are used to harmonize practice in this area and to serve as references for the technical expertise of the assessment bodies, thereby enhancing the credibility and reliability of the results.

The three keystones described above are interdependent. Metrology and physical standards provide the necessary means to ensure that measurements are accurate; admissible production quality may be specified in international standards which, in turn, may serve as references for assessing compliance. Used by companies and governments to optimize production and health care services, protect the consumer and the environment, and improve safety and quality, efficient implementation promotes sustainable development and helps further social progress, while also encouraging trade.

Scientific progress over the last few decades has led to sustainable development through the emergence of a vast array of technologies and innovative products. Metrology is crucial to this process to ensure the quality of new products and services, through increasingly accurate measuring techniques developed in close cooperation with the International System of Units.

In the area of neutron dosimetry, various studies carried out in the late 1990s demonstrated the difficulty involved in satisfactorily ensuring dosimetric monitoring of workers exposed to neutrons [Bordy et *al.*, 2000]. This has resulted in the development of new generations of personal electronic neutron dosimeters.

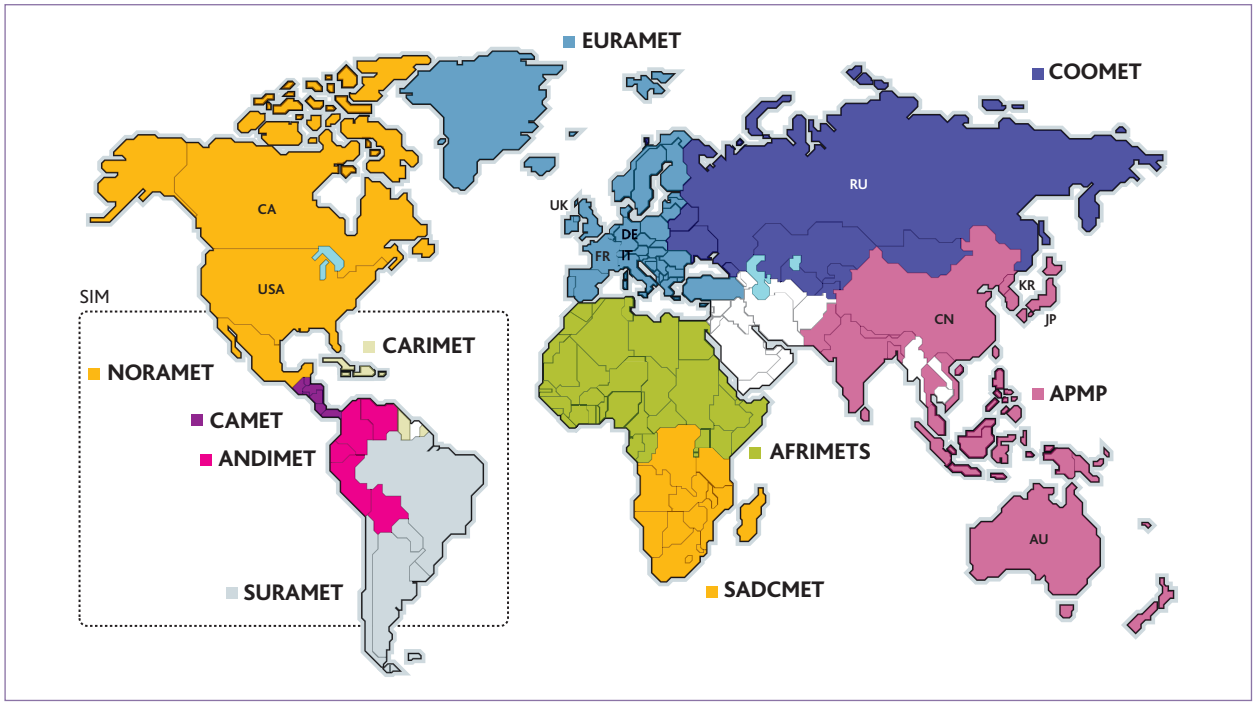

Figure 2 *Regional metrology organizations around the world.*

Metrology facilities at IRSN that produce reference neutron radiation fields are used to "link" measurements taken using these dosimeters to the dosimetry standard units. The calibration methods used comply with the recommendations of ISO and IEC international standards, and the fact that this activity has been accredited by Cofrac, the French accreditation committee, in accordance with ISO 17025, guarantees the Institute's expertise and ensures that its results are compliant.

After this general introduction to metrology and a brief explanation of how metrology activities relate to neutron dosimetry at IRSN, the rest of this article describes the facilities and methods used to obtain a reference neutron radiation field, together with studies in progress and avenues for future development.

Neutron metrology in France

How metrology is organized

Metrology around the world

International metrology was created following the Meter Convention signed in Paris in 1875, which founded three organizations.

- The BIPM (*Bureau international des poids et mesures*) was set up to ensure international harmonization of physical measures and ensure traceability regarding the International System of Units (SI). It cooperates directly with national metrology laboratories.
- The CIPM (*Comité international des poids et mesures*) supervises the BIPM and its activities. The CIPM is advised on scientific and technical matters by various advisory committees made up of international experts.

The General Conference on Weights and Measures (CGPM) has authority over the CIPM. It consists of delegates representing the governments of the Member States and meets every four years. Based on the CIPM's report, the CGPM makes decisions regarding international metrology.

The Meter Convention is currently supported by 51 Member States [BIPM].

The Mutual Recognition Arrangement (MRA)

On October 14, 1999, a mutual recognition arrangement was signed by 38 national metrology institutes (NMIs) and two international organizations. The aims of this arrangement, coordinated by the BIPM, are to establish the degree of equivalence(2) between national measurement standards maintained by NMIs, to ensure the mutual recognition of the calibration and measurement certificates issued by NMIs, thereby providing governments and other parties with a sound technical basis for future (and more extensive) agree-

(2) Deviation, with the associated uncertainty value, between a standard value and the reference value in a CIPM key comparison.

ments regarding international trade and regulatory activities. For example, the French national standard for measuring length (the standard meter) is recognized as a measurement standard by all the other national metrology laboratories that have signed the MRA. Consequently, a calibration certificate for a neutron detector issued by IRSN will also be recognized by these national metrology laboratories.

To establish the degree of equivalence between measurement standards, the MRA defines the procedure for implementing international measurement comparisons, referred to as key or supplementary comparisons, and provides that national metrology institues are to establish quality systems and procedures for demonstrating their competence.

The MRA has resulted in documents stating the Calibration and Measurement Capabilities (CMCs) of each NML. CMCs are registered in the Key Comparison Data base (KCDB) managed by the BIPM, which can be viewed by the public on the Internet.

Metrology in Europe

Various international metrology organizations have been developed at a more local level to strengthen relations and cooperation between metrology institutes. Thoughout the world, there are five regional metrology organizations (RMO), shown in ***Figure 2***: Euramet for Europe, Sim for North and South America, APMP for Southern Asia and the Pacific, Coomet for the former Soviet bloc countries and certain European countries and, lastly, SADCMET for South Africa. Most of the national metrology laboratories are members of these RMOs. Metrology institutes that are not NMLs can nonetheless become involved in RMO activities.

Beginning in 1988, metrology in Europe was coordinated by Euromet, the European Collaboration in Measurement Standards. The need for smoother integration and better coordination of research in metrology at European level (within the framework of a European Metrology Research Program, or EMRP), led to a new organization set up on July 1, 2007, with association status, known as the European Association of National Metrology Institutes (Euramet).

Metrology in France

Since 2005 the French national metrology and test laboratory LNE (*Laboratoire national de métrologie et d'essais*) has been France's national metrology laboratory. It has replaced the former organization, the BNM, that had been responsible for this function since 1969. The LNE coordinates metrology activities in France. For historical reasons, assessment and research activities in scientific and industrial metrology are performed by several different laboratories attached to various public institutions. Thus, there are four national metrology laboratories (NMLs)[3] operating under the authority of the LNE, constituting the main metrology laboratories in France, together with seven LNE associate laboratories, including IRSN, involved in specific areas and whose expertise complements that of the NMLs.

IRSN'S LNE Asssociate Laboratory

Presentation of LNE-IRSN

Among the national metrology laboratories in France, the CEA's *Laboratoire national Henri Becquerel* (LNE-LNHB) is the one responsible for ionizing radiation. In the case of neutron measurement units, the LNHB deals with metrology involving radioactivity (activity and emission rate). For units working in neutron dosimetry, the IRSN's Neutron Metrology and Dosimetry Laboratory (DRPH/SDE/LMDN) has neutron sources, the required methods and accredited associate activity. To complement the LNHB's activities, IRSN was recognized as an Associate Laboratory (LNE-IRSN) for neutron dosimetry on November 27, 2001.

This laboratory and the facilities used are based at the CEA's site in Cadarache. In addition to the 11 permanent staff, a growing number of doctoral researchers (three as of October 2008), post-doc employees (two to date) and student trainees work there. This change highlights two points: first, the increasingly important role played by research and development in the laboratory's activities, and second, the increasingly powerful facilities used (notably, startup of the AMANDE facility in 2005, together with technical and conceptual developments relative to existing facilities and detectors). As specified in Chapter 3, only one facility (the radioactive neutron source irradiator) has been accredited and fully integrated in the LNE-IRSN, along with two employees. One of IRSN's short- to medium-term goals is to obtain accreditation and associate laboratory status for all activities throughout its facilities and a large part of its measuring equipment.

Responsibilities of LNE-IRSN

The status of associate laboratory entails the following responsibilities for LNE-IRSN:

- LNE-IRSN must implement the following SI derived units of measure: fluence rate[4] ($m^{-2}.s^{-1}$), kerma rate[5] in tissue ($Gy.s^{-1}$) and ambient and personal dose equivalent rates[6] ($Sv.s^{-1}$). The fluence rate is the only quantity that is measured. The dosimetric quantities (kerma and dose equivalents) are obtained by applying a dose conversion factor (with no uncertainty) that depends on neutron energy values, as given in the [ICRP74, 1997] tables. To implement these units, the LNE-IRSN must develop, maintain, improve and use reference measurement standards and transfer[7]

measurement standards. It must also deploy reference resources and methods for the different quantities across the entire range of energy values and fluence rates encountered in radiological protection.

- The associate laboratory must conduct research to improve the definition and implementation of the units of measure mentioned above.
- It must carry out and, as necessary, coordinate all comparisons of use in ensuring international equivalence of national measurement standards and methods developed by national metrology laboratories. Within the framework of this task, it must ensure that France is represented on the CIPM's Advisory Committee for Ionizing Radiation, Section 3 (neutrons) (CCRI(III)), within Euramet and in any other working groups involved in metrology.
- The laboratory must study, develop and use transfer and calibration resources to "interconnect" French laboratories in order to ensure traceability of calibration measurement standards for users.
- It provides calibration services that cannot be undertaken by accredited laboratories, mainly because they are not directly profitable enough or for scientific, technical or strategic reasons.
- It is involved in training programs.

In return, the LNE helps fund certain clearly-defined metrology projects, through an annual contribution of € 100,000.

General method for defining references

As described above, dosimetric quantities are calculated on the basis of the neutron fluence rate.

Two methods can be used to determine the fluence rate. In the case of radioactive sources, it is obtained by measuring the source emission rate (i.e. the number of neutrons emitted in the entire space), taken as the reference measurement standard. For other devices, the fluence rate is obtained on the basis of measurements taken using detectors, working measurement standards or transfer measurement standards. These different methods are described in detail in the next section.

The factors used to convert fluence rates to kerma or dose equivalent rates varies according to the neutron energy. Defining references for dosimetric quantities therefore implies knowing the distribution of neutron fluence energy.

In the case of radioactive neutron sources, international standards recommend an average energy distribution and conversion factor for every type of source. For other neutron fields, the LMDN has a full range of spectrometers, in other words, detectors that can be used to measure the distribution of fluence energy within different energy ranges. These are transfer measurement standards connected to reference measurement standards at a national metrology laboratory outside France (PTB in Germany or NPL in the United Kingdom).

The metrology methods associated with reference neutron fields (production and calibration) are described in ISO 8529 and 12789 [ISO 8529-1, 2001] [ISO 8529-2, 2000] [ISO 8529-3, 1998] [ISO 12789-1, 2008] [ISO 12789-2, 2008]. Ensuring traceability for national measurement standard references requires that the method used to define these references be described in as much detail as possible, accounting for all the different parameters, together with a fully-documented evaluation of uncertainty components and including details of an organization acting as guarantor for the definition and maintenance of the reference standards.

To this end, a "quality system" must be established in accordance with ISO 17025, 2005 recommendations. The assessment of compliance and recognition of expertise are then formalized through accreditation awarded by the French accreditation body, Cofrac. Accreditation and ranking as an associate laboratory of the LNE implies that the LNE-IRSN can test its references by taking part in international comparisons: CIPM Key Comparisons (through the CCRI Advisory Committee) which are held once every ten years, and Supplementary Comparisons (CIPM or Euramet) scheduled as required.

(3) In France, the four national metrology laboratories are the LNE (French national laboratory of metrology and testing), the LNE-LNHB (*Laboratoire National Henri Becquerel*, CEA), the LNE-INM (national institute of metrology, CNAM) and the LNE-SYRTE (laboratory of time-space reference systems at the Paris observatory).

(4) Fluence: the relation between the number of particles incident on a sphere and the surface area of the sphere's cross-section – a definition often simplified to the number of incident particles per unit of area. The unit of measure for fluence is m^{-2}. The fluence rate is the same thing as neutron flux density, expressed in $m^{-2}.s^{-1}$.

(5) Tissue kerma is the dose absorbed in human tissue, assuming that all the secondary particles generated by neutron reactions in the tissue have totally lost all their energy. The dose absorbed in a substance, or the absorbed dose, is the relation between the average energy lost by all ionizing particles in a sample of that substance and the mass of the sample. Kerma and dose are expressed as $J.kg^{-1}$, i.e. in Gy.

(6) The equivalent dose is the absorbed dose to which a (dimensionless) weighting factor is applied to take into account the specific toxicity of different types of radiation. The unit of measure used is also the $J.kg^{-1}$, but it is known as the Sievert (Sv) in order to distinguish it from the unit used for absorbed dose. Equivalent dose, a biological quantities, is not directly measurable and is approached *via* dose equivalents. Put simply, the ambient dose equivalent H*(10) used for neutrons is the dose equivalent that would be produced by a neutron field in which all the neutrons move in the same direction, at a depth of 10 mm inside a sphere, known as an Icru sphere, measuring 30 cm in diameter, filled with a liquid having a density of 1 $g.cm^{-3}$, made up of oxygen (76.2%), carbon (11.1%), hydrogen (10.1%) and nitrogen (2.6%). The individual, or personal, dose equivalent Hp(10,α) is the dose equivalent in soft tissue at a depth of 10 mm beneath the skin and depends on the direction of the neutrons. For personal dose equivalent calibration, the device is placed on a calibration phantom (a slab of polymethyl methacrylate, or a water slab, measuring 30 cm x 30 cm x 15 cm), which simulates backscatter from the human body. Calibration for other quantities is performed with the device in the air.

(7) There are three types of measurement standard: the reference measurement standard, featuring the highest level of metrological quality available in a given place or within a given organization; transfer measurement standards, used as intermediaries to compare measurement standards; and, lastly, working measurement standards currently used to calibrate or check measurements, measuring devices or reference materials. Working measurement standards are connected to the reference measurement standard either directly or *via* a transfer measurement standard.

Following international comparisons, declarations of Calibration and Measurement Capabilities (CMC) are updated in the BIPM database. Under the Mutual Recognition Arrangement, these capabilities are automatically recognized worldwide by all the signatory members of the MRA.

Resources implemented at IRSN

The resources implemented at IRSN are designed to meet the requirements of metrology as described above and also to comply with the recommendations set out under the various standards:

- ISO standards (8529 and 12789 as mentioned above), defining the methods used to produce neutron reference fields and calibration methods;
- standards developed by the International Electrotechnical Commission (IEC), specifying the irradiation tests to be performed on radiological protection instruments [IEC 61005, 2003] [IEC 61526, 2005] [IEC 61322, 1994].

A detailed description of IRSN's various facilities dedicated to metrology can be found in [Gressier and Pochat, 2006].

Neutron radioactive sources

Producing neutron fields

Radioactive sources are the most widely used neutron sources, given the fact that:

- it is relatively simple to determine the fluence rate (cm^{-2}) and the dosimetric quantities by measuring the source's initial activity at the time of fabrication;
- the cost of using such neutron sources is reasonable.

For routine calibration of neutron measuring equipment that has already undergone all operating tests under irradiation conditions as part of the design or certification process, radioactive sources using ^{241}AmBe (neutrons produced by α,n reaction) and ^{252}Cf (neutrons from spontaneous fission of the radionuclide) are recommended under ISO 8529-1, since the average energy of the neutrons (4.2 MeV[8] for AmBe and 2.1 MeV for ^{252}Cf) is of the same order of magnitude as that of neutrons produced by fission reactions in the nuclear industry. In order to calibrate a device in a moderated neutron field, in line with the recommendations of ISO 8529-1, the ^{252}Cf source can be placed in the center of a 15-cm radius moderating sphere of heavy water, as shown in ***Figure 3***.

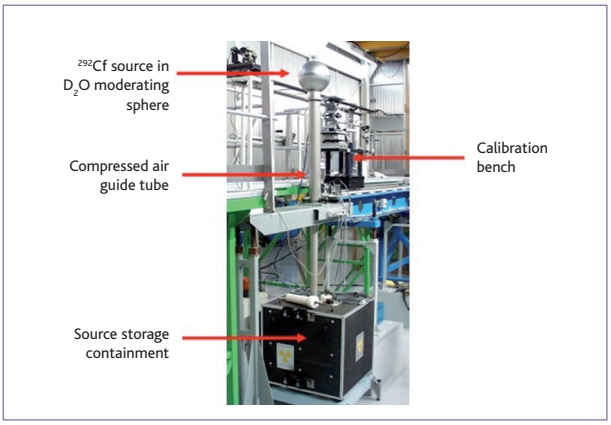

Figure 3 *IRSN's reference radioactive neutron source irradiator.*

Traceability and references

The fluence rate is determined by measuring the source emission rate, applying various corrections to take into account emission anisotropy or attenuation in the air[9], and the scattered neutrons (neutrons deviated from their path by interaction with elements surrounding the source and the measuring points, such as the support on which the source is placed, the floor and walls of the building, etc.). The emission rate for the ^{252}Cf source was measured using the manganese bath method[10] at the LNHB [MB]. This method serves to define the emission rate of a source as a fluence reference measurement standard. A transfer measurement standard (a neutron survey meter) was used to "connect" IRSN's ^{241}AmBe source references to the NPL's ^{241}AmBe source references. The NPL and the LNHB took part in the CCRI(III)-K9 Key Comparison involving measurement of the emission rate of a ^{241}AmBe source, thus ensuring the quality of the primary references for the emission rate.

(8) The electronvolt (symbol: eV) is the unit of measure for energy defined as the kinetic energy acquired by an electron accelerating through a potential difference of one volt. An electronvolt is therefore approximately 1.6×10^{-19} joules. It is not included in the International System (SI).

(9) If the source emission was isotropic, fluence Φ at a distance d (in cm) from the source would be directly related to the emission rate A (in s^{-1}) by the relation:

$$\phi = \frac{A}{4\pi d^2}$$

Given the geometry of the metal capsule (usually cylindrical) surrounding the radioactive material, and the non-uniform nature of the radioactive substance in the source volume, an anisotropic correction is required depending on the neutron emission angle.

Some of the neutrons traveling through the distance d between the source and the measuring point have a nuclear reaction (diffusion, capture) with nuclei of the atoms that make up the air. These neutrons do not, therefore, reach the measuring point. This reduction in the number of neutrons is known as attenuation in the air.

(10) The radioactive source is placed in the center of a sphere (~ 1 m in diameter) containing a solution of manganese sulfate. The manganese nuclei capture the neutrons to form the unstable isotope ^{56}Mn, which emits gamma rays through its de-excitation process. By measuring the gamma radiation, it is possible to determine the neutron emission rate of the source with great accuracy.

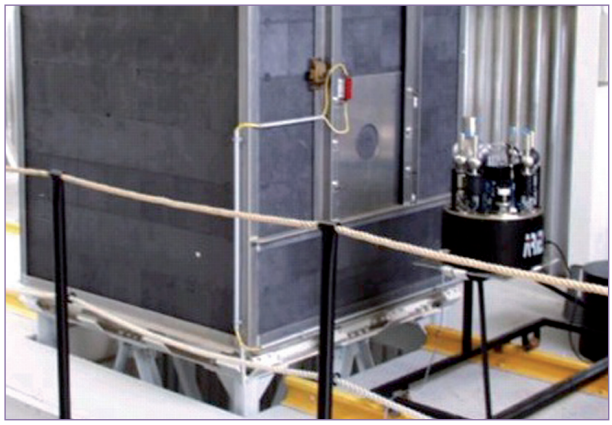

Figure 4 *Calibrating the ROSPEC multi-detector spectrometer using a graphite pile to produce a "thermal" neutron reference field.*

The irradiator consisting of two sources, ^{241}AmBe and ^{252}Cf, is, to date, the only Cofrac-accredited facility at the LMDN, and the only one to have been integrated into the LNE-IRSN. Nine CMCs are associated with this activity (four units in the three neutron fields described above).
An international comparison supervised by the CCRI and Euramet is currently in progress (Euromet.RI(III)- S1). This work consists of determining the ambient dose equivalent H*(10) and involves calibration of a shared instrument (a neutron survey meter) that is being moved from one facility to another.

Research in progress focuses on minimizing uncertainty, improving knowledge on the distribution of neutron energy [Magalotti et *al.*, 2007; Lebreton et *al.*, 2007] and the role of scattered neutrons, controlling the photon field associated with the neutron field [Langner et *al.*, 2007], and defining new calibration methods.

Thermal neutron field

Producing a neutron field

"Thermal" neutron fields are fields in which the energy of practically all the neutrons is lower than 0.5 eV. This type of field is used to check the response of very-low-energy measuring instruments, as recommended by international standards. Such fields are usually produced by research reactors. Without a reactor, IRSN moderates one or more radioactive sources in a graphite cube measuring 1.5 m along each edge. Six ^{241}AmBe sources, distributed throughout the block of graphite, were used up until 2006. Given that these sources (over ten years old) needed to be removed, IRSN decided to upgrade the facility's performance by replacing them with a single high-activity ^{252}Cf source, placed in the center of the moderating cube [Lacoste, 2007].

Traceability and references

The method used to establish the "thermal" neutron fluence reference related to this facility is by activation using a gold foil pellet. The activity of the gold foil, placed at the calibration point for a given amount of time, will be measured by the LNHB and the NPL, and will serve as a reference measurement standard. The distribution of neutron fluence energy will be determined using all the spectrometers at the IRSN laboratory and will make it possible to validate the Monte Carlo simulations of the neutron field.

This method forms the technical basis required for Cofrac accreditation, which will allow this facility to take part in a Key Comparison organized by the CCRI on measuring fluence in "thermal" neutron fields.

Monoenergetic neutron fields

Producing neutron fields

By studying variations in the response of measuring instruments as a function of neutron energy, it is possible to validate the responses calculated by the instruments, or determine and verify the appropriateness of the calibration methods used for these instruments, i.e., to determine and check whether calibration using a radioactive neutron source is sufficient.

To carry out such a study, the neutron fields used must have an energy distribution limited to a narrow energy range. For energy values higher than a few keV, monoenergetic fields are used.

These fields are produced by accelerating charged particles (protons or deuterons) onto a target consisting of a deposit of scandium, lithium, tritium or deuterium on a thin metallic foil. Interaction between the incident charged particles and the nuclei of these deposits produces neutrons emitted in all directions in space. The specific feature of these nuclear reactions is that they produce monoenergetic neutrons for a given energy value of incident charged particles and a given neutron emission angle [Marion and Fowler, 1960].

Because of energy loss due to ionization of the charged beam particles in the thickness of the target (a few µm), fluence energy distribution shows a peak with mid-height width ranging from a few keV to a few hundred keV, as shown in ***Figure 5***.

For this purpose, IRSN uses three accelerators(11), shown in ***Figure 6***:

- the SAMES J25 and T400 accelerators, which produce high neutron emission rates, but for which the neutron energy range is limited

to approx. 14.8 MeV per reaction (d,T) and 3 MeV per reaction (d,D) respectively;

- the AMANDE accelerator, which produces monoenergetic neutron fields, ranging from a few keV to 20 MeV, at lower rates.

Traceability and references

In the case of monoenergetic neutron fields, two quantities are taken as reference values: neutron fluence (or fluence rate) and average energy at the monoenergetic peak.

SAMES accelerators

For the J25 accelerator, the method used to determine fluence is based on detecting the associated particle: this means detecting the alpha particle created at the same time as the neutron, during the reaction of deuterons in the target [Texier, 2007]. This method can be used as a reference measurement standard, provided that the detection efficiency (intrinsic and geometric) of the charged particle detectors used is known precisely. Another difficulty involved in establishing this reference measurement standard is due to contamination of the incident deuteron beam by deuterons with two or three times less energy than expected(12). The energy reference is determined using a transfer measurement standard "connected" to the AMANDE energy references.

For the T400 accelerator, the same principle applies, but the charged particle used is generated by a reaction occurring at the same time as the reaction producing the neutrons. It is therefore essential to know the exact cross section of each reaction. A study is being conducted on the possibility of using a transfer measurement standard based on AMANDE energy and fluence references in parallel.

The AMANDE facility

Fluence references developed using the AMANDE facility are based on references applicable to radioactive sources, using a transfer measurement standard (IRSN Long Counter [Lacoste, 2006]). In the short term (as of 2010 or 2011), energy references will be determined using the time-of-flight method (which measures neutron velocity).

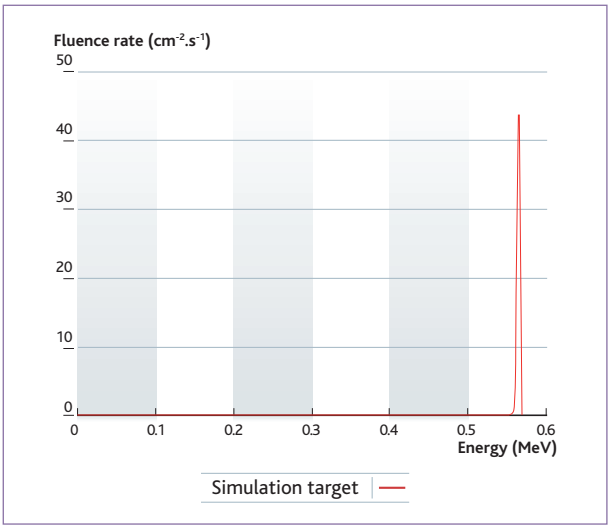

Figure 5 *Simulation of neutron fluence energy distribution in a field of monoenergetic neutrons at 565 keV produced by the AMANDE facility.*

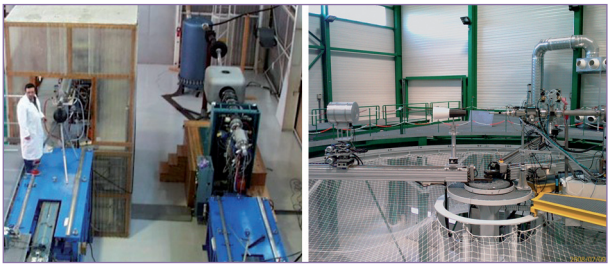

Figure 6 *Accelerators used to produce "monoenergetic" neutron fields. Photo on the left: J25 (on the left) and T400 (on the right). Photo on the right: end of the line of the AMANDE accelerator and measurement of scattered neutron fluence using IRSN's Long Counter and a shadow cone(13).*

This is currently being studied at the IRSN's LMDN laboratory. The method, directly traceable to national time and distance measurement standards, will be used to define a reference measurement standard for neutron energy. To date, recoil proton spectrometers (spherical proportional gas counters and a liquid scintillator), "related" to Germany's national metrology laboratory (PTB) reference measurement standards for monoenergetic fields [Pichenot et *al.*, 2002], have been used as transfer measurement standards and have been compared with the theoretical energy values obtained using nuclear reaction kinematics. They will then be "connected" to the AMANDE reference measurement standard (time-of-flight) to be used as transfer measurement standards on other AMANDE fields different from those used for connection purposes and on other facilities at the laboratory.

The application for Cofrac accreditation for determining fluence (and dosimetric quantities) with AMANDE is currently being pro-

(11) These accelerators are based on applying an electric potential difference to accelerate the charged particles. The relation between energy E of the ion beam (in eV) and the potential difference V (in V) is direct: E = qV, where q is the charge of the charged particle (here, q = 1, so E = V). The J25 accelerator can therefore be used to accelerate ions up to 150 keV, while the T400 accelerates up to 400 keV and AMANDE to 4 MeV. Neutron energy depends on the kinetic energy transferred during the reaction.

(12) This comes from polyatomic ions (molecules with two or three deuterium atoms), generated within the accelerators' ion source and which are not eliminated due to the purely rectilinear geometry of the SAMES accelerators.

(13) A shadow cone is a shield made of iron and polyethylene placed between the target that produces the neutrons and the detector. All the neutrons produced in the solid angle masked by the shadow cone are stopped. This is one of the methods used to determine the role of scattered neutrons in measurement.

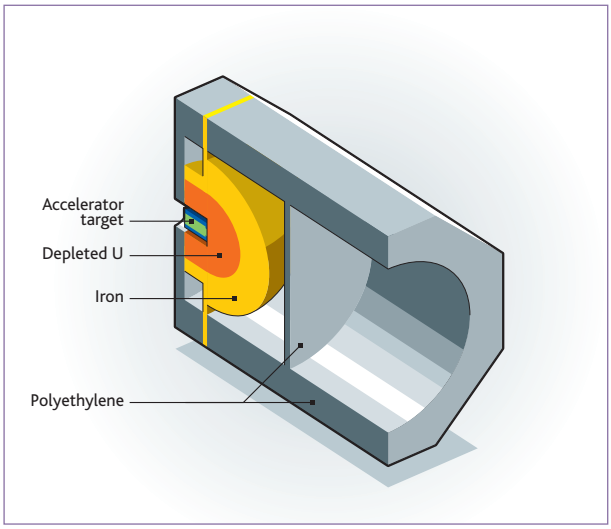

Figure 7 *Cross-section diagram of the CANEL facility.*

cessed. This accreditation should be granted at the beginning of 2010. A second stage, following the study on the time-of-flight method, will involve extending accreditation to include neutron energy.

With regards to fluence, the long counter developed by IRSN was used in mid-2008 in a Euramet international supplementary comparison (TC-936), initiated within the framework of scientific cooperation between IRSN and the German (PTB) and British (NPL) national metrology laboratories. In 2011, a CIPM Key Comparison will be organized using AMANDE, in which a range of different reference instruments will measure fluence in four monoenergetic fields.

There are many research projects to be pursued, mainly focusing on managing uncertainty, the evolution of targets under irradiation, understanding the role played by scattered neutrons, controlling the photon field associated with neutron fields, defining calibration methods, studying new nuclear reactions, developing specific reference instruments (one possible option is currently under study in thesis work [Allaoua, 2007]), etc.

Realistic fields

Concept

The response of personal dosimeters and, generally speaking, all neutron measuring devices, depends on neutron energy. This means that it is impossible to correctly calibrate an instrument that will be used in a neutron field in which the emission angle and energy distributions are significantly different from those in the reference radiation field used for calibration. That is why ISO 12789-1, developed with significant contributions from IRSN, introduces the notion of Simulated Workplace Neutron Fields, also known as Realistic Neutron Fields. Once they have been accurately characterized, these neutron fields can be used as reference fields for calibration and are recommended in the latest IEC standards.

The aim is to be able to calibrate any device in a neutron field that resembles as closely as possible the field in which it is to be used. Calibration in "realistic" fields provides more reliable dose measurements with better of each individual workplace.

Producing neutron fields

The moderated ^{252}Cf source mentioned above is a realistic neutron field. Nonetheless, IRSN has a unique facility unlike any other worldwide, called CANEL. It can produce this type of field using the monoenergetic fields of the J25 and T400 accelerators. CANEL is a modular assembly that can be placed around the target of these accelerators and in which the "primary monoenergetic" neutrons generate a spectrum of "secondary" fission neutrons through reaction with CANEL's uranium shell. The fission neutrons then pass through different shields made of iron and polyethylene, as illustrated in ***Figure 7***, to produce a degraded spectrum representative of the spectra found in certain workplaces.

Traceability and references

The reference method used will be the same as for the SAMES accelerators, plus a measurement of the fluence energy distribution with all the spectrometers at the IRSN laboratory. The spectrometers will eventually transfer the energy and fluence references from AMANDE, as soon as the latter receives accreditation for the energy reference.

However, a Euromet international research comparison (TC-670) was carried out using a slightly different version of CANEL. A satisfactory level of agreement was attained between the various spectrometry systems at the laboratories that took part in this comparison, involving mainly Bonner sphere systems(14) enabling the entire energy distribution to be measured [Gressier et *al.*, 2004]. If one of the instruments participating in this exercise is involved in or related to a Key Comparison, then traceability relative to international references can be established. This solution is currently being examined.

(14) The Bonner sphere system consists of a "thermal" neutron detector (i.e. that mainly detects very low-energy neutrons), placed in the center of polyethylene spheres of various diameters. Sensitivity to neutrons of a given energy then depends on the size of the sphere. By combining the measurements performed using all the spheres, it is possible, using dedicated codes, to determine the neutron fluence energy distribution in a range between a few meV to 20 MeV.

Conclusion and outlook

Role and advantages of neutron metrology at IRSN

IRSN's facilities for producing neutron reference fields make it possible to:

- test, calibrate and certify any kind of measuring equipment (spectrometers, survey-meters, passive and active dosimeters, multi-detectors, etc.) that are sensitive to neutrons;
- ensure traceability relative to international references for French calibration laboratories that produce neutron fields.

They are currently used by:

- industry, to develop or test measuring instruments for radiological protection;
- research institutes, to develop detectors for fundamental research in astrophysics, nuclear physics and particle physics;
- IRSN, for research and development in dosimetry and radiobiology.

IRSN thus has a full range of technical resources to maintain and develop the tools and skills required to conserve a high level of expertise in the field of neutron dosimetry.

A new domain of metrology?

Thanks to its experience in neutron metrology, IRSN now proposes an alternative approach to research and development involving the AMANDE facility, at least initially.

It is possible, based on a metrological approach, to control the dose deposited in a single cell using charged particles, ranging from protons to heavier ions, such as carbon and oxygen. A project is currently being set up to integrate a prototype version of a µ-beam line into AMANDE. This new line will be used to deliver individually controlled ions, accelerated across a broad range of energy values, to cell samples, within a few micromillimeters accuracy. In light of initial results, the options of developing of a new dedicated facility or extending the AMANDE facility may be considered.

This type of development would open the way to measuring doses at the microscopic and cellular level, thereby extending the fields of application for metrology at IRSN.

References

- A. Allaoua (2007). Définition et caractérisation d'un détecteur à noyaux de recul pour l'établissement de références de champs neutroniques mono-énergétiques pour l'installation AMANDE. États des lieux au 1er septembre 2007, Rapport SDE 2007-28.
- BIPM: www.bipm.org
- J.M. Bordy, H. Stadtmann, P. Ambrosi, D.J. Bartlett, P. Christensen, H. Hyvönen (2000). *Performance test of dosimetric services in the EU member states and Switzerland for the routine assessment of individual doses (photon, beta, neutron), Radiation Protection Dosimetry, 89 (1-2), p.107-154.*
- CEI 61005 (2003). Instrumentation pour la radioprotection. Appareils de mesure de l'équivalent de dose ambiant neutron (ou de son débit d'équivalent de dose).
- CEI 61322 (1994). Instrumentation pour la radioprotection. Débitmètres à poste fixe, ensembles d'alarme et moniteurs pour rayonnements neutroniques compris entre l'énergie des neutrons thermiques et 15 MeV.
- CEI 61526 (2005). Instrumentation pour la radioprotection. Mesure des équivalents de dose individuels Hp(10) et Hp(0,07) pour les rayonnements X, gamma, neutron et bêta. Appareils de mesure à lecture directe et moniteurs de l'équivalent de dose individuel.
- Cofrac: www.cofrac.fr
- Euramet: www.euramet.org
- V. Gressier, V. Lacoste, L. Lebreton, H. Muller, G. Pelcot, M. Bakali, F. Fernández, M. Tómas, N.J. Roberts, D.J. Thomas, M. Reginatto, B. Wiegel, J. Wittstock (2004). *Characterisation of the IRSN CANEL/T400 facility producing realistic neutron fields for calibration and test purposes, Radiation Protection Dosimetry, 110 (1-4), p.523–527.*
- V. Gressier, J.L. Pochat (2006). Les installations de l'IRSN dédiées à la métrologie des neutrons, Radioprotection 41 vol. 1 11-32.
- *International Commission on Radiological Protection Publication 74 (1997). Conversion Coefficients for use in Radiological Protection against External Radiation.*
- ISO (2006). Métrologie, normalisation et évaluation de la conformité. Bâtir une infrastructure pour le développement durable, http://www.iso.org/iso/fr/devt_3pillars_2006-fr.pdf
- ISO 12789-1 (2008). Champs de rayonnement de référence. Champs de neutrons simulant ceux de postes de travail. Partie 1 : Caractéristiques et méthodes de production.
- ISO 12789-2 (2008). Champs de rayonnement de référence. Champs de neutrons simulant ceux de postes de travail. Partie 2 : Concepts d'étalonnage en relation avec les grandeurs fondamentales.
- ISO 17025 (2005). Norme NF en ISO/CEI 17025. Exigences générales concernant la compétence des laboratoires d'étalonnage et d'essais.
- ISO 8529-1 (2001). Rayonnements neutroniques de référence. Partie 1 : Caractéristiques et méthodes de production.
- ISO 8529-2 (2000). Rayonnements neutroniques de référence. Partie 2 : Concepts d'étalonnage des dispositifs de radioprotection en relation avec les grandeurs fondamentales caractérisant le champ de rayonnement.
- ISO 8529-3 (1998). Rayonnements neutroniques de référence. Partie 3 : Étalonnage des dosimètres de zone (ou d'ambiance) et individuels, et détermination de leur réponse en fonction de l'énergie et de l'angle d'incidence des neutrons.
- V. Lacoste (2006). Étude et modélisation d'un long compteur pour l'établissement des références neutroniques en fluence de l'installation AMANDE, Rapport SDE 2006-48.
- V. Lacoste (2007). *Design of a new IRSN thermal neutron field facility using Monte Carlo simulations, Rapport SDE 2007-14.*
- F. Langner, S. Löb, R. Nolte, V. Gressier, B. Asselineau, V. Lacoste, L. Lebreton (2007). *Photon contribution to ambient dose equivalent H*(10) in the wide-spectrum neutron reference fields of the IRSN, Radiation Protection Dosimetry 126(1-4),145-150.*
- L. Lebreton, A. Zimbal, D. Thomas (2007). *Experimental comparison of ^{241}Am-Be Neutron fluence energy distributions, Radiation Protection Dosimetry 126(1-4), 3-7.*
- LNE : www.metrologiefrancaise.fr
- LNHB : www.nucleide.org
- N. Magalotti, V. Lacoste, L. Lebreton, V. Gressier (2007). *Investigation of the neutron energy distribution of the IRSN ^{241}Am-Be(α,n) source, Radiation Protection Dosimetry, doi:10.1093/rpd/ncl537.*
- J.B. Marion, J. L. Fowler (1960). *Fast Neutron Physics, Interscience Publishers, London.*
- MB. Description du bain de manganèse sur le site internet du *National Physical Laboratory:* http://www.npl.co.uk/server.php?show=ConWebDoc.2016
- G. Pichenot, S. Guldbakke, B. Asselineau, V. Gressier, C. Itié, H. Klein, K. Knauf, L. Lebreton, S. Löb, L. Pochon-Guérin, D. Schlegel, W. Sosaat (2002). *Characterisation of spherical recoil proton proportional counters used for neutron spectrometry, Nuclear Instruments and Methods in Physics Research, A 476, p. 165-169.*
- E. Texier (2007). Caractérisation du champ neutronique monoénergétique de 14,8 MeV de l'accélérateur J25, Rapport SDE 2007-37.

4.9 ENVIRONMENTAL AND HEALTH IMPACT OF CHEMICAL EFFLUENT RELEASES: the CALIES computer code

Caroline RINGEARD, Nathalie PIRES
Occupational and Population Radiological Protection Assessment Unit

A new task for IRSN that began in 2001

Since 2001, the ASN, the French nuclear safety authority, has called on IRSN to carry out technical assessments on the production, treatment and release of chemical effluent, in order to process applications for water intake and effluent release permits, as well as assessments on the environmental and health impact of these releases.

Several IRSN divisions are involved in this task. The Institute bases this work on regulatory texts and guides produced by the European Commission and organizations such as Ineris, the French national institute for the study of industrial environments and hazards, while making sure that the methods used are consistent with those implemented for assessing the consequences of radioactive effluent releases.

CALIES: an assessment tool developed by IRSN

IRSN has designed and developed a tool named CALIES (for the calculation of environmental and health impact), used in assessing releases into freshwater, the sea and air. This computer tool uses equations that characterize the transfer of contaminants into water, air, soil, plants, aquatic organisms and humans. CALIES is used to meet assessment needs in situations involving chronic, sub-chronic and acute exposure for a given population, classified in five age groups.

Designed as a platform, Version 3.0 now includes a database (listing the characteristics of over a hundred chemicals that have been analyzed since 2001), an atmospheric dispersion module (COTRAM4, which calculates concentrations added in the air based on the quantities of chemicals released and meteorological data), as well as a module that calculates environmental and health impact.

For a person exposed to a substance that has a threshold effect, the health impact is expressed in terms of a risk index, IR. This index is the result of comparing the person's exposure levels, calculated using CALIES, with toxicological reference values (TRV). If the risk index is less than one, a toxic effect is unlikely. Over one, a toxic effect cannot be ruled out.

For substances that do not have a threshold effect, the individual's excess risk value (Eri) is calculated. The individual's excess risk represents the probability of an individual developing, during his or her lifetime, the effect(s) associated with the substance(s) in question. In France, the reference value(1) is 10^{-5}.

Each year, a bibliographic review of toxicity studies is produced to update the monographs available in CALIES. Based on the state of current knowledge, the impact data to be used in calculating the health risk is selected.

Students from EHESP, an institute of higher eduction in public health, and ENSCR, a higher education school of chemistry in Rennes, are regularly welcomed at IRSN to

(1) Circular of December 10, 1999, relative to guidelines on defining objectives for the remediation of contaminated sites and soils.

conduct studies on modeling transfer to the environment, aimed at enhancing the computer code, as in a recent study involving the transfer of organic substances to plants.
Since 2001, IRSN has submitted around thirty assessments to the authorities, mostly in response to applications for effluent release permits. CALIES was recently used to assess health impact in a case involving exposure to contaminated soils.

4.10 RADON in the Martian atmosphere

Jean-Christophe SABROUX
Airborne Pollutants and Containment Study and Research Department
Pierre-Yves MESLIN
Aerosol Physics and Metrology Laboratory

Radon, an inert radioactive gas and a decay product of uranium-238, has long been a favorite tracer among hydrogeologists. The project to conduct a scientific study on radon in the Martian atmosphere and to develop an instrument designed to measure radon aboard the future Mars Lander or Rover is based on a simple idea: there is a high correlation between soil humidity and radon exhalation. Inspired by the slogan *Follow the water!*, which has long been the guiding principle behind Nasa's programs to explore the Red Planet, it seemed only natural to suggest focusing on radon in the atmosphere as a natural indicator of water in the near-surface soil of Mars. The question is of particular interest at low latitudes, where the neutron spectrometer on Nasa's Mars Odyssey orbiter has revealed evidence of large quantities of hydrogen, although it is not yet clear whether this signals the presence of ice or of hydrated minerals.

Co-funded by Cnes, the French space agency, IRSN supervised a thesis(1) on the scientific study of radon on Mars, a subject which has so far escaped the attention of planetologists. Although the technical feasibility of measuring radon had been demonstrated during development of "Phase A" instrumentation, also co-financed by Cnes, the link between water and radon in the temperature and pressure conditions on the surface of Mars, factoring in its physical and chemical characteristics, needed to be established more soundly. This has now been achieved, in what seems to be one of the major conclusions drawn in this thesis: the near-surface soil on Mars, including at low latitudes, is not nearly as dry as that of the Moon (where, since the Surveyor missions, radon has been measured on numerous occasions, including in orbit), and the difference in humidity levels is great enough to increase radon exhalation significantly.

Of course, the link between atmospheric radon and near-surface water is far from being incontestable, on Mars as here on Earth. This was confirmed in a model of radon transport in porous media developed to reflect the specific characteristics of Martian soil, where low pressure and low temperature make it essential to take into account Knudsen diffusion (diffusion in a micro- to nano-porous medium) and adsorption (the same applies, for example, to clay on Earth, but for quite different

(1) Pierre-Yves Meslin defended his thesis on "Radon as a geophysical tracer on Mars: study of its transport, first evidence and development of an instrument to measure radon on the surface of the planet", at Pierre & Marie Curie University in Paris.

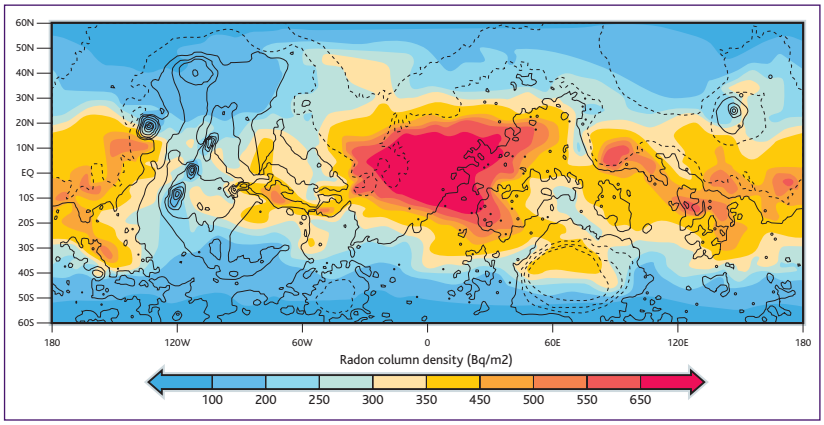

Figure 1 *Map of radon "column density" measured in Bq.m^{-2} drawn up using a global atmospheric circulation model for Mars (LMDZ, developed by the CNRS' Dynamic Meteorology Laboratory) and input data that takes into account the water and thorium content in the soil on Mars (determined from measurements taken in space by the Mars Odyssey gamma ray and neutron spectrometer). This map assumes, as an initial approximation, a constant relation between uranium and thorium on the surface of Mars.*

reasons). Combined with a global atmospheric circulation model, the transport model traces radon to its source and, in particular, to soil humidity, albeit based on a certain number of assumptions. These are conditioned by other, observable assumptions, regularly furnished by the Mars orbiters and rovers that are still in operation. This original and rigorous approach provides predictive mapping of the potential exhalation of radon on Mars, an approach that is equally valid for use on Earth. Last, meticulous analysis of the data supplied by the Alpha spectrometer on the Opportunity rover has revealed the presence of polonium-210 deposited on Martian atmospheric dust. Similarly, the hypothesis that bismuth-214 is present in the planet's atmosphere, as formulated in this thesis, should make it possible to map uranium on Mars using data from the gamma ray spectrometer on the Mars Odyssey orbiter.

Thanks to these two scientific developments, which would not be possible without incredible progress in ionizing radiation metrology, together with the many links forged between IRSN and French and foreign space laboratories, an instrument designed to measure radon on Mars is now in a much stronger position than four years ago, in the race to be included aboard a Martian probe – such as ESA's MarsNEXT mission, possibly launched by the end of the next decade.

KEY EVENTS and dates

DISSERTATIONS DEFENDED

May 20, 2008

Pierre-Yves MESLIN submitted a thesis on "Radon as a geophysical tracer on Mars: study of its transport, first evidence and development of an instrument to measure radon on the surface of the planet", at Pierre & Marie Curie University in Paris.

OTHER MAJOR EVENTS

February 2008

The ASAMPSA2 Project (Advanced Safety Assessment Methodologies: Level 2 PSA) was launched on February 19, 2008 for a period of 36 months, under the European Commission's 7th Framework Program. The goal of the project is to draw up a guide to best practices regarding Level 2 probabilistic safety assessment methodologies (Level 2 PSA), with a view to harmonization at European level. The guide deals primarily with nuclear power plants in Europe, but the possibility of applying it to future reactors (GEN III and GEN IV) will also be examined. Twenty-one organizations in 12 EU Member States are involved in this project, coordinated by IRSN.

December 2008

A cooperation agreement was signed between IRSN and its counterparts, PTB (Germany), NPL (United Kingdom) and IRMM (European Commission's Joint Research center, based in Belgium), in the field of neutron metrology and dosimetry.